Chapter 8
Irradiation-Induced Voids and Bubbles

The formation and growth of *voids* and *bubbles* is of intense interest for material performance in radiation environments at elevated temperature. The first observation of voids in irradiated metals was published by Cauthorne and Fulton in 1967 [1]. Voids can have a profound influence on material properties because solids undergo *volumetric swelling* when voids form and grow. It has been suggested that the US breeder reactor program experienced a setback of nearly a decade by this surprising observation, as scientists scrambled to understand this phenomenon and the consequences to reactor internals. Since that time, a great deal of effort has been expended toward understanding their formation and growth. Figure 8.1 shows examples of voids in irradiated stainless steel, aluminum, and magnesium. Voids of this size and number density can cause tens of percent increases in volume, translating into significant changes in linear dimensions as well. The challenge of designing a reactor to accommodate swelling of this magnitude quickly becomes monumental.

The formation and growth of voids shares much in common with bubbles. Yet because of their nature—a void is essentially an empty cavity—bubble mechanics are more complicated. It is by virtue of the fact that insoluble gases are formed by transmutation when certain metals are irradiated that drew attention to the subject of bubbles in irradiated metals. Under irradiation, it is possible for large numbers of inert gas bubbles to form, which significantly alter the physical and mechanical properties of metals. Fast and thermal spectrum reactors generate helium via transmutation, and the first wall of a fusion reactor is susceptible to bubble formation due to the high gas loading from reaction products in the plasma. Numerous examples exist in reactor systems where bubbles form and alter material properties, one of the most important being the structural materials of fission reactors. This chapter will address the theory of void and bubble nucleation and growth, along with elucidating the most important factors affecting these processes in reactor systems.

G.S. Was, *Fundamentals of Radiation Materials Science*,
DOI 10.1007/978-1-4939-3438-6_8

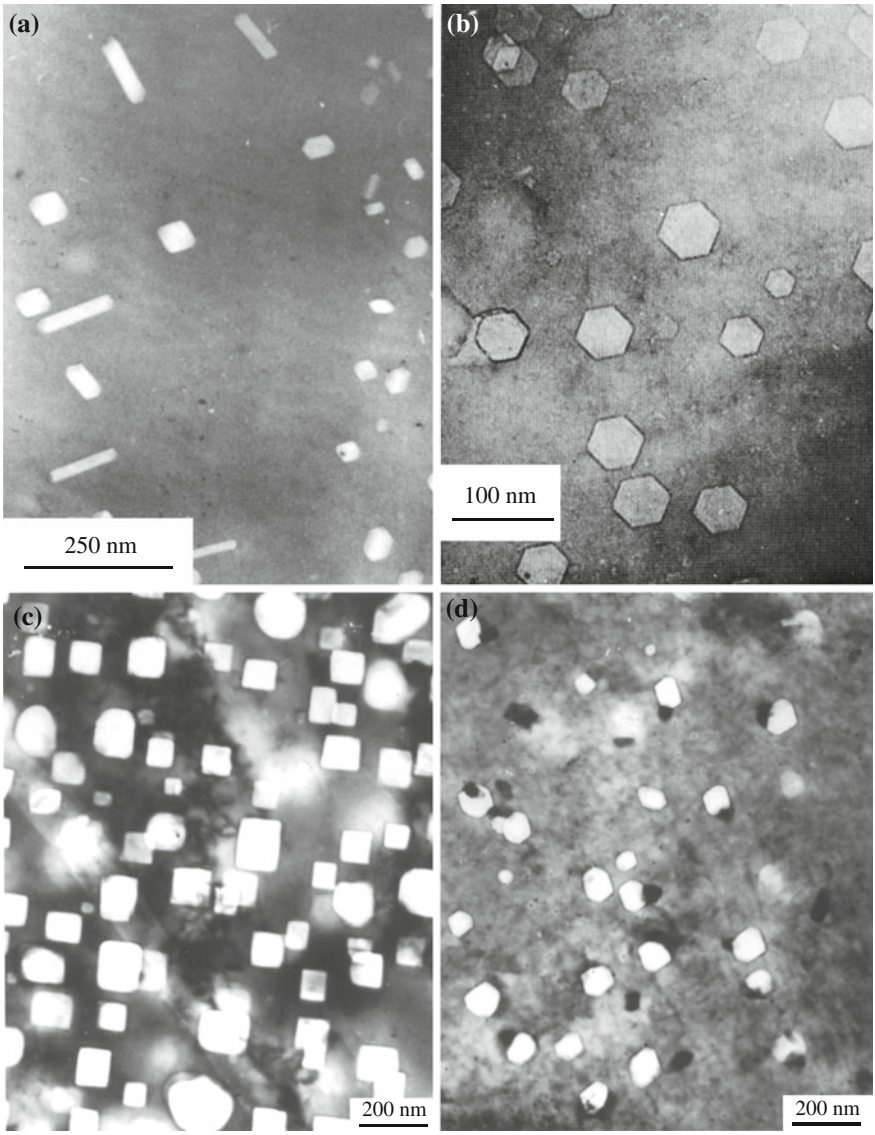

Fig. 8.1 Micrographs of irradiation-induced voids in (**a**) stainless steel, (**b**) aluminum, (**c**) and (**d**) magnesium [2, 3]

8.1 Void Nucleation

The driving force for the formation of voids in solids is the supersaturation of vacancies due to irradiation defined by:

$$S_v = \frac{C_v}{C_v^0}, \tag{8.1}$$

where C_v^0 is the thermal equilibrium concentration of vacancies. During irradiation, defects react to form clusters and the clusters either grow by absorption of defects of the same type, or shrink by absorption of defects of the opposite type. For a cluster of vacancies to grow into a void, there must be a net increase in the number of vacancies absorbed over the number of interstitials absorbed. Thus, we will be interested in the equilibrium void distribution function, $\rho^0(n)$ (where n is the number of vacancies in the void), which is developed by a supersaturation of vacancies in the solid. The distribution function gives the number of vacancy clusters in each size class. Under non-equilibrium conditions, there will be a net flux, J, of voids from one size class to the next larger size class. This is the nucleation current and is the quantity we are interested in finding. The presence of an inert gas in the nucleation process is then considered.

8.1.1 Equilibrium Void Size Distribution

Analogous to the case of point defects (discussed in Chap. 4) and following the derivation in [4], the equilibrium void size distribution is determined from the change in Gibbs free energy of a system containing a distribution $\rho^0(n)$ of vacancy clusters:

$$G = G_0 + \sum_n \rho^0(n) G_n - kT \sum_n \ln w_n, \tag{8.2}$$

where G_0 is the free energy of the perfect lattice, the second term is the work to form a void distribution, and the last term is the entropy contribution to the number of ways that the voids can be distributed in a lattice. The quantity G_n is the Gibbs free energy (reversible work) required to form a void of size n:

$$G_n = H_n - TS_n = E_n + p\upsilon_n - TS_n, \tag{8.3}$$

where

E_n the energy required to form a void of n vacancies
υ_n volume change (= $n\Omega$)
p hydrostatic stress
S_n the excess entropy associated with the process
w_n the number of ways of placing $\rho^0(n)$ voids of size n in the solid.

Neglecting the last two terms on the right, G_n reduces to $G_n \cong E_n$.

For large values of n, the energy of the void can adequately be represented by the surface energy:

$$E_V = 4\pi R_V^2 \gamma, \tag{8.4}$$

where γ is the surface energy of the solid per unit area and R_V is the void radius which is related to the number of vacancies in the void by:

$$n = \frac{4\pi R_V^3}{3\Omega}, \tag{8.5}$$

where Ω is the atomic volume. The reader should note that the expression in Eq. (8.4) is the same as was developed in Eq. (7.58) and for the limiting case of a vacancy, as in Eq. (4.22). Equation (8.4) is, however, an approximation since the energy should properly include terms for the contraction of the surface and for the elastic energy stored in the solid (see Eq. 4.23). Combining Eqs. (8.4) and (8.5) gives:

$$E_n = \left(36\pi\Omega^2\right)^{1/3} \gamma n^{2/3}. \tag{8.6}$$

The last term in Eq. (8.2) is the product of the temperature and the mixing entropy. It can be obtained by calculating the number of ways in which voids can be distributed in a crystal containing N_0 lattice sites per unit volume. The procedure is the same as that used for vacancies in Sect. 4.2 and results in:

$$w_n = \frac{n^{\rho^0(n)}(N_0/n)!}{(N_0/n - \rho^0(n))!(\rho^0(n))!}. \tag{8.7}$$

We now define the chemical potential of a void of size n as μ_n that is related to the Gibbs free energy by:

$$\mu_n = \left.\frac{\partial G}{\partial \rho^0_{(n)}}\right|_{T,p,n}. \tag{8.8}$$

Substituting Eq. (8.7) into Eq. (8.2), using Stirling's approximation for the factorial term in Eq. (8.7), and taking the derivative as required by Eq. (8.8) ($\partial G = \partial \Delta G$ since $\Delta G = G - G_0$) gives:

$$\mu_n = E_n + kT \ln\left[\frac{\rho^0(n)}{N_0}\right]. \tag{8.9}$$

We have neglected $\rho^0(n)$ compared to N_0 because the void concentration is low. For monovacancies ($n = 1$), Eq. (8.9) reduces to:

$$\mu_v = E_v + kT \ln\left(\frac{C_v}{N_0}\right). \tag{8.10}$$

Since the equilibrium concentration of vacancies in a solid is given by:

$$C_v^0 = N_0 \exp\left(\frac{-E_f^v}{kT}\right), \tag{8.11}$$

substituting for N_0 from Eq. (8.11) into Eq. (8.10) gives:

$$\mu_v = kT \ln\left(\frac{C_v}{C_v^0}\right) = kT \ln S_v. \tag{8.12}$$

The criterion for chemical equilibrium is that the chemical potential of reactants and products in the system be the same, i.e.,

$$n\mu_v = \mu_n. \tag{8.13}$$

Substituting Eqs. (8.9) and (8.12) into the criterion for chemical equilibrium, Eq. (8.13) gives:

$$\rho^0(n) = N_0 \exp\left(n \ln S_v - \xi n^{2/3}\right), \tag{8.14}$$

where

$$\xi = \left(36\pi\Omega^2\right)^{1/3} \frac{\gamma}{kT}. \tag{8.15}$$

Substituting Eq. (8.15) into Eq. (8.14) and considering only the term inside the exponent, we have:

$$n \ln S_v - \xi n^{2/3} = n \ln S_v - \frac{\left(36\pi\Omega^2\right)^{1/3} \gamma n^{2/3}}{kT}. \tag{8.16}$$

Expressing Eq. (8.14) as $\rho^0(n) = N_0 \exp(-\Delta G_n^0/kT)$ gives the following expression for ΔG_n^0:

$$\Delta G_n^0 = -nkT \ln S_v + \left(36\pi\Omega^2\right)^{1/3} \gamma n^{2/3}, \tag{8.17}$$

which is just the free energy change in the solid on forming a spherical void consisting of n vacancies on some particular site. A schematic of Eq. (8.17) is shown in Fig. 8.2 in which the free energy is plotted as a function of the number of

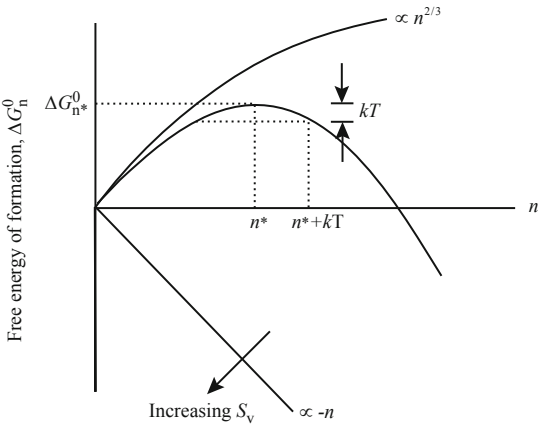

Fig. 8.2 Schematic illustration of ΔG^0_n, the free energy of formation of a spherical void consisting of n vacancies and the effect of thermal fluctuations on the critical size void embryo

vacancies in a void. Note that the first term decreases linearly with n, while the second term increases as $n^{2/3}$. Accounting for the magnitude of the factors in each term, the resulting sum is a curve with a maximum at a value of n^*. This is the critical size of a void embryo which must be achieved in order for the embryo to grow into a void. At the critical point, vacancy addition and removal both cause a reduction in the Gibbs free energy of the system, so this is an unstable point. Above the critical size, addition of vacancies to the embryo causes a decrease in the free energy, which means that void growth is favored, while loss of vacancies causes an increase in the free energy, so this reaction is not favored. Note also that thermal fluctuations add an increment to the embryo size, pushing the critical size to a higher value and thus making it more difficult to nucleate a stable void.

8.1.2 Void Nucleation Rate

The nucleation rate of void embryos (consisting of n vacancies) can be described using the same formalism that was used to describe vacancy loop nucleation in Chap. 7 and developed in [5–7]. However, for the sake of continuity, that derivation will be repeated here for the case of void embryos. Recall from Eq. (7.74) that the nucleation rate of a void embryo of size n is given by:

$$J_n = \rho^0(n)\beta_v(n)Z, \tag{8.18}$$

where $\rho^0(n)$ is the concentration of voids of size n vacancies, $\beta_v(n)$ is the absorption rate, and Z, the Zeldovich factor (defined in Sect. 7.6.1) and the void concentration is given by:

$$\rho^0(n) = N_0 \exp\left(\frac{-\Delta G_n^0}{kT}\right), \tag{8.19}$$

where N_0 is the number of sites on which voids can be formed and ΔG_n^0 is the change in free energy in the solid upon formation of the void and is given in Eq. (8.17). The value of ΔG_n^0 for the critical void embryo size, ΔG_k^0 (for embryo size n_k), is the activation barrier for void formation shown in Fig. 8.3 by the lower curve and is given as:

$$\Delta G_k^0 = -n_k kT \ln S_v + \left(36\pi\Omega^2\right)^{1/3} \gamma n_k^{2/3}. \tag{8.20}$$

The void nucleation rate is the nucleation current given in Eq. (8.18). The void nucleation current, J_n, and activation barrier, ΔG_k^0, apply to the case where only vacancies are present. However, under irradiation, vacancies and interstitials are produced in equal numbers, so the presence of interstitials must be accounted for. We now consider the case where interstitials can also impinge on voids. The analysis is similar to that just presented, but more complicated due to the introduction of another specie that will make void nucleation more difficult.

Consider now the nucleation of vacancy clusters on one particular kind of attractive site [4–6] such as the compressive stress field around a dislocation. The following assumptions are made:

1. The lattice is in thermal and dynamic equilibrium, which are minimally affected by displacement and thermal spikes.
2. Monovacancies and solvent monointerstitials are the only mobile point defects present.
3. The defects obey dilute solution thermodynamics.
4. A steady-state concentration of vacancies and interstitials exists.

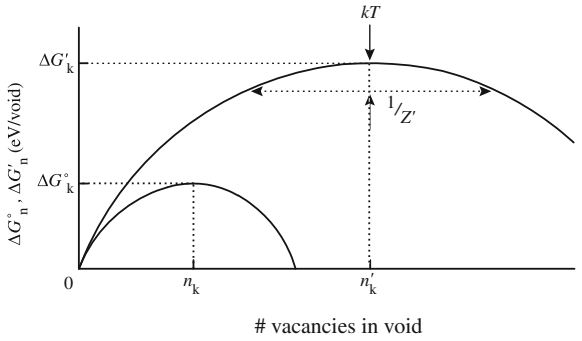

Fig. 8.3 Schematic nucleation curves showing the various parameters which are important in void nucleation. ΔG_k^0 is the activation barrier to nucleation if interstitials are not present, while $\Delta G_k^{'}$ is the same quantity if interstitials are present during the nucleation process (after [6])

Assumption (1) is reasonable as thermal spike lifetimes are very short (10^{-12} s) and dynamical equilibrium should be attained in similar time intervals. Assumption (2) is generally not valid since gas atoms are often present and are known to play an important role in nucleation (treated in Sect. 8.1.3). Assumption (3) should be valid for low defect concentration ($\leq 10^{-4}$ atomic fraction). The final assumption is a gross oversimplification since the microstructure continues to evolve with increasing dose causing sink strength, and therefore defect concentrations, to continually change.

The following derivation of the void nucleation rate from kinetic considerations is similar to that for loops, in which the nucleation rate is expressed as the flux of clusters between adjacent size classes in a phase space of cluster size. A flux is the concentration times velocity or the product of concentration, jump frequency, and jump distance. The flux between any two size classes, say n and $n + 1$, is:

$$J_n = \beta_v(n)\rho(n) - \alpha_v(n+1)\rho(n+1) - \beta_i(n+1)\rho(n+1), \tag{8.21}$$

where $\rho(n)$ and $\rho(n + 1)$ are the number of n-mer (voids containing a net of n vacancies) and $(n + 1)$-mers per unit volume. $\beta_v(n)$ is the rate of vacancy capture by a n-mer, and $\alpha_v(n + 1)$ and $\beta_i(n + 1)$ are the rates of vacancy loss and interstitial capture by a $(n + 1)$-mer, respectively. The first term in Eq. (8.21) represents an addition to the $n + 1$ size class by capture of a vacancy by a void of n-mer size class. The second term is a loss from the $(n + 1)$-mer size class by loss of a vacancy, and the third term is a loss from the $(n + 1)$-mer size class by capture of an interstitial. Interstitial emission is of low probability and is neglected. Figure 8.4 shows the various processes described by Eq. (8.21) in phase space.

Setting $J = 0$ in Eq. (8.21) is equivalent to equilibrating the size classes since there is no net flux between size classes (as we did in Sect. 7.6). If we neglect interstitials, then we can write Eq. (8.21) as:

$$\alpha_v(n+1) = \frac{\beta_v(n)\rho^0(n)}{\rho^0(n+1)}. \tag{8.22}$$

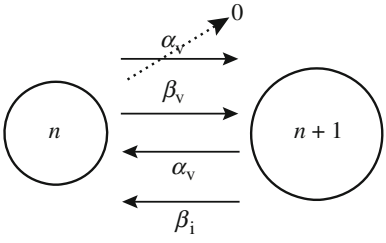

Fig. 8.4 Illustration of the processes governing the flux between adjacent void sizes in a phase space of void size

Combining Eqs. (8.21) and (8.22) gives:

$$J_n = \beta_v(n)\left\{\rho(n) - \rho(n+1)\left[\frac{\rho^0(n)}{\rho^0(n+1)} + \frac{\beta_i(n+1)}{\beta_v(n)}\right]\right\}. \tag{8.23}$$

Since $\rho^0(n) = N_0 \exp(-\Delta G_n^0/kT)$, we note that:

$$\frac{\rho^0(n)}{\rho^0(n+1)} = \exp\left(\frac{\delta G_n^0}{kT}\right), \tag{8.24}$$

where $\delta G_n^0 \equiv \Delta G_{n+1}^0 - \Delta G_n^0$. We now define new functions of n, $\rho'(n)$, and $\delta G_n'$ such that by analogy with Eq. (8.24):

$$\frac{\rho'(n)}{\rho'(n+1)} = \frac{\rho^0(n)}{\rho^0(n+1)} + \frac{\beta_i(n+1)}{\beta_v(n)} = \exp\left(\delta G_n'/kT\right), \tag{8.25}$$

where

$$\delta G_n' = \Delta G_{n+1}' - \Delta G_n', \tag{8.26}$$

and $\Delta G_n'$ is not generally a free energy because of the term $\dfrac{\beta_i(n+1)}{\beta_v(n)}$ in Eq. (8.25). Using the expression in Eq. (8.25), we can rewrite the equation for J_n in terms of $\dfrac{\rho'(n)}{\rho'(n+1)}$ by substituting Eq. (8.25) into Eq. (8.23) to give:

$$J_n = \beta_v(n)\left\{\rho(n) - \rho(n+1)\frac{\rho'(n)}{\rho'(n+1)}\right\}. \tag{8.27}$$

Rearranging Eq. (8.27) gives:

$$J_n = -\beta_v(n)\rho'(n)\left[\frac{\rho(n)}{\rho'(n)} - \frac{\rho(n+1)}{\rho'(n+1)}\right], \tag{8.28}$$

and noting that:

$$\frac{\left[\dfrac{\rho(n)}{\rho'(n)} - \dfrac{\rho(n+1)}{\rho'(n+1)}\right]}{\Delta n} = \frac{\partial\left(\dfrac{\rho(n)}{\rho'(n)}\right)}{\partial n}, \tag{8.29}$$

gives:

$$J_n = -\beta_v(n)\rho'(n)\frac{\partial[\rho(n)/\rho'(n)]}{\partial n}, \tag{8.30}$$

which is the basic flux equation. Rearranging Eq. (8.25) by taking the natural log of both sides and summing from $j = 0$ to $n - 1$ gives:

$$\sum_{j=0}^{n-1} \ln\left(\frac{\rho'(j)}{\rho'(j+1)}\right) = \sum_{j=0}^{n-1} \left\{ -\ln\left[\frac{\beta_i(j+1)}{\beta_v(j)} + \exp\left(\frac{\delta G_j^0}{kT}\right)\right]\right\}, \tag{8.31}$$

and:

$$\ln\left(\frac{\rho'(n)}{\rho'(0)}\right) = \sum_{j=0}^{n-1} \left\{ -\ln\left[\frac{\beta_i(j+1)}{\beta_v(j)} + \exp\left(\frac{\delta G_j^0}{kT}\right)\right]\right\}. \tag{8.32}$$

We can identify two boundary conditions. The first is the quantity $\rho'(0)$, which may be evaluated by noting that as $\beta_i(n)/\beta_v(n) \rightarrow 0$, $\rho'(0) = \rho^0(0)$ and that $\rho^0(0) \rightarrow N_0$, which is simply the number of nucleation sites per unit volume. Since N_0 (and hence $\rho^{'}(0)$) is independent of void concentration, we can write:

$$\begin{aligned} \ln\left(\frac{\rho'(n)}{\rho'(0)}\right) &= \sum_{j=0}^{n-1} \left\{ -\ln\left[\frac{\beta_i(j+1)}{\beta_v(j)} + \exp\left(\frac{\delta G_j^0}{kT}\right)\right]\right\} \\ &= \frac{-\Delta G_n'}{kT}. \end{aligned} \tag{8.33}$$

Since as $\beta_i(n)/\beta_v(n) \rightarrow 0$, $\rho^{'}(0) \rightarrow \rho^0(0)$, and $\rho^0(0)$ is just N_0, the number of nucleation sites per unit volume, we have then:

$$\rho'(n) = N_0 \exp\left(\frac{-\Delta G_n'}{kT}\right), \tag{8.34}$$

and

ΔG_n^0 activation barrier without interstitials,
$\Delta G_n^{'}$ activation barrier with interstitials.

The upper curve in Fig. 8.3 shows $\Delta G_n^{'}$ as functions of n. Note that $\Delta G_n^{'}$ is larger than ΔG_k^0 and requires a larger void size due to the hindering effect of interstitials on the void nucleation process. The maxima in the two curves occur at n_k, ΔG_k^0 and $n_k^{'}$, $\Delta G_k^{'}$.

Now, the steady-state void nucleation rate may be calculated from the expression for J_n in Eq. (8.30):

$$J_k = Z' \beta_k \rho_k', \tag{8.35}$$

which is the rate at which voids escape over the potential barrier of height $\Delta G_k^{'}$ in units of [voids/cm^3 s]. The term β_k is the rate of single vacancy impingement on a void of size $n_k^{'}$. If clusters are assumed to be spherical, then the vacancy impingement rate is expressed by the rate constant for point defect absorption by spherical sinks, as in Eq. (5.84). Since void embryos are small, the capture rate is of

mixed-control type in which both diffusion and reaction rate limitations are of comparable magnitude:

$$\beta_{\mathrm{v}}(n) = \frac{4\pi R_{\mathrm{V}} D_{\mathrm{v}} C_{\mathrm{v}}}{1 + a/R_{\mathrm{V}}}, \tag{8.36}$$

where a is the lattice parameter, assuming that the rate at which vacancies leave a void depends on the size of the void but not on the concentration of vacancies or interstitials or details of the dynamics. Note that for large voids, $a/R_{\mathrm{V}} \rightarrow 0$ and $\beta_{\mathrm{v}}(n)$ has a pure diffusion character.

The term Z', analogous to Z but in the presence of interstitials, is:

$$Z' = \left[-\frac{1}{2\pi kT} \frac{\partial^2 \Delta G'_n}{\partial n^2} \right]^{1/2}_{n'_k}. \tag{8.37}$$

The subscript indicates that the second derivative is to be evaluated at $n = n'_k$. Its value is the width of $\Delta G'_k$ at kT units below the maximum and is in the order of 0.05. The second derivative is found from Eq. (8.25) to be:

$$\frac{1}{kT}\left(\frac{\partial^2 \Delta G'_n}{\partial n^2}\right)_{n'_k} = \left\{ \left[\frac{1}{kT} \frac{\partial^2 \Delta G^0_n}{\partial n^2} \right] \left[\exp\left(\frac{1}{kT} \frac{\partial \Delta G^0}{\partial n} \right) \right] \right\}_{n'_k}, \tag{8.38}$$

giving:

$$\rho'_k = N_0 \exp\left(-\Delta G'_k / kT\right), \tag{8.39}$$

where $\Delta G'_k$ is determined by evaluating Eq. (8.33) at n'_k.

Since the critical void nucleus size is taken as the maximum of the $\Delta G'_n$ curve, differentiating Eq. (8.17) and substituting the result into Eq. (8.33) permit evaluation of $\Delta G'_n$. The maximum in $\Delta G'_n$ is determined by setting $\partial \Delta G'_n / \partial n = 0$:

$$n'_k = \frac{32\pi\gamma^3\Omega^2}{3(k\mathrm{T})^3 \left[\ln\left(\dfrac{\beta_{\mathrm{v}}(n) - \beta_{\mathrm{i}}(n+1)}{\beta^0_{\mathrm{v}}(n)} \right) \right]^3}, \tag{8.40}$$

where $C_{\mathrm{v}}/C^0_{\mathrm{v}} = \beta_{\mathrm{v}}(n)/\beta^0_{\mathrm{v}}(n)$. Since $R_{\mathrm{V}} = \left(\dfrac{3}{4} \dfrac{n\Omega}{\pi} \right)^{1/3}$, the radius corresponding to n'_k is:

$$r'_k = \frac{2\gamma\Omega}{kT \ln\left[\left(\dfrac{\beta_{\mathrm{v}}(n) - \beta_{\mathrm{i}}(n+1)}{\beta^0_{\mathrm{v}}(n)} \right) \right]}. \tag{8.41}$$

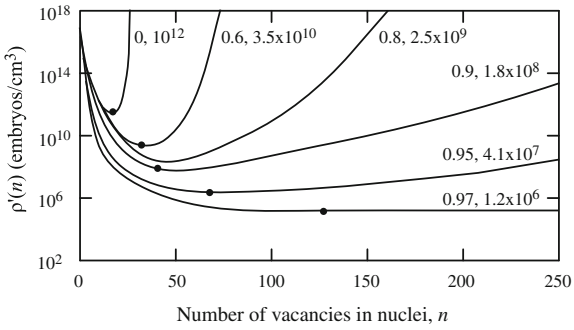

Fig. 8.5 Concentration of void embryos as a function of their size when the net flow of embryos is constrained to be zero. The parameters are the arrival rate ratios β_i/β_v and the nucleation rates (in s^{-1} cm^{-3}) of the unconstrained system. For this example, $T = 627$ °C and $S_v = 430$. *Solid circles* indicate the minima of $n(x)$ (after [8])

Note that as $\beta_i \rightarrow \beta_v$, $r_k' \rightarrow \infty$, which says that if the capture rate for vacancies and interstitials is the same, then the critical void embryo size would need to be ∞.

Figure 8.5 plots $\rho'(n)$ as a function of cluster size n for various values of β_i/β_v for $S_v = 430$ and $T = 627$ °C. Note the effect of increasing the interstitial arrival rate for a fixed vacancy arrival rate. With increasing arrival rate ratio, (β_i/β_v), the slope of the distribution, $d\rho/dn$, decreases everywhere. The reason is that increasing the interstitial flux increases the fraction of embryos of a given size n which actually shrink to the next smallest size $(n - 1)$, whereas to maintain the constrained distribution requires that the increased fraction be balanced by a decreased concentration of nuclei of size n relative to that of size $(n - 1)$.

Increasing the arrival rate ratio also shifts the minimum in the distribution $\rho'(n)$ to larger sizes and to lower concentrations. Since the nucleation rate is proportional to $\rho'(n)$, it decreases tremendously by the deepening and widening of the minimum in $\rho(n)$ as the arrival rate ratio increases. The nucleation rate in Fig. 8.5 decreases about 6 orders of magnitude as the arrival rate ratio is increased from 0 to 0.97.

To obtain void nucleation as β_i/β_v approaches 1 requires higher vacancy supersaturation. The strong dependence of nucleation on vacancy supersaturation is affected only very slightly by the arrival rate ratio. Figure 8.6 shows that a factor of 10 increase in supersaturation causes the nucleation rate to increase from 1 to 10^{15} nuclei/cm^3/s at 627 °C.

The effect of temperature on the vacancy concentration, C^*, required to give a fixed nucleation rate is shown in Fig. 8.7 by the set of curves identified by the arrival rate ratios, β_i/β_v. Over most of the temperature range, C^* increases with

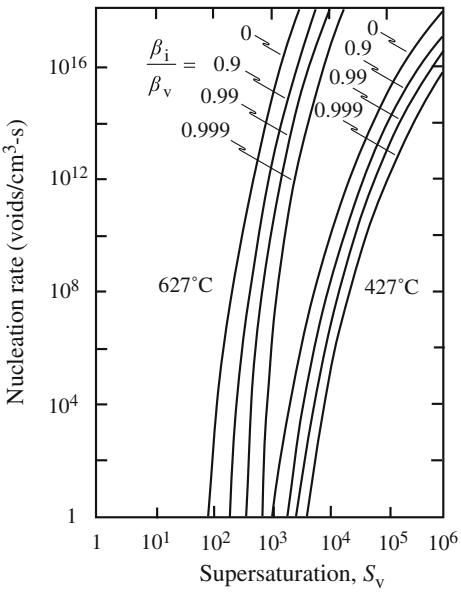

Fig. 8.6 Nucleation rate as a function of the vacancy supersaturation. The parameters are the arrival rate ratios, β_i/β_v, and the temperature (after [8])

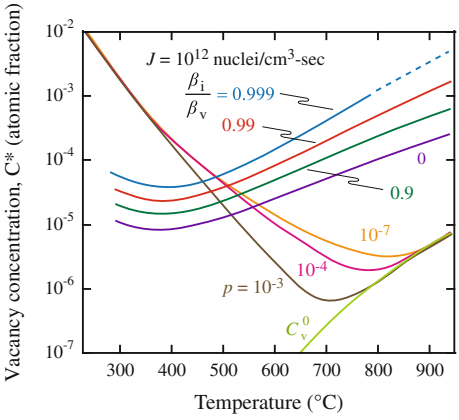

Fig. 8.7 Steady-state vacancy concentration, C^*, caused by a production rate of $K_0 = 10^{-3}$ atom fraction of defect pairs per second. The parameter p on the curves is the probability per jump that a defect is annihilated at existing sinks, such as dislocations. The curve labeled C_v^0 is the thermal equilibrium concentration of vacancies. The set of curves labeled by the arrival rate ratio, β_i/β_v, indicates the vacancy concentration required to give a nucleation rate of 10^{12} void nuclei/cm^{3}s. This nucleation rate is obtained at the temperature and vacancy concentration at the intersection of the curves under the conditions characterized by the curve parameters. The nucleation rate will be higher (*lower*) at temperatures below (*above*) the intersection temperature at fixed values of the parameters (after [8])

temperature even though the supersaturation $S_v = C_v/C_v^0$ decreases. Note that C_v is high at low temperature where the diffusion coefficient is small and there is not much loss. C_v is small at intermediate temperature where annihilation and loss to sinks are great. But C_v is high again at high temperature where $C_v^0 \sim C_v$. The parameter p is the probability per defect jump that the defect is annihilated at a sink. The values of p range from 10^{-7}, typical of an annealed metal to 10^{-3}, which is typical of a heavily cold-worked metal.

Figure 8.8 gives the steady-state vacancy concentrations for several defect production rates K_0 and several nucleation rates J and for a sink-annihilation probability of 10^{-7} and an arrival rate ratio of 0.99. The intersection of the defect production rate and the nucleation rate provides the vacancy concentration at the temperature of the intersection. Higher vacancy production rates promote greater vacancy concentration and a higher nucleation rate.

In summary, the void nucleation rate is a function of the height of the activation barrier. Inclusion of interstitials raises the activation barrier and reduces the nucleation rate. The critical void size radius for survival and growth as a void is a function of the activation barrier height with greater heights requiring larger critical void sizes. Nucleation rate is strongly increased by vacancy supersaturation and a reduced interstitial-to-vacancy arrival rate ratio.

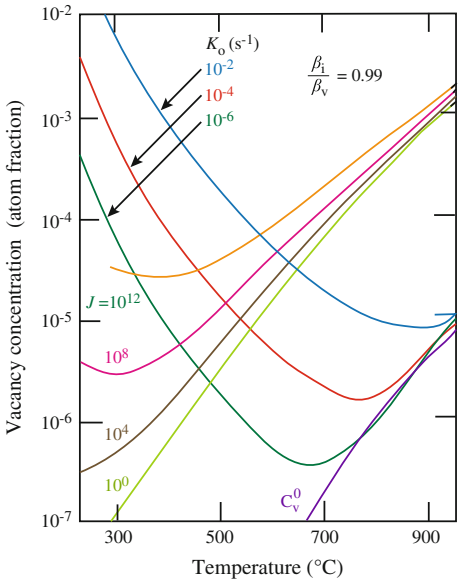

Fig. 8.8 Steady-state vacancy concentrations for several defect production rates and a sink annihilation probability $p = 10^{-7}$ and vacancy concentrations required for several nucleation rates J (in cm^{-3} s^{-1}) at an arrival rate ratio of 0.99. Such nucleation rates are obtained at the indicated defect production rates at the temperature where the curves intersect (after [8])

8.1.3 *Effect of Inert Gas*

Up to this point, we have assumed that a supersaturation of vacancies was sufficient to create a void embryo. It is well known that inert gas atoms may act to stabilize a void embryo and assist in the nucleation process. In fact, there is evidence to suggest that gas atoms are *always* involved in the void nucleation process [6–10]. Hence, several theories have been proposed that involve void nucleation in the presence of inert and non-inert gases [9, 11]. Here, we will consider a simple treatment [4, 9] of an immobile, inert gas, which is just an extension of the theory already developed. We will focus on helium since it is commonly produced by transmutation reactions in core structural materials.

Helium is very immobile compared to vacancies or interstitials in the temperature range of void formation. Once helium is trapped by a void embryo, its return to the matrix is very unlikely. Therefore, nucleation in the presence of helium does not require us to consider the interaction between helium atoms, vacancies, and interstitials in the formation of a void embryo. We may analyze the problem instead, by treating the inert gas atoms as sites for the formation of void embryos by migration of the point defects. In essence, this is a form of heterogeneous void nucleation rather than the homogeneous process described in Sect. 8.1.2.

The phase space description of the gas-containing void behavior is similar to that given in Sect. 8.1.2 and in [6]. The void is assigned coordinates specifying its vacancy content (n) and the number of gas atoms it contains (x) (Fig. 8.9). The void moves in the $+n$ direction by capturing vacancies and in the opposite direction by either thermal emission of vacancies or capture of interstitials:

$$\dot{n} = \beta_{\mathrm{v}}^{0} n^{1/3} - \alpha_{\mathrm{v}} - \beta_{\mathrm{i}}^{0} n^{1/3}, \tag{8.42}$$

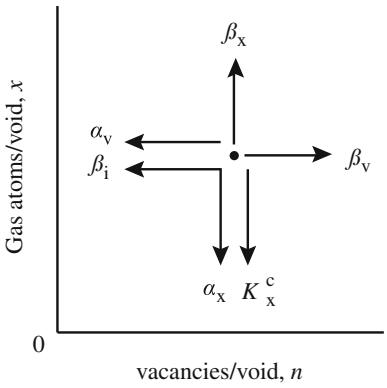

Fig. 8.9 Phase space for void nucleation showing movements of a void following point defect capture (β_i, β_v, β_x) or loss (α_v, α_x, K_x^c) (after [6])

where β_{v}^0 and β_{i}^0 are the arrival rates of vacancies and interstitials to the void, α_{v} is the emission rate of vacancies from the void, and the factor $n^{1/3}$ accounts for the dependence of the capture rate on the void size. Similarly, movement in the positive x-direction occurs by gas atom capture and in the opposite direction by resolution of gas atoms (return of the gas atom to the matrix due to knockout by irradiation) or by thermal emission of gas atoms:

$$\dot{x} = \beta_x^0 n^{1/3} - \alpha_x - xK_x^c, \tag{8.43}$$

where β_{x}^0 is the arrival rate of gas atoms, α_{x} is the emission rate of gas atoms, and $K_{\mathrm{x}}^{\mathrm{c}}$ is the rate of gas atom resolution.

For the case where the voids are in equilibrium with the vacancy and gas atom concentrations, the distribution of gas-filled void embryos containing n vacancies and x gas atoms is:

$$\rho^0(n,x) = N \exp\left(\frac{-\Delta G^0(n,x)}{kT}\right), \tag{8.44}$$

where $\Delta G^0\,(n, x)$ is the free energy of formation of the gas-filled void, also referred to as an (n, x)-mer. For every $(n - 1, x)$-mer capturing a vacancy, a (n, x)-mer will emit a vacancy, and for every $(n, x - 1)$-mer capturing a gas atom, a (n, x)-mer will emit one. Then,

$$\rho^0(n-1,x)\beta_{\mathrm{v}}^0(n-1)^{1/3} = \rho^0(n,x)\alpha_{\mathrm{v}}(n,x), \tag{8.45}$$

and

$$\rho^0(n,x-1)\beta_x^0(x-1)^{1/3} = \rho^0(n,x)\alpha_x(n,x), \tag{8.46}$$

and substituting Eqs. (8.45) and (8.46) into Eq. (8.42) to eliminate $\alpha_{\mathrm{v}}(n, x)$ and $\alpha_x(n, x)$ gives:

$$\dot{n} = \beta_{\mathrm{v}}^0 n^{1/3}\left[1 - \frac{\beta_{\mathrm{i}}^0}{\beta_{\mathrm{v}}^0} - \exp\left(\frac{1}{kT}\frac{\partial \Delta G^0(n,x)}{\partial n}\right)\right] \tag{8.47}$$

$$\dot{x} = \beta_x^0 n^{1/3}\left[1 - \frac{xK_x^c}{\beta_x^0 n^{1/3}} - \exp\left(\frac{1}{kT}\frac{\partial \Delta G^0(n,x)}{\partial x}\right)\right], \tag{8.48}$$

which are the velocities of the void in (n, x) phase space. However, we are interested in the nucleation rate, which requires more development and is described in detail in [4].

We start with a distribution of gas atom clusters, M_x, which is the number of gas atom clusters per unit volume composed of x gas atoms. The total helium concentration in the solid is:

$$M = \sum_{x=1} xM_x, \tag{8.49}$$

and is determined by the helium production rate due to transmutation reactions. We assume that nucleation of voids occurs independently and simultaneously on each of the gas atom clusters characterized by M_x nucleation sites per unit volume. Nucleation is driven by the vacancy and interstitial supersaturation. In addition to heterogeneous nucleation at gas cluster sites, homogenous nucleation is assumed to occur also on the N_0 lattice sites in the solid. The total nucleation rate is the sum of the contributions of the homogeneous and heterogeneous nucleation rates:

$$J = J_{\text{hom}} + \sum_{x=1} J_x, \tag{8.50}$$

where J_{hom} is given by Eq. (8.35). In order to obtain the total nucleation rate, we need to determine the heterogeneous nucleation rate J_x on the M_x gas cluster sites.

The distribution of helium void embryos containing n vacancies and x gas atoms, $\rho^0(n, x)$, is governed by the reaction:

$$n\text{v} = \text{v}_{nx}, \tag{8.51}$$

where v_{nx} denotes a void consisting of n vacancies and x gas atoms. Since helium is immobile, there is no chemical reaction expressing the equilibration of gas atoms between the voids and the bulk. The criterion of chemical equilibrium is then:

$$n\mu_{\text{v}} = \mu_{nx}, \tag{8.52}$$

and the chemical potential of a void with n vacancies and x gas atoms is:

$$\mu_{nx} = \frac{\partial G}{\partial \rho^0(n,x)}. \tag{8.53}$$

The formulation of the total Gibbs free energy for the gas–vacancy cluster is similar to the analysis presented earlier for vacancies alone. Analogous to Eq. (8.2) for voids, the total Gibbs free energy is:

$$G = G_0 + \sum_x \sum_n \left[\rho^0(n,x)G_{nx} - kT \ln w_{nx}\right]. \tag{8.54}$$

As before, w_{nx} *is* the number of ways of arranging ρ^0 $(n\ x)$ voids on M_i sites:

$$w_{nx} = \frac{M_x(M_x-1)\ldots\{M_x-[\rho^0(n,x)-1]\}}{[\rho^0(n,x)]!} = \frac{M_x!}{[M_x-\rho^0(n,x)]![\rho^0(n,x)]!}. \quad (8.55)$$

Using Eq. (8.55) in Eq. (8.54) and using Eq. (8.54) to determine the chemical potential as given in Eq. (8.53) yield:

$$\mu_{nx} = G_{nx} + kT\ln\left[\frac{\rho^0(n,x)}{M_x}\right]. \quad (8.56)$$

The reversible work to form a void embryo from n vacancies and x gas atoms is [4, 12]:

$$G_{nx} = \left(36\pi\Omega^2\right)^{1/3}\gamma n^{2/3} - xkT\ln\left(\frac{MHn\Omega}{xkT}\right). \quad (8.57)$$

The first term is the work to create a gas-free void consisting of n vacancies and is the same as that given in Eq. (8.6) for void formation. The second term is work to move the helium from the solid into the void. H in the second term is the Henry's law constant for the dissolution of helium in the metal. The expression for G_{nx} in Eq. (8.57) is substituted into the expression for the chemical potential of a void with n vacancies and x gas atoms, as in Eq. (8.56). Using the equality in Eq. (8.52) with μ_v given by Eq. (8.12) and solving for ρ^0 (n, x) give:

$$\rho^0(n,x) = M_x\exp\left[n\ln S_v - \xi n^{2/3} + x\ln\left(\frac{MHn\Omega}{xkT}\right)\right], \quad (8.58)$$

which is identical to Eq. (8.14) except for the extra term in the exponent and the pre-exponential factor. In fact, for $x = 0$ and $M_x = N_0$, the result reduces to Eq. (8.14).

Using Eq. (8.44) with M_x substituted for N_0 gives:

$$\Delta G^0(n,x) = -nkT\ln S_v + \left(36\pi\Omega^2\right)^{1/3}\gamma n^{2/3} - xkT\ln\left(\frac{MHn\Omega}{xkT}\right). \quad (8.59)$$

Figure 8.10 shows the free energy of void formation as a function of n and x. The intercept of this surface at $x = 0$ (no gas) corresponds to the $\beta_i/\beta_v = 0$ curve in Fig. 8.5 in which ρ' is plotted as a function of n in Eq. (8.34), $\rho'(n) = N_0\exp(-\Delta G_k'/kT)$, and for $\beta_i/\beta_v = 0$, then $\Delta G_n' = \Delta G(n, x = 0)$. Note that gas atoms in the void reduce the energy barrier for nucleation below that value characteristic of gas-free voids. The saddle point on the surface shown in Fig. 8.10 occurs at $n = 11$ and $x = 6$. The plot, however, does *not* include interstitials (as would a plot of $\Delta G_n'$), which are included in the analysis in exactly the same manner as in the case of homogeneous nucleation.

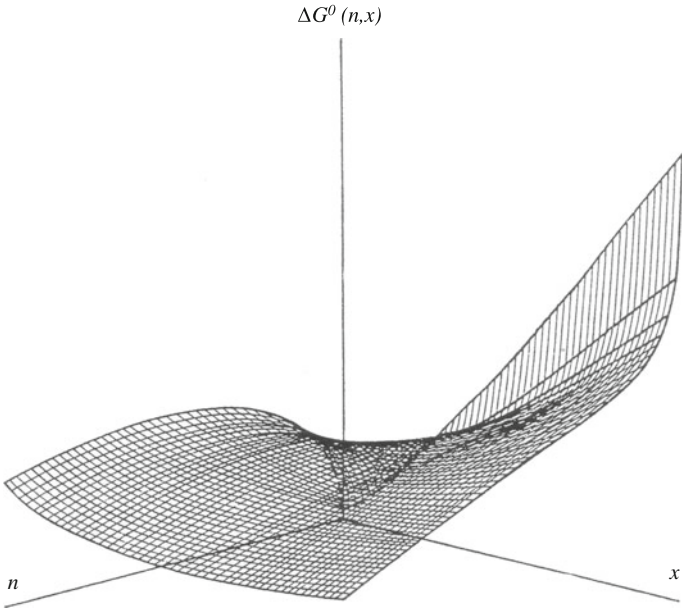

Fig. 8.10 Plot of the free energy of void formation as a function of the number of vacancies (n) and the number of gas atoms (x) in the void. Conditions are as follows: S_v = 600, p_0 = 507 MPa, T = 500 °C, γ = 1 J/m^2 (after [12])

The determination of the nucleation rate is done in the same manner as for homogeneous nucleation, resulting in a nucleation current:

$$J_{k,x} = Z'_x \beta_{kx} \rho'_k(n,x), \tag{8.60}$$

where

$$Z'_x = \left[\frac{-1}{2\pi kT}\frac{\partial^2 \Delta G'(n,x)}{\partial n^2}\right]^{1/2}_{n=n_k}, \tag{8.61}$$

$$\rho'(n,x) = M_x \exp(-\Delta G'(n,x)/kT), \tag{8.62}$$

and

$$\Delta G'(n,x) = kT \sum_{x=0}^{n} \left[\ln\left(\frac{\beta_i^0}{\beta_v^0}\right) + \exp\left(\frac{1}{kT}\frac{\partial \Delta G^0(n,x)}{\partial n}\right)\right], \tag{8.63}$$

and the values of Z'_k and $\rho'(n_k, x)$ are evaluated at the critical void size, n_k, and β_{kx} is the rate of impingement of vacancies on a critical size void.

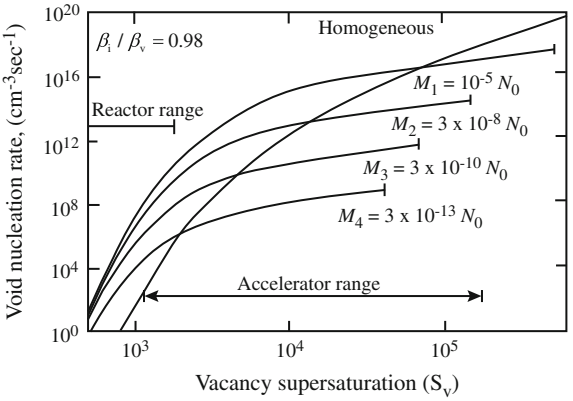

Fig. 8.11 Void nucleation rates (J) on helium atom clusters and the homogeneous nucleation rate (J_{hom}) as functions of vacancy supersaturation at 500 °C. Total helium content of 10 ppm (after [13])

To determine the nucleation rate on the gas atom clusters in the metal, we must estimate the distribution of the available gas (M atoms/cm^3) among the various cluster sizes. For simplicity, the distribution $M_x = M_1^{-(x+1)}$ is assumed. This distribution must satisfy Eq. (8.49). Figure 8.11 shows the results of calculations based on Eqs. (8.60) to (8.62) for M equivalent to 10 ppm helium (equivalent to the amount of helium expected in stainless steel cladding after a fluence of 5×10^{22}n/cm^2). Note that in the regime of vacancy supersaturation expected in a reactor, heterogeneous nucleation on helium atom clusters far outweighs homogeneous nucleation. This behavior constitutes theoretical confirmation of the often-observed enhancement of void nucleation of helium. The relative importance of homogeneous and heterogeneous nucleation shifts according to the helium concentration because $J_{hom}(n)$ is proportional to N_0, whereas $J_x\ (n)$ is proportional to M_x. At low fluence, homogeneous nucleation is dominant because there is not enough helium to drive heterogeneous nucleation. However, since J_{hom} is quite low, no voids are observed until sufficient helium has been generated by transmutation reactions to give the high heterogeneous nucleation rate. This incubation time is physically the relaxation time for the approach to steady state after a step increase in supersaturation. For void formation with or without the presence of gas:

$$\tau = \left(2\beta_k Z_k'\right)^{-1}. \tag{8.64}$$

This value is equivalent to a fluence of 10^{22} n/cm^2 for fast reactor irradiation conditions.

In summary, the effect of gas atoms is to substantially increase the void nucleation rate by lowering the critical radius for a stable void embryo below that for a gas-free void. Therefore, gas atom introduction into the lattice (either by transmutation or by accelerator injection) promotes the formation of voids relative to the pristine lattice.

8.1.4 Void Nucleation with Production Bias

The evolution of dislocation loops under cascade damage conditions was discussed in Sects. 7.5 and 7.6.2 for interstitial clusters. We can use the same treatment to develop a formulation specific to void nucleation [14]. Given that the number of vacancies in a spherical void can be written as:

$$\frac{\mathrm{d}n_\mathrm{v}}{\mathrm{d}t} = \frac{3n_\mathrm{v}^{1/3}}{a^2}\left[D_\mathrm{v}C_\mathrm{v} - D_\mathrm{i}C_\mathrm{i} - D_\mathrm{v}C_\mathrm{v}^0\right] \tag{8.65}$$

$$C_\mathrm{v}^\mathrm{V} = C_\mathrm{v}^0 \exp(2\gamma\Omega/kTR_\mathrm{V}), \tag{8.66}$$

where $a = (3\Omega/4\pi)^{1/3}$, n_v is the number of vacancies in a void, $R_\mathrm{V} = an_\mathrm{v}^{1/3}$, and Ω is the atomic volume, the drift velocity, $F(n)$ (from the Fokker–Planck treatment), is now a single term equal to the RHS of Eq. (8.65). The diffusive spread, described by the term $D(n)$, is a sum of contributions due to single defect jumps, cascades, and vacancy emission as:

$$D(n) = D^s(n) + D^c(n) + D^e(n), \tag{8.67}$$

where

$$D^s(n) = \frac{3n^{1/3}}{2a^2}\left[D_\mathrm{v}\left(C_\mathrm{v} - C_\mathrm{v}^0\right) + D_\mathrm{i}C_\mathrm{i}\right], \tag{8.68}$$

$$D^c(n) = \frac{3n^{2/3}}{4a}\left[\frac{K_\mathrm{v}^\mathrm{eff}\left\langle N_\mathrm{dv}^2\right\rangle}{k_\mathrm{v}N_\mathrm{dv}} + \frac{K_\mathrm{i}^\mathrm{eff}\left\langle N_\mathrm{di}^2\right\rangle}{k_\mathrm{i}N_\mathrm{di}}\right], \tag{8.69}$$

$$D^e(n) = \frac{9D_\mathrm{v}C_\mathrm{v}^0 n^{2/3}}{2a^2}, \tag{8.70}$$

and K_j^eff is the effective generation rate of free point defects, $N_{\mathrm{d}j}$ and $\left\langle N_{\mathrm{d}j}^2\right\rangle$ are the average number and the average square number of free point defects generated in a single cascade, respectively, and k_j^2 is the total sink strength for point defects of the type j. The solution to the general kinetic equation is similar to that for the case of interstitial clusters and is given in [14]. For the case of small critical vacancy size, the void nucleation probability, P_m, is:

$$P_m \cong \left[\frac{\beta}{6\pi R_{\mathrm{cr}} n_{\mathrm{cr}}} \frac{(D_{\mathrm{v}}C_{\mathrm{v}} - D_{\mathrm{i}}C_{\mathrm{i}})}{D_{\mathrm{i}}C_{\mathrm{i}}\left(1 + d n_{\mathrm{cr}}^{1/3}\right)} (n_0 - n_{\mathrm{v0}})\right]^{1/2} \times \exp\left(-\frac{\eta(\beta/R_{\mathrm{cr}}) n_{\mathrm{cr}}^{2/3} - n_0^{2/3}}{1 + 1/\left(d^e n_{\mathrm{cr}}^{1/3}\right) + d^c/d^e}\right), \tag{8.71}$$

where n_0 is the initial void embryo size (generally $\sim$4 vacancies), n_{v0} is a minimum size of a void embryo below which it is no longer a void (generally $\sim$2–3 vacancies), $d = d^{\mathrm{c}} + d^{\mathrm{e}}$, $\beta = 2\gamma\Omega/kT$, and R_{cr} and n_{cr} are the size and vacancy content of the critical size embryo. Assuming that production bias is the main driving force for void growth at elevated temperatures, the ratio $(D_{\mathrm{v}}C_{\mathrm{v}} - D_{\mathrm{i}}C_{\mathrm{i}})/D_{\mathrm{i}}C_{\mathrm{i}}$ is estimated as ε_{i}, the fraction of interstitials produced in cascades in the form of immobile clusters. The term R_{cr} is determined from Eqs. (8.65) and (8.66) under that condition that a void will grow if it receives a net vacancy flux ($D_{\mathrm{v}}C_{\mathrm{v}} > D_{\mathrm{i}}C_{\mathrm{i}}$):

$$R_{\mathrm{cr}} = \frac{\beta D_{\mathrm{v}} C_{\mathrm{v}}^{\mathrm{V}}}{D_{\mathrm{v}}C_{\mathrm{v}} - D_{\mathrm{i}}C_{\mathrm{i}} - D_{\mathrm{v}}C_{\mathrm{v}}^{\mathrm{V}}}, \tag{8.72}$$

and $R(n) = an^{1/3}$. The terms d^{c} and d^{e} are strengths of the diffusive spread for clusters and for vacancy emission relative to single point defects:

$$d^{\mathrm{c}} = \frac{D^{\mathrm{c}}(n_{\mathrm{cr}})}{n_{\mathrm{cr}}^{1/3} D^{\mathrm{s}}(n_{\mathrm{cr}})}, \quad d^{\mathrm{e}} = \frac{D^{\mathrm{e}}(n_{\mathrm{cr}})}{n_{\mathrm{cr}}^{1/3} D^{\mathrm{s}}(n_{\mathrm{cr}})}, \tag{8.73}$$

and the function η has a value between 0.55 and 0.84.

Application of Eq. (8.71) for various values of d^{c} and d^{e} and for a void embryo size of 4 vacancies leads to nucleation probabilities in the range 10^{-6} to 10^{-4} for critical vacancy clusters of size ~100 vacancies (Fig. 8.12). The nucleation rate is then:

$$J \cong \frac{K_{\mathrm{cl}}^{\mathrm{eff}}}{N_{\mathrm{d}}} P_m, \tag{8.74}$$

where $K_{\mathrm{cl}}^{\mathrm{eff}}$ is the effective generation rate of point defects in cluster and free form, N_{d} is the average total number of point defects generated in a single cascade, and ε_{i} is the fraction of interstitials produced in cascades in the form of immobile clusters. Figure 8.13 shows the void nucleation rate calculated for annealed copper compared with experimental data at 250, 300, and 350 °C and different surface energies, γ_{s}, and for different values of d^{e}. In terms of void nuclei created $\mathrm{cm}^{-3}\ \mathrm{s}^{-1}$, the nucleation rate is in the range 10^{15} to 10^{18}, which is larger than what was predicted by conventional nucleation theory. Thus, the effect of production bias is to increase the nucleation rate.

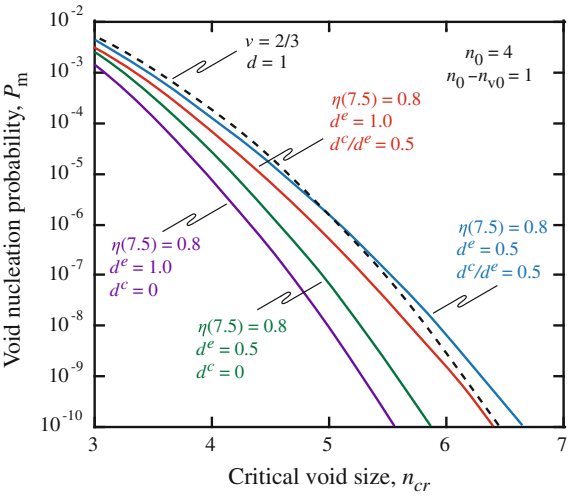

Fig. 8.12 Nucleation probability plotted from Eq. (8.71) for initial void size of four vacancies and minimum size of one vacancy and for different values of d^c and d^e versus the critical void size, n_{cr}. The term $\nu = \frac{(D_v C_v - D_i C_i)[1-\exp(-\beta/R_{cr})]}{D_i C_i}$ (after [14])

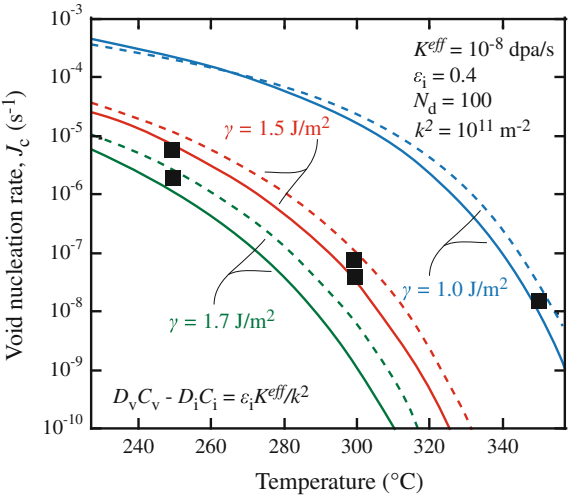

Fig. 8.13 Void nucleation rate versus irradiation temperature for the case of copper under a displacement rate of 10^{-8} dpa/s (after [14])

8.2 Treatment of Defect Sinks in the Growth of Voids

Having determined expressions for the rate at which voids are nucleated in the solid, we now turn to determining the rate at which the void nuclei grow into stable voids. As mentioned earlier, we will assume that the nucleation and growth stages are separated in time and that only after the void embryos are established does growth begin. Of course, this is a simplification of the true in-reactor situation in which the growth of stable nuclei is occurring simultaneously with nucleation.

Void growth is determined by solving the point defect balance equations developed in Chap. 5. These equations provide the vacancy and interstitial supersaturations that drive the nucleation and growth processes. The concentrations of vacancies and interstitials in the solid are determined by equating the rates of defect production and removal by all mechanisms. By doing so, the time derivatives are removed and the resulting solution has the form of a steady-state solution. However, since the defect concentrations are changing with time (dose), the *steady-state* solution is valid over only short time periods and is termed *quasi-steady state*. The quasi-steady-state solution has value because the changes in sink strength due to microstructure evolution are slow compared to the response time of the defect populations. So in essence, the problem can be solved by assuming an initial condition that properly characterizes the sink strengths, solving the point defect balance equations for those sink strengths, then updating the sink strengths, and iterating.

Rates of production and removal are assumed to be uniform throughout the metal. Clearly, strong gradients will exist close to the sink. But they can be neglected by *homogenizing* or *smearing* the sink strengths, that is, by replacing discrete sinks by spatially uniform absorbers of point defects so that the aggregate effect on defect absorption is the same in the homogenized sink case as in the heterogeneous sink case. The sink strengths are those described in Chap. 5. Void growth is then calculated according to rate theory as developed by Brailsford and Bullough [14] subject to the following simplifications:

1. Discrete sinks are replaced by a continuous or *smeared* distribution of sinks.
2. Each sink is given a *strength* so that the current of defects to the *smeared* sink is the same as the current to the actual sinks in the real material.
3. Steps 1 and 2 remove the spatial dependence of C_v and C_i, and the point defect balance equations become:

$$\begin{aligned} \frac{\partial C_v}{\partial t} &= K_0 - \sum_X A_v^X - R_{iv} \\ \frac{\partial C_i}{\partial t} &= K_0 - \sum_X A_i^X - R_{iv}, \end{aligned} \tag{8.75}$$

   where the first term on the right is the production rate of vacancies and interstitials, the second term is the loss rate to all sinks, X, and the last term is the loss rate due to vacancy–interstitial recombination.
4. Vacancy and interstitial concentrations, C_v and C_i, are calculated from Eq. (8.75). The change in sink strength due to the flow of defects to the sink is calculated, and the process, starting with Step 1, is iterated in order to advance in time and dose.

Reaction rate constants for defect–sink reactions and sink strengths for the relevant sinks were determined in Chap. 5 and summarized in Table 5.2. Recall that sinks are classified as neutral (voids, grain boundaries, incoherent precipitates), biased (dislocation network and dislocation loops), or variable biased (coherent precipitates

and over/undersized solutes). For all sink types, the defect absorption rate is proportional to the diffusion coefficient of the point defect and the difference in defect concentration between the bulk and the sink surface. With the exception of dislocation loops, the interstitial concentration at the sink surface is insignificant compared to the bulk value and may be neglected. In the case of vacancies, their concentration at the network dislocation core is maintained at the equilibrium concentration. For voids and loops, the vacancy concentration at the sink surfaces must also be determined. Once the sink strengths and the defect concentrations at the sink surfaces are all known, then we can determine the net absorption rate of defects by void nuclei and use this information to determine the growth rate of the voids.

8.2.1 Defect Absorption Rates and Concentrations at Sink Surfaces

We seek to determine expressions for the absorption rates of defects for each of the relevant sinks, categorized according to sink type. The general form of the absorption rate is:

$$A_j^X = k_X^2 D_j \left(C_j - C_j^X \right) = k_X^2 D_j C_j - L_j^X, \tag{8.76}$$

where A_j^X is the absorption rate of defect j by sink X, k_X^2 is the strength of sink X, D_j is the diffusion coefficient of defect j, C_j and C_j^X are the bulk concentration and sink surface concentration of defect j, respectively, and L_j^X is the thermal emission rate of defect j by sink X. Note that for neutral sinks, the sink strengths are dependent only on the character of the sink and not the defect. This is the advantage of writing the loss terms using sink strengths rather than reaction rate constants.

Neutral Sinks

The loss rate of point defects to voids can be written as:

$$\begin{aligned} A_\mathrm{v}^\mathrm{V} &= k_\mathrm{V}^2 D_\mathrm{v} \left(C_\mathrm{v} - C_\mathrm{v}^\mathrm{V} \right) = k_\mathrm{V}^2 D_\mathrm{v} C_\mathrm{v} - L_\mathrm{v}^\mathrm{V} \\ A_\mathrm{i}^\mathrm{V} &= k_\mathrm{V}^2 D_\mathrm{i} C_\mathrm{i}, \end{aligned} \tag{8.77}$$

where k_V^2 is the sink strength of a void given in Table 5.2, C_v^V is the vacancy concentration at the void surface, L_v^V is the thermal emission rate of vacancies at the sink surface, and all voids are assumed to be the same size. The loss rate of defects to incoherent precipitates is:

$$\begin{aligned} A_\mathrm{v}^\mathrm{IP} &= k_\mathrm{IP}^2 D_\mathrm{v} C_\mathrm{v} \\ A_\mathrm{i}^\mathrm{IP} &= k_\mathrm{IP}^2 D_\mathrm{i} C_\mathrm{i}, \end{aligned} \tag{8.78}$$

and to grain boundaries, the rate is:

$$\begin{aligned} A_{\mathrm{v}}^{\mathrm{gb}} &= k_{\mathrm{gb}}^2 D_{\mathrm{v}} C_{\mathrm{v}} \\ A_{\mathrm{i}}^{\mathrm{gb}} &= k_{\mathrm{gb}}^2 D_{\mathrm{i}} C_{\mathrm{i}}, \end{aligned} \tag{8.79}$$

where the sink strengths are given in Table 5.2, and thermal emission terms have been neglected.

Among Eqs. (8.77), (8.78), and (8.79), the term that is yet to be determined is the vacancy concentration at the void surface, $C_{\mathrm{v}}^{\mathrm{V}}$. This is done as follows. Recall from Eq. (4.15) that the thermal equilibrium concentration of vacancies in a solid is:

$$C_{\mathrm{v}}^0 = \frac{1}{\Omega} \exp\left(\frac{S_{\mathrm{f}}}{k}\right) \exp\left(\frac{-H_{\mathrm{f}}}{kT}\right),$$

where

$$H_{\mathrm{f}} = E_{\mathrm{f}} + p\Omega, \tag{8.80}$$

and the $p\Omega$ term was neglected for single vacancies embedded in the lattice. This simplification does not hold in the solid surrounding a void where forces such as surface tension, pressure due to gas in the void, or an external hydrostatic stress are acting. For example, the existence of a void surface produces a surface tension that can be determined, using Fig. 8.14, as follows:

$$\frac{\text{Force}}{\text{unit area}} = \frac{2\pi r\gamma \sin\theta}{A} \cong \frac{2\pi r\gamma}{\pi r^2}\theta = \frac{2\pi r\gamma}{\pi r^2}\left(\frac{r}{R}\right) = \frac{2\gamma}{R}, \tag{8.81}$$

where the approximation is that sin θ is replaced with θ for small θ. Hence, the p term in Eq. (8.80) becomes:

$$p = -\frac{2\gamma}{R}, \tag{8.82}$$

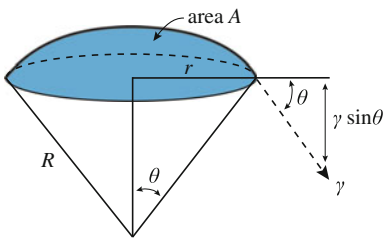

Fig. 8.14 Schematic of the surface tension on a void of radius R

where the minus sign enters because the surface tension acts in an inward direction to shrink the void. The vacancy concentration at the void surface then becomes:

$$C_{\mathrm{v}}^{\mathrm{V}} = \frac{1}{\Omega}\exp\left(\frac{S_{\mathrm{f}}}{k}\right)\exp\left(-\frac{E_{\mathrm{f}}}{kT}\right)\exp\left(-\frac{p\Omega}{kT}\right), \tag{8.83}$$

where

$$C_{\mathrm{v}}^{0} = \frac{1}{\Omega}\exp\left(\frac{S_{\mathrm{f}}}{k}\right)\exp\left(-\frac{E_{\mathrm{f}}}{kT}\right), \tag{8.84}$$

and substituting for $p\Omega$ from Eq. (8.82) gives:

$$C_{\mathrm{v}}^{\mathrm{V}} = C_{\mathrm{v}}^{0}\exp\left(\frac{2\gamma\Omega}{RkT}\right), \tag{8.85}$$

and Eq. (8.77) becomes:

$$A_{\mathrm{v}}^{\mathrm{V}} = k_{\mathrm{V}}^{2}D_{\mathrm{v}}\left[C_{\mathrm{v}} - C_{\mathrm{v}}^{0}\exp\left(\frac{2\gamma\Omega}{RkT}\right)\right]. \tag{8.86}$$

Biased Sinks

The defect loss rate to network dislocations is given by:

$$\begin{aligned} A_{\mathrm{v}}^{N} &= k_{\mathrm{vN}}^{2}D_{\mathrm{v}}\left(C_{\mathrm{v}} - C_{\mathrm{v}}^{0}\right) = k_{\mathrm{vN}}^{2}D_{\mathrm{v}}C_{\mathrm{v}} - L_{\mathrm{v}}^{N} \\ A_{\mathrm{i}}^{N} &= k_{\mathrm{iN}}^{2}D_{\mathrm{i}}C_{\mathrm{i}}, \end{aligned} \tag{8.87}$$

where the sink strengths are given in Table 5.2 and the term C_{v}^{0} is the thermal equilibrium concentration of vacancies. For interstitial dislocation loops, the loss term is:

$$\begin{aligned} A_{\mathrm{v}}^{\mathrm{L}} &= k_{\mathrm{vL}}^{2}D_{\mathrm{v}}\left(C_{\mathrm{v}} - C_{\mathrm{v}}^{\mathrm{L}}\right) = k_{\mathrm{vL}}^{2}D_{\mathrm{v}}C_{\mathrm{v}} - L_{\mathrm{v}}^{\mathrm{L}} \\ A_{\mathrm{i}}^{\mathrm{L}} &= k_{\mathrm{iL}}^{2}D_{\mathrm{i}}\left(C_{\mathrm{i}} - C_{\mathrm{i}}^{\mathrm{L}}\right) = k_{\mathrm{iL}}^{2}D_{\mathrm{i}}C_{\mathrm{i}} - L_{\mathrm{i}}^{\mathrm{L}}, \end{aligned} \tag{8.88}$$

where the sink strengths are the same as for network dislocations since the dislocation core is the same. However, the defect concentration at the sink surface is different from the thermal equilibrium value because addition of a vacancy or an interstitial to the dislocation loop contracts or expands, respectively, the size of the loop and this requires a change in energy. The concentration of vacancies and interstitials in equilibrium with a loop is $C_{\mathrm{v}}^{\mathrm{L}}$ and $C_{\mathrm{i}}^{\mathrm{L}}$, respectively. Following the analysis in [4], the defect concentration in equilibrium with the loop is determined

by considering the Gibbs free energy of a piece of metal containing n_v vacancies and n_i interstitials at concentrations C_v^L and C_i^L, and a single interstitial loop containing m_i interstitials:

$$G = G_0 + E_L(m_i) + n_v\mu_v + n_i\mu_i, \tag{8.89}$$

where G_0 is the free energy of solid without the loop but with C_v and C_i defects, $E_L(m_i)$ is the energy of the loop, and $\mu_{i,v}$ are the chemical potentials of interstitials and vacancies in the solid. For the system to be in chemical equilibrium, the transfer of point defects between the solid and the loop must cause no change in the free energy of the system:

$$\delta G = \left(\frac{dE_L}{dm_i}\right)\delta m_i + \mu_v\delta n_v + \mu_i\delta n_i = 0, \tag{8.90}$$

and

$$\delta m_i = \delta n_v - \delta n_i, \tag{8.91}$$

since the number of interstitials in the loop must come from the bulk. Eliminating δm_i from Eqs. (8.90) and (8.91) gives:

$$\left(\frac{dE_L}{dm_i}\right)\delta n_v - \left(\frac{dE_L}{dm_i}\right)\delta n_i + \mu_v\delta n_v + \mu_i\delta n_i = 0. \tag{8.92}$$

Since changes in vacancy and interstitial concentrations are arbitrary and independent of each other, the coefficients of both changes are set equal to zero, leading to:

$$\begin{aligned} \frac{dE_L}{dm_i} + \mu_v &= 0 \\ \frac{dE_L}{dm_i} - \mu_i &= 0. \end{aligned} \tag{8.93}$$

From Eq. (8.12), the chemical potential of vacancies and interstitials in a solid with concentrations C_v^L and C_i^L is:

$$\begin{aligned} \mu_v &= kT\ln\frac{C_v^L}{C_v^0} \\ \mu_i &= kT\ln\frac{C_i^L}{C_i^0}. \end{aligned} \tag{8.94}$$

For vacancies and interstitials in equilibrium,

$$C_{\mathrm{v}}^{\mathrm{L}} C_{\mathrm{i}}^{\mathrm{L}} = C_{\mathrm{v}}^{0} C_{\mathrm{i}}^{0}, \tag{8.95}$$

or from Eq. (8.93):

$$\mu_{\mathrm{v}} = -\mu_{\mathrm{i}}. \tag{8.96}$$

Combining Eqs. (8.93) and (8.94) for vacancies and then for interstitials yields:

$$\begin{aligned} C_{\mathrm{v}}^{\mathrm{L}} &= C_{\mathrm{v}}^{0} \exp\left(-\frac{\mathrm{d}E_{\mathrm{L}}/\mathrm{d}m_{\mathrm{i}}}{kT}\right) \\ C_{\mathrm{i}}^{\mathrm{L}} &= C_{\mathrm{i}}^{0} \exp\left(\frac{\mathrm{d}E_{\mathrm{L}}/\mathrm{d}m_{\mathrm{i}}}{kT}\right). \end{aligned} \tag{8.97}$$

Using Eq. (7.62) for the energy of a Frank loop:

$$E_{\mathrm{L}} = 2\pi\mu b^2 \left(\frac{\sqrt{3}a^2 m_{\mathrm{i}}}{4\pi}\right)^{1/2} + \pi\left(\frac{\sqrt{3}a^2 m_{\mathrm{i}}}{4\pi}\right)\gamma_{\mathrm{SFE}},$$

and dropping the second term for simplicity, then $\mathrm{d}E_{\mathrm{L}}/\mathrm{d}m_{\mathrm{i}}$ becomes:

$$\frac{\mathrm{d}E_{\mathrm{L}}}{\mathrm{d}m_{\mathrm{i}}} = \frac{\Theta}{2\sqrt{m_{\mathrm{i}}}}, \tag{8.98}$$

where Θ is $2\pi\mu b^2 \left(\frac{\sqrt{3}a^2}{4\pi}\right)^{1/2}$. Substituting into Eq. (8.97) yields:

$$\begin{aligned} C_{\mathrm{v}}^{\mathrm{L}} &= C_{\mathrm{v}}^{0} \exp\left(-\frac{\Theta}{2\sqrt{m_{\mathrm{i}}}kT}\right) \\ C_{\mathrm{i}}^{\mathrm{L}} &= C_{\mathrm{i}}^{0} \exp\left(\frac{\Theta}{2\sqrt{m_{\mathrm{i}}}kT}\right). \end{aligned} \tag{8.99}$$

Note that the vacancy concentration in equilibrium with an interstitial loop is less than the equilibrium vacancy concentration in the solid, while the reverse is true for interstitials. The absorption rates of vacancies and interstitials at loops then become, from Eq. (8.88):

$$\begin{aligned} A_{\mathrm{v}}^{\mathrm{L}} &= z_{\mathrm{v}} D_{\mathrm{v}} \rho_{\mathrm{L}} \left[C_{\mathrm{v}} - C_{\mathrm{v}}^{0} \exp\left(-\frac{\Theta}{2\sqrt{m_{\mathrm{i}}}kT}\right)\right] \\ A_{\mathrm{i}}^{\mathrm{L}} &= z_{\mathrm{i}} D_{\mathrm{i}} \rho_{\mathrm{L}} \left[C_{\mathrm{i}} - C_{\mathrm{i}}^{0} \exp\left(\frac{\Theta}{2\sqrt{m_{\mathrm{i}}}kT}\right)\right]. \end{aligned} \tag{8.100}$$

Variable Biased Sinks

The sink strengths for variable biased sinks are given in Eq. (5.120) and are:

$$k_{\mathrm{vCP}}^2 = 4\pi R_{\mathrm{CP}} \rho_{\mathrm{CP}} Y_{\mathrm{v}}$$
$$k_{\mathrm{iCP}}^2 = 4\pi R_{\mathrm{CP}} \rho_{\mathrm{CP}} Y_{\mathrm{i}},$$

where $Y_{\mathrm{v,i}}$ are sink strengths for coherent precipitates for vacancies and interstitials and the loss rate of point defects to coherent precipitates is:

$$\begin{aligned} A_{\mathrm{v}}^{\mathrm{CP}} &= k_{\mathrm{vCP}}^2 D_{\mathrm{v}} C_{\mathrm{v}} = 4\pi R_{\mathrm{CP}} \rho_{\mathrm{CP}} C_{\mathrm{v}} Y_{\mathrm{v}} \\ A_{\mathrm{i}}^{\mathrm{CP}} &= k_{\mathrm{iCP}}^2 D_{\mathrm{i}} C_{\mathrm{i}} = 4\pi R_{\mathrm{CP}} \rho_{\mathrm{CP}} C_{\mathrm{i}} Y_{\mathrm{i}}. \end{aligned} \tag{8.101}$$

8.2.2 Point Defect Balances

Now that we have expressions for the absorption rates of defects for each type of sink, we can construct the steady-state, point defect balances for the solid under irradiation:

$$\begin{aligned} K_0 - \sum_X A_{\mathrm{v}}^X - R_{\mathrm{iv}} &= 0 \\ K_0 - \sum_X A_{\mathrm{i}}^X - R_{\mathrm{iv}} &= 0, \end{aligned} \tag{8.102}$$

and in the most general form:

$$\begin{aligned} K_0 - k_{\mathrm{v}}^2 D_{\mathrm{v}} \left(C_{\mathrm{v}} - C_{\mathrm{v}}^X \right) - K_{\mathrm{iv}} C_{\mathrm{v}} C_{\mathrm{i}} &= 0 \\ K_0 - k_{\mathrm{i}}^2 D_{\mathrm{i}} \left(C_{\mathrm{i}} - C_{\mathrm{i}}^X \right) - K_{\mathrm{iv}} C_{\mathrm{v}} C_{\mathrm{i}} &= 0, \end{aligned} \tag{8.103}$$

where k_{v}^2 and k_{i}^2 are the total sink strengths for vacancy and interstitial loss:

$$\begin{aligned} k_{\mathrm{v}}^2 &= k_{\mathrm{vV}}^2 + k_{\mathrm{vIP}}^2 + k_{\mathrm{vgb}}^2 + k_{\mathrm{vN}}^2 + k_{\mathrm{vL}}^2 + k_{\mathrm{vCP}}^2 \\ k_{\mathrm{i}}^2 &= k_{\mathrm{iV}}^2 + k_{\mathrm{iIP}}^2 + k_{\mathrm{igb}}^2 + k_{\mathrm{iN}}^2 + k_{\mathrm{iL}}^2 + k_{\mathrm{iCP}}^2, \end{aligned} \tag{8.104}$$

and the C_{v}^X and C_{i}^X are concentrations of vacancies and interstitials at the sink surface. Now, since defect production rates and recombination rates in Eq. (8.103) are equal and there is no net accumulation of point defects at coherent precipitates, then:

$$\sum_X A_{\mathrm{v}}^X = \sum_X A_{\mathrm{i}}^X, \tag{8.105}$$

or

$$A_{\mathrm{v}}^{\mathrm{V}} + A_{\mathrm{v}}^{\mathrm{IP}} + A_{\mathrm{v}}^{\mathrm{gb}} + A_{\mathrm{v}}^{N} + A_{\mathrm{v}}^{\mathrm{L}} + A_{\mathrm{v}}^{\mathrm{CP}} = A_{\mathrm{i}}^{\mathrm{V}} + A_{\mathrm{i}}^{\mathrm{IP}} + A_{\mathrm{i}}^{\mathrm{gb}} + A_{\mathrm{i}}^{N} + A_{\mathrm{i}}^{\mathrm{L}} + A_{i}^{\mathrm{CP}}, \quad (8.106)$$

and therefore,

$$\begin{aligned}&(k_{\mathrm{vV}}^2 + k_{\mathrm{vIP}}^2 + k_{\mathrm{vgb}}^2 + k_{\mathrm{vN}}^2 + k_{\mathrm{vL}}^2 + k_{\mathrm{vCP}}^2) D_{\mathrm{v}} C_{\mathrm{v}} - L_{\mathrm{v}}^{\mathrm{V}} - L_{\mathrm{v}}^{N} - L_{\mathrm{v}}^{\mathrm{L}} \\ &= (k_{\mathrm{iV}}^2 + k_{\mathrm{iIP}}^2 + k_{\mathrm{igb}}^2 + k_{\mathrm{iN}}^2 + k_{\mathrm{iL}}^2 + k_{\mathrm{iCP}}^2) D_{\mathrm{i}} C_{\mathrm{i}} - L_{\mathrm{i}}^{\mathrm{L}}.\end{aligned} \quad (8.107)$$

where the L terms are the thermal emission of the defect from the sink.

Substituting in for the expressions for sink strength and thermal emission from the respective equations in Chaps. 5 and 7 gives:

$$\begin{aligned}4\pi R_{\mathrm{V}} \rho_{\mathrm{V}} D_{\mathrm{v}} &\left[C_{\mathrm{v}} - C_{\mathrm{v}}^0 \exp\left(\frac{2\gamma\Omega}{RkT}\right)\right] + z_{\mathrm{v}} \rho_N D_{\mathrm{v}} (C_{\mathrm{v}} - C_{\mathrm{v}}^0) + 4\pi R_{\mathrm{CP}} \rho_{\mathrm{CP}} D_{\mathrm{v}} C_{\mathrm{v}} Y_{\mathrm{v}} \\ &+ z_{\mathrm{v}} \rho_{\mathrm{L}} D_{\mathrm{v}} \left[C_{\mathrm{v}} - C_{\mathrm{v}}^0 \exp\left(-\frac{\Theta}{2\sqrt{m_{\mathrm{i}} kT}}\right)\right] \\ &= \pi R_{\mathrm{V}} \rho_{\mathrm{V}} D_{\mathrm{i}} C_{\mathrm{i}} + z_{\mathrm{i}} \rho_{\mathrm{N}} D_{\mathrm{i}} C_{\mathrm{i}} + 4\pi R_{\mathrm{CP}} \rho_{\mathrm{CP}} D_i C_i Y_{\mathrm{i}} \\ &+ z_{\mathrm{i}} \rho_{\mathrm{L}} D_{\mathrm{i}} \left[C_{\mathrm{i}} - C_{\mathrm{i}}^0 \exp\left(\frac{\Theta}{2\sqrt{m_{\mathrm{i}} kT}}\right)\right],\end{aligned} \quad (8.108)$$

where terms for grain boundaries and incoherent precipitates are neglected for simplicity. Since the thermal equilibrium interstitial concentration, C_{i}^0, is extremely small, the thermal emission of interstitials from loops can be neglected.

8.3 Void Growth

Now that we have determined the absorption rate of defects for each sink in the solid, we focus on the void with the objective of developing an expression describing its rate of growth. The void growth equation has its origins in the net flux of vacancies to a void embryo. The *net* rate of absorption of vacancies by a void is:

$$A_{\mathrm{net}}^{\mathrm{V}} = A_{\mathrm{v}}^{\mathrm{V}} - A_{\mathrm{i}}^{\mathrm{V}} = 4\pi R D_{\mathrm{v}} (C_{\mathrm{v}} - C_{\mathrm{v}}^{\mathrm{V}}) - 4\pi R D_{\mathrm{i}} C_{\mathrm{i}}, \quad (8.109)$$

where

R is void radius (we have dropped the subscript V for simplicity)
$C_{\mathrm{v,i}}$ is vacancy/interstitial concentration in the solid
$C_{\mathrm{v}}^{\mathrm{V}}$ is vacancy concentration at the void surface, and thermal emission of interstitials from voids is neglected.

The rate of change in volume of the void is just the net absorption rate times the defect volume, Ω:

$$\frac{dV}{dt} = 4\pi R\Omega\left[D_v(C_v - C_v^V) - D_i C_i\right], \tag{8.110}$$

and since

$$V = \frac{4}{3}\pi R^3, \tag{8.111}$$

we obtain the common form of the void growth equation:

$$\frac{dR}{dt} = \dot{R} = \frac{\Omega}{R}\left[D_v(C_v - C_v^V) - D_i C_i\right]. \tag{8.112}$$

Our objective is to determine an expression for the void growth equation, which amounts to determining the values for C_v, C_i, and C_v^V. The general solution procedure is thus to solve the point defect balance equations in Eq. (8.75) for C_v and C_i at some initial value of the void radius, R_0, and then to use those values of C_v and C_i in Eq. (8.112) to increment the void size from R_0 to R'. Since sink strength changes with void size, updated values of C_v and C_i must be obtained for the next void growth increment. The process is then iterated to describe the change in void size with time or dose. This process can be carried out numerically and with small time steps in order to minimize the time increment over which the sink strengths are assumed to be constant. In solving for void size in this way, changes to the microstructure can also be incorporated at the time step boundaries.

While a numerical solution of the void growth equation will produce the most accurate result, it provides no insight into the governing processes during void growth. Brailsford and Bullough [15] inserted the solution of Eq. (8.75) into Eq. (8.112) to obtain an approximate analytical result that provides an excellent tool for understanding the parameters governing void growth. Mansur [5, 16] advanced the analysis to develop expressions for the dependence on critical parameters affecting void growth. We begin by returning to the point defect balance equations at steady state in order to determine the bulk concentrations of vacancies and interstitials, C_v and C_i. Setting the time rate of change of the vacancy and interstitial concentrations equal to zero in Eq. (8.75) gives:

$$\begin{aligned} K_0 - \sum_X A_v^X - R_{iv} &= 0 \\ K_0 - \sum_X A_i^X - R_{iv} &= 0, \end{aligned} \tag{8.113}$$

or

$$\begin{aligned} K_0 - K_{\mathrm{iv}} C_{\mathrm{i}} C_{\mathrm{v}} - K_{\mathrm{vs}} C_{\mathrm{v}} C_{\mathrm{s}} &= 0 \\ K_0 - K_{\mathrm{iv}} C_{\mathrm{i}} C_{\mathrm{v}} - K_{\mathrm{is}} C_{\mathrm{i}} C_{\mathrm{s}} &= 0, \end{aligned} \tag{8.114}$$

with solutions:

$$\begin{aligned} C_{\mathrm{v}} &= \frac{-K_{\mathrm{is}} C_{\mathrm{s}}}{2K_{\mathrm{iv}}} + \left[\frac{K_0 K_{is}}{K_{\mathrm{iv}} K_{\mathrm{vs}}} + \frac{K_{is}^2 C_{\mathrm{s}}^2}{4K_{\mathrm{iv}}} \right]^{1/2} \\ C_{\mathrm{i}} &= \frac{-K_{\mathrm{vs}} C_{\mathrm{s}}}{2K_{\mathrm{iv}}} + \left[\frac{K_0 K_{\mathrm{vs}}}{K_{\mathrm{iv}} K_{is}} + \frac{K_{\mathrm{vs}}^2 C_{\mathrm{s}}^2}{4K_{\mathrm{iv}}} \right]^{1/2}, \end{aligned} \tag{8.115}$$

where C_{s} is the sink concentration. Using Table 5.2 to write the reaction rate constants for vacancies and interstitials at sinks as sink strengths gives:

$$\begin{aligned} C_{\mathrm{v}} &= \frac{-k_{\mathrm{i}}^2 D_{\mathrm{i}}}{2K_{\mathrm{iv}}} + \left[\frac{K_0 k_{\mathrm{i}}^2 D_{\mathrm{i}}}{K_{\mathrm{iv}} k_{\mathrm{v}}^2 D_{\mathrm{v}}} + \frac{(k_{\mathrm{i}}^2)^2 D_{\mathrm{i}}^2}{4K_{\mathrm{iv}}} \right]^{1/2} \\ C_{\mathrm{i}} &= \frac{-k_{\mathrm{v}}^2 D_{\mathrm{v}}}{2K_{\mathrm{iv}}} + \left[\frac{K_0 k_{\mathrm{v}}^2 D_{\mathrm{v}}}{K_{\mathrm{iv}} k_i^2 D_{\mathrm{i}}} + \frac{(k_{\mathrm{v}}^2)^2 D_{\mathrm{i}}^2}{4K_{\mathrm{iv}}} \right]^{1/2}. \end{aligned} \tag{8.116}$$

Defining:

$$\eta = \frac{4K_{\mathrm{iv}} K_0}{D_{\mathrm{i}} D_{\mathrm{v}} k_{\mathrm{v}}^2 k_{\mathrm{i}}^2}, \tag{8.117}$$

and

$$\begin{aligned} k_{\mathrm{v}}^2 &= z_{\mathrm{v}} \rho_{\mathrm{d}} + 4\pi R \rho_{\mathrm{V}} + 4\pi R_{\mathrm{CP}} \rho_{\mathrm{CP}} \\ k_{\mathrm{i}}^2 &= z_{\mathrm{i}} \rho_{\mathrm{d}} + 4\pi R \rho_{\mathrm{V}} + 4\pi R_{\mathrm{CP}} \rho_{\mathrm{CP}}, \end{aligned} \tag{8.118}$$

where, for simplicity, we have neglected grain boundaries, incoherent precipitates and bias factors on voids and coherent precipitates, and the network dislocations and dislocation loops are represented by a single term with density $\rho_{\mathrm{d}} = \rho_{\mathrm{N}} + \rho_{\mathrm{L}}$. Using Eqs. (8.117) and (8.118), then Eq. (8.116) can be written as:

$$\begin{aligned} C_{\mathrm{v}} &= \frac{D_{\mathrm{i}} k_{\mathrm{i}}^2}{2K_{\mathrm{iv}}} \left[(\eta + 1)^{1/2} - 1 \right] \\ C_{\mathrm{i}} &= \frac{D_{\mathrm{v}} k_{\mathrm{v}}^2}{2K_{\mathrm{iv}}} \left[(\eta + 1)^{1/2} - 1 \right]. \end{aligned} \tag{8.119}$$

The void growth rate from Eq. (8.112) can be written in the form:

$$\dot{R} = \dot{R}_0 X(\eta), \tag{8.120}$$

where

$$\dot{R}_0 = \frac{\dfrac{K_0(z_i - z_v)\rho_d \Omega}{R(z_v\rho_d + 4\pi R\rho_V)}}{z_i\rho_d + 4\pi R\rho_V + 4\pi R_{CP}\rho_{CP}\left[1 + \dfrac{(z_i - z_v)\rho_d}{z_v\rho_d + 4\pi R\rho_V}\right]}. \tag{8.121}$$

Equation (8.121) can be simplified by dropping the last term in the square brackets in the denominator, since the difference $(z_i - z_v)$ is small, giving:

$$\dot{R}_0 = \frac{K_0(z_i - z_v)\rho_d \Omega}{R(z_v\rho_d + 4\pi R\rho_V)(z_i\rho_d + 4\pi R\rho_V + 4\pi R_{CP}\rho_{CP})}. \tag{8.122}$$

This growth term is independent of temperature and is proportional to the dislocation bias for interstitials $(z_i - z_v)$ and the defect production rate. Note that $\dot{R}_0$ is:

- Independent of temperature;
- Proportional to the dislocation bias $(z_i - z_v)$;
- Proportional to the defect production rate, K_0.

The term $X(\eta)$ is given by:

$$X(\eta) = F(\eta) - 2\zeta, \tag{8.123}$$

where

$$F(\eta) = \frac{2}{\eta}\left[(\eta + 1)^{1/2} - 1\right], \tag{8.124}$$

and η is a dimensionless parameter defined in Eq. (8.117). Substituting Eq. (8.123) into Eq. (8.120) gives:

$$\dot{R} = \dot{R}_0 F(\eta) - 2\dot{R}_0\zeta. \tag{8.125}$$

The quantity η in the function $F(\eta)$ can be simplified by substituting in for k_v^2 and k_i^2 from Eq. (8.104) (or Table 5.2), giving:

$$\eta = \frac{4K_{iv}K_0}{D_i D_v(z_i\rho_d + 4\pi R\rho_V + 4\pi R_{CP}\rho_{CP})(z_v\rho_d + 4\pi R\rho_V + 4\pi R_{CP}\rho_{CP})}. \tag{8.126}$$

Using the approximation that $z_i \cong z_v$ and eliminating K_{iv} by using Eq. (5.61) gives:

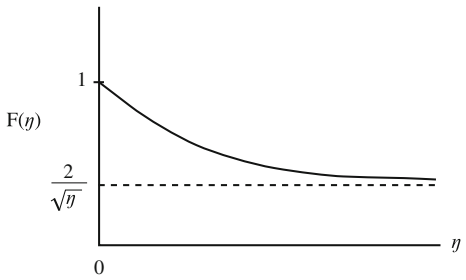

Fig. 8.15 The behavior of $F(\eta)$ in Eq. (8.124) as a function of η

$$\eta = \frac{4z_{iv}K_0\Omega}{D_v a^2(z\rho_d + 4\pi R\rho_V + 4\pi R_{CP}\rho_{CP})^2}. \tag{8.127}$$

The expression for η is substituted into Eq. (8.124) to obtain an expression for $F(\eta)$. This function describes the effect of homogeneous recombination on void growth (Fig. 8.15). When recombination is negligible, $K_{iv} \to 0$ and $\eta \to 0$, and $F \to 1$, or $\lim_{\eta \to 0} F(\eta) = 1$.

Turning now to the second term in Eq. (8.125), we define for simplicity:

$$\dot{R}_{th} = -2\dot{R}_0\zeta, \tag{8.128}$$

so that Eq. (8.125) can now be written as:

$$\dot{R} = \dot{R}_0 F(\eta) + \dot{R}_{th}, \tag{8.129}$$

The term ζ is a function of temperature and is expressed as:

$$\begin{aligned}\zeta = \zeta(T) = {} & \frac{D_v(z_v\rho_d + 4\pi R\rho_v)[z_i\rho_d + 4\pi(R\rho_V + R_{CP}\rho_{CP})]}{2K_0(z_i - z_v)[z_v\rho_d + 4\pi(R\rho_V + R_{CP}\rho_{CP})]} \\ & \times [4\pi R_{CP}\rho_{CP}C_v^V + z_v\{\rho_N(C_v^V - C_v^0) + \rho_L(C_v^V - C_v^L)\}].\end{aligned} \tag{8.130}$$

so that:

$$\begin{aligned}\dot{R}_{th} = -2\dot{R}_0\zeta = {} & \frac{-2D_v(z_v\rho_d + 4\pi R\rho_V)[z_i\rho_d + 4\pi(R\rho_V + R_{CP}\rho_{CP})]}{2K_0(z_i - z_v)\rho_d[z_v\rho_d + 4\pi(R\rho_V + R_{CP}\rho_{CP})]} \\ & \times \frac{\dfrac{K_0(z_i - z_v)\rho_d\Omega}{R(z_v\rho_d + 4\pi R\rho_V)}}{z_i\rho_d + 4\pi R\rho_V + 4\pi R_{CP}\rho_{CP}\left[1 + \dfrac{(z_i - z_v)\rho_d}{z_v\rho_d + 4\pi R\rho_V}\right]} \\ & \times [4\pi R_{CP}\rho_{CP}C_v^V + z_v[\rho_N(C_v^V - C_v^0) + \rho_L(C_v^V - C_v^L)]].\end{aligned} \tag{8.131}$$

By approximating $z_i \cong z_v$, numerous terms in Eq. (8.131) cancel, leaving:

$$\dot{R}_{th} = \frac{-D_v \Omega}{R(z_i \rho_d + 4\pi R \rho_V + 4\pi R_{CP} \rho_{CP})} \times \left[4\pi R_{CP} \rho_{CP} C_v^V + z_v \left[\rho_N (C_v^V - C_v^0) + \rho_L (C_v^V - C_v^L)\right]\right]. \tag{8.132}$$

Substituting in for C_v^V and C_v^L from Eqs. (8.85) and (8.99), respectively, gives:

$$\dot{R}_{th} = \frac{-D_v \Omega}{R(z_i \rho_d + 4\pi R \rho_V + 4\pi R_{CP} \rho_{CP})} \times \left[4\pi R_{CP} \rho_{CP} C_v^0 \exp\left(\frac{2\gamma\Omega}{RkT}\right) + z_v \left[\rho_N \left(C_v^0 \exp\left(\frac{2\gamma\Omega}{RkT}\right) - C_v^0\right) + \rho_L \left(C_v^0 \exp\left(\frac{2\gamma\Omega}{RkT}\right) - C_v^0 \exp\left(-\frac{\Theta}{2\sqrt{m_i kT}}\right)\right)\right]\right]. \tag{8.133}$$

Approximating $\exp(x) \sim x + 1$ for small x in all but the first of the exponential terms of Eq. (8.133) gives:

$$\dot{R}_{th} = \frac{-D_v \Omega}{R(z_i \rho_d + 4\pi R \rho_V + 4\pi R_{CP} \rho_{CP})} \times \left[4\pi R_{CP} \rho_{CP} C_v^0 \exp\left(\frac{2\gamma\Omega}{RkT}\right) + z_v C_v^0 \left[\rho_N \frac{2\gamma\Omega}{RkT} + \rho_L \left(\frac{2\gamma\Omega}{RkT} + \frac{\Theta}{2\sqrt{m_i kT}}\right)\right]\right], \tag{8.134}$$

and pulling the term C_v^0 out into the coefficient yields:

$$\dot{R}_{th} = \frac{-D_v \Omega C_v^0}{R(z_i \rho_d + 4\pi R \rho_V + 4\pi R_{CP} \rho_{CP})} \times \left[4\pi R_{CP} \rho_{CP} \exp\left(\frac{2\gamma\Omega}{RkT}\right) + z_v \rho_N \frac{2\gamma\Omega}{RkT} + z_v \rho_L \left(\frac{2\gamma\Omega}{RkT} + \frac{\theta}{2\sqrt{m_i kT}}\right)\right], \tag{8.135}$$

which is the simplified expression for the thermal emission term. This term represents the thermal emission of defects from sinks. It is independent of defect production rate and is strongly temperature dependent. Note that at very low temperature, $\dot{R}_{th} \to 0$, because of the terms D_v and C_v^0.

The rate of change in the void radius with time, $\dot{R}$, determined from Eq. (8.120), can be used to determine the volumetric swelling rate:

$$\frac{dV}{dt} = 4\pi R^2 \dot{R}. \tag{8.136}$$

Void swelling can be represented in terms of the void size distribution as follows. If $\rho_V(R)\,dR$ is the number of voids/cm^3 with radii between R and $R + dR$, then the total void number density is:

$$\rho_V = \int_0^\infty \rho_V(R)\,dR, \tag{8.137}$$

the average void size is:

$$\bar{R} = \frac{1}{\rho_V}\int_0^\infty R\rho_V(R)dR, \tag{8.138}$$

and the amount of void swelling is defined by the change in volume of the solid:

$$\frac{\Delta V}{V} = \frac{4}{3}\pi \int_0^\infty R^3 \rho_V(R)dR. \tag{8.139}$$

If the void distribution is narrow, then we can approximate the integral in Eq. (8.139) with:

$$\frac{\Delta V}{V} = \frac{4}{3}\pi \bar{R}^3 \rho_V. \tag{8.140}$$

The equations provided in this section allow the determination of the rate of growth of voids in a solid under irradiation and consequently the rate of swelling of that solid. The following sections address the effects of various parameters on void growth.

8.3.1 Temperature Dependence

Figure 8.16 provides a typical plot of void swelling as a function of temperature. Note that swelling is characterized by a peak at intermediate temperature. This behavior should look familiar from the temperature dependence of RIS since the origin is essentially the same. Low defect mobility limits void growth at low temperature, and the approach of the defect concentration to the thermal equilibrium value limits void growth at high temperature due to a loss of supersaturation. In the preceding analysis of the void growth equation, the two highly

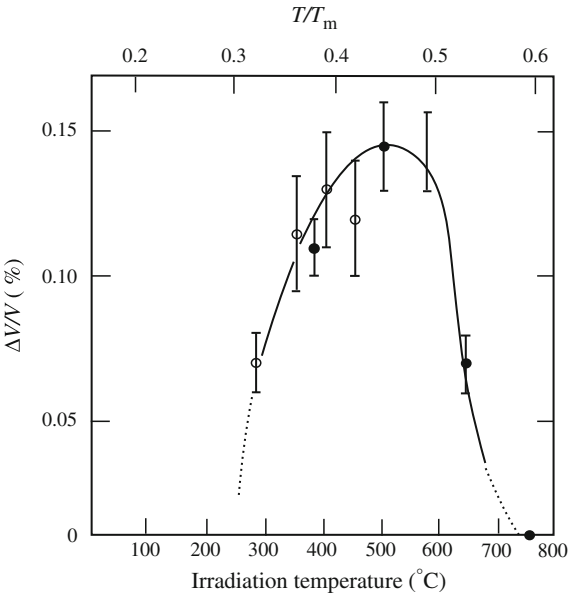

Fig. 8.16 Swelling in nickel as a function of irradiation temperature for a fluence of 5×10^{19} n/cm^2 (after [17])

temperature-sensitive parameters are the vacancy diffusion coefficient D_v and the equilibrium vacancy concentration C_v^0. The temperature dependence of the term $\dot{R}_0 F(\eta)$ is contained in the parameter η, which is controlled by D_v. At low temperatures, swelling is low because vacancies are practically immobile. A low value of D_v makes η large and forces F to become small, resulting in a low value for the term $\dot{R}_0 F(\eta)$. The term $\dot{R}_{th}$ approaches zero since it is proportional to $D_v C_v^0$. Since both $F(\eta)$ and $\dot{R}_{th}$ become small at low temperature, void growth ceases. Under these conditions, the concentration of vacancies builds up and vacancies and interstitials are lost to recombination.

At high temperature, the emission of vacancies by voids counterbalances the net vacancy influx driven by irradiation and suppresses swelling. When in the void growth equation η becomes small and F approaches unity, the term $\dot{R}_{th}$ also increases (but in the negative direction) and dominates at the highest temperatures. Hence, a maximum in the growth rate is predicted at intermediate temperature where both thermal emission and mutual recombination are less important and the net flow of vacancies to voids is maximized. Figure 8.17 shows how the components of the void growth rate combine to result in a peak at intermediate temperature. This is found to be true with all metals.

Figure 8.18(a) shows an example of the sharp dependence of void swelling on temperature in an Fe–Cr–Ni alloy irradiated in the BN-350 reactor as a function of dose and temperature. All the data were for irradiation over a fixed time period, reflecting the variation of dose rates with position in the core. Closed symbols represent samples in which voids were found, and open symbols were samples that

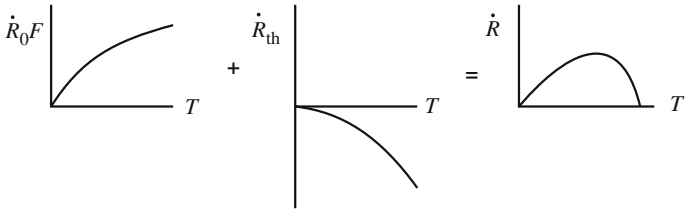

Fig. 8.17 Construction of the total void swelling rate $\dot{R}$ from its components $\dot{R}_0F$ and $\dot{R}_{th}$

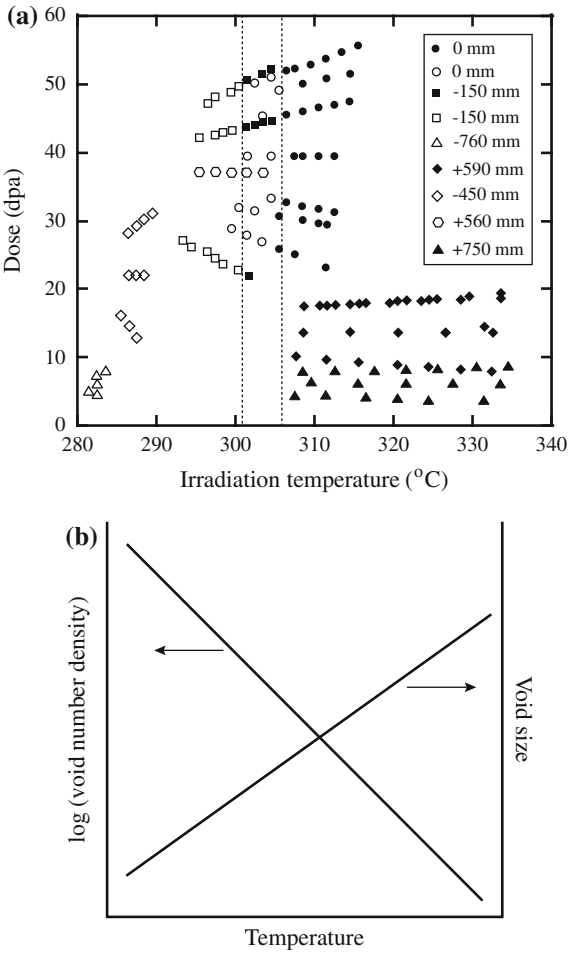

Fig. 8.18 (**a**) Dose–temperature plot of swelling in a Fe–Cr–Ni alloy irradiated in the BN-350 fast reactor showing the sharp temperature threshold for swelling (after [18]). (**b**) Schematic of the temperature dependence of void density and void size

exhibited no voids. Note that despite the differing doses and dose rates, void nucleation occurs with a very sharp temperature threshold at about 302–307 °C, illustrating the high sensitivity of void formation to temperature. The general

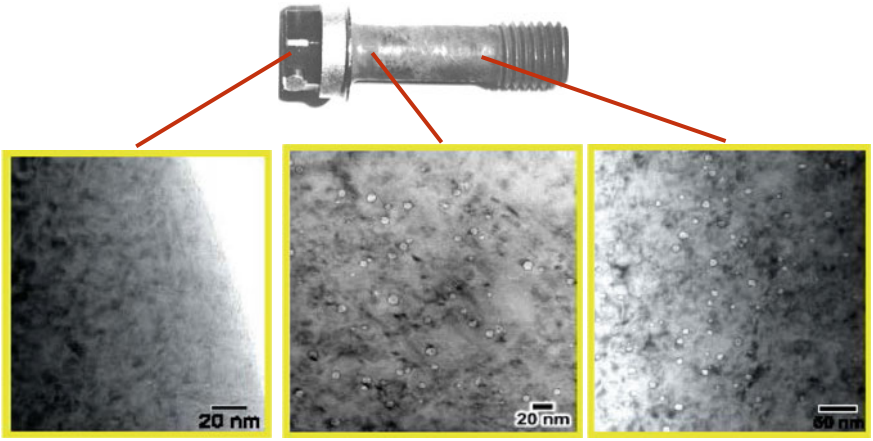

Fig. 8.19 Swelling in a cold-worked 316 SS baffle bolt in a PWR as a function of position along the bolt length. The bolt head was closest to the core, and the temperature distribution is caused by a combination of gamma heating and whether the bolt was exposed to the coolant (*courtesy* S.M. Bruemmer and Garner FA, PNNL)

behavior of the void number density and size with temperature is shown in Fig. 8.18(b). With increasing temperature, the void density falls logarithmically and the size increases, which is the typical behavior for a process that is dominated by nucleation at low temperatures where the void growth is slow and by growth at high temperature where the free energy difference driving void growth is small.

Figure 8.19 shows images of the microstructure in a baffle bolt used to secure baffle–former plates against the baffle in a pressurized water reactor. In this case, the head was closest to the core (received the highest dose) and was exposed to the coolant, hence the lowest temperature. Gamma heating caused the temperature to exceed the coolant temperature ($\sim$320 °C) along the length of the bolt. While the doses differ somewhat, the dominant influence of temperature is noted by both the lack of voids in the lowest temperature location (head) and the largest void size at the highest temperature (top shank).

8.3.2 Dose Dependence

Understanding how swelling depends on dose is critical in the design and operation of components in radiation environments in which voids have the potential to form and grow. From the discussion in the previous section, the dependence is complicated by the occurrence of the defect production rate, K_0, in the terms $\dot{R}_0$ and $F(\eta)$. So we will take a different approach in determining the void growth rate

dependence on dose, following that of Mansur [5]. Recall the expressions for C_v and C_i given in Eq. (8.119):

$$C_v = \frac{D_i k_i^2}{2K_{iv}}\left[(\eta+1)^{1/2}-1\right]$$
$$C_i = \frac{D_v k_v^2}{2K_{iv}}\left[(\eta+1)^{1/2}-1\right],$$

and for η as given in Eq. (8.117):

$$\eta = \frac{4K_{iv}K_0}{D_i D_v k_v^2 k_i^2}.$$

We can write the term in brackets in Eq. (8.119) as:

$$\left[(\eta+1)^{1/2}-1\right] = \left[\left(1+\frac{4K_{iv}K_0}{D_i D_v k_v^2 k_i^2}\right)^{1/2}-1\right]. \tag{8.141}$$

Then, $D_v C_v$ and $D_i C_i$ can be written as:

$$\begin{aligned} D_v C_v &= \frac{D_v D_i k_i^2 z_v}{2K_{iv}}\left[\left(1+\frac{4K_{iv}K_0}{D_i D_v k_v^2 k_i^2}\right)^{1/2}-1\right] \\ D_i C_i &= \frac{D_v D_i k_v^2 z_i}{2K_{iv}}\left[\left(1+\frac{4K_{iv}K_0}{D_i D_v k_v^2 k_i^2}\right)^{1/2}-1\right]. \end{aligned} \tag{8.142}$$

Neglecting thermal emission and substituting into Eq. (8.112) give:

$$\dot{R} = \frac{\Omega D_v D_i}{2RK_{iv}}\left[\left(1+\frac{4K_{iv}K_0}{D_i D_v k_v^2 k_i^2}\right)^{1/2}-1\right]\left(k_v^2 z_v - k_i^2 z_i\right). \tag{8.143}$$

Substituting for k_v^2 and k_i^2 from Eq. (8.104) and considering only coherent precipitates, network dislocations, and loops give:

$$\begin{aligned} \dot{R} = {} & \frac{\Omega D_v D_i}{2RK_{iv}}\left[\left(1+\frac{4K_{iv}K_0}{D_i D_v k_v^2 k_i^2}\right)^{1/2}-1\right] \\ & \times\left[4\pi R_{CP}\rho_{CP}\left(z_i^{CP} z_v - z_v^{CP} z_i\right) + \rho_L\left(z_i^{L} z_v - z_v^{L} z_i\right) + \rho_N\left(z_i^{N} z_v - z_v^{N} z_i\right)\right]. \end{aligned} \tag{8.144}$$

Simplifying Eq. (8.144) for the case of voids and total dislocation density only, we have:

$$\dot{R} = \frac{\Omega D_v D_i}{2RK_{iv}} \left[\left(1 + \frac{4K_{iv}K_0}{D_i D_v k_v^2 k_i^2} \right)^{1/2} - 1 \right] \rho_d \left(z_i^d z_v - z_v^d z_i \right). \tag{8.145}$$

The term $\left(z_i^d z_v - z_v^d z_i\right)$ is the bias of dislocations versus that for voids and is the determinant of the propensity for a void to grow or shrink. Growth will occur if $z_i^d z_v > z_v^d z_i$, or stated as ratios, $\frac{z_i^d}{z_v^d} > \frac{z_i}{z_v}$, and shrinkage will occur if the inequality is in the other direction. The presence of other sinks will affect swelling through their inclusion in the terms k_v^2 and k_i^2. The larger the sink strengths, the lower will be the void growth rate due to the loss of defects to those sinks.

The limiting behaviors of Eq. (8.145) are the cases in which recombination dominates $\frac{4K_{iv}K_0}{D_i D_v k_v^2 k_i^2} \gg 1$ (loss of defects to recombination is much larger than that lost to sinks) and loss to sinks dominates $\frac{4K_{iv}K_0}{D_i D_v k_v^2 k_i^2} \ll 1$[5]. Assuming that the only sinks besides voids are network dislocations, we have:

$$\dot{R} = \frac{\Omega}{R} \left(\frac{D_i D_v K_0}{z_i^N z_v^N K_{iv}} \right)^{1/2} \frac{Q_i^{1/2} Q_v^{1/2} \left(z_i^N z_v - z_v^N z_i \right)}{(1+Q_v)^{1/2}(1+Q_i)^{1/2}} : \text{ recombination dominant} \tag{8.146}$$

$$\dot{R} = \frac{\Omega K_0 Q_i Q_v}{R\rho_N (1+Q_v)(1+Q_i)} \left(z_i^N z_v - z_v^N z_i \right) : \text{sink dominant}, \tag{8.147}$$

where

$$Q_{i,v} = \frac{z_{i,v}^N \rho_N}{4\pi R \rho_V z_{i,v}} \tag{8.148}$$

is the ratio of dislocation sink strength to void sink strength. Note that the growth rate is dependent on $K_0^{1/2}$ when recombination is dominant, as in Eq. (8.146). However, when sinks are dominant, Eq. (8.147) shows that the growth rate is proportional to K_0. Multiplying Eq. (8.147) by $4\pi R^2 \rho_V$ and given that $\Omega = 1/N_0$, the site density gives the volume swelling rate:

$$\frac{d(\Delta V/V)}{dt} = K_0 \left(\frac{z_i - z_v}{z_v} \right) \frac{Q}{(1+Q)^2}. \tag{8.149}$$

This is the same expression that can be obtained from Eq. (8.122) by neglecting the effect of coherent precipitates. For $Q = 1$ and $z_i - z_v = 0.01$, we have:

$$\frac{\Delta V}{V}\% \cong 1/4 \times (\text{dose in dpa}). \tag{8.150}$$

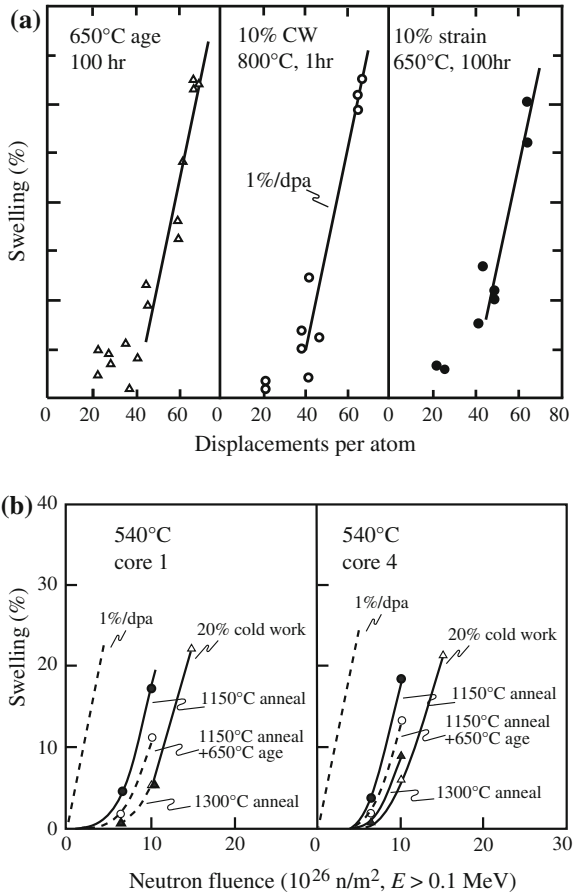

Fig. 8.20 (**a**) Early development of 1 %/dpa swelling rates in aged OKH16N15M3B steel during irradiation in the BOR-60 reactor at 400–500 °C (after [20]). (**b**) Variations in swelling at 540 °C in EBR-II for two nominally similar heats of 316 stainless steel as a function of starting condition (after [21])

Garner [19] has shown that over a wide dose range, the steady-state swelling rate in austenitic stainless steels is of the order of ~ 1 %/dpa (Fig. 8.20). The linear dependence is consistent with a sink-dominated process, but the magnitude of the coefficient is a factor of four greater than that predicted by Eq. (8.150). The discrepancy is likely due to the effect of clusters that is not accounted for in the rate theory model. A closer look at the behavior of vacancies and interstitials in the cascade shows that the fraction of vacancies and interstitials that form clusters is larger than has been accounted for thus far. Vacancy clusters form near the cascade core, and interstitial clusters form near the cascade periphery. Mobile interstitial clusters can reach sinks by migration of the cluster as a whole. Vacancies emitted by vacancy clusters by thermal emission are also free to reach sinks. Since the fraction of interstitials and vacancies in clusters is not the same, nor is their thermal stability, the difference between vacancy and interstitial clusters results in a difference in the effective production rates of vacancies compared to that of interstitials, termed the *production bias*, and can influence void swelling. The net result is

that the sink strength of the clusters is much greater than that of the measurable dislocation loops, resulting in a much greater driving force for void swelling than is accounted for by the rate equation formulation. This is one of the reasons that the observed steady-state swelling dependence on dose is greater than that predicted by the rate equation formulation.

8.3.3 Role of Dislocations as Biased Sinks

The dislocation structure of an alloy can exert a profound effect on the swelling behavior. Equation (8.122) demonstrates that both a biased sink (e.g., dislocations) and a neutral sink are necessary for void growth. If the bias is removed, $z_i = z_v$, then $\dot{R}_0 = 0$ and swelling will not occur as defects will flow equally to each sink.

The Q-dependence of $\dot{R}_0$ is shown in Fig. 8.21. Note that $\dot{R}_0$ is a maximum at $Q = 1$, or when the flow of vacancies to voids and dislocations is equal. The regime $Q > 1$ is representative of the low-dose regime in which both R and ρ_V are small, so vacancy loss to the existing dislocation network dominates. This is why cold-worked alloys swell less. When $Q \sim 1$, then the flow of vacancies to voids and dislocations is approximately equal. This is the regime where bias exerts its greatest influence. If the flow of vacancies and interstitials to sinks is equal, and more interstitials go to dislocations, then more vacancies must flow to voids. At $Q \sim 1$, the flows are equal, so the bias is most effective in promoting void growth. When $Q < 1$, defect flow to voids dominates the loss terms, and since few defects flow to dislocations, the bias is not very effective in creating an imbalance in point defect fluxes, so the flow of vacancies and interstitials to voids is similar in magnitude and void growth slows or ceases. Although dislocations exhibit a slight preference for interstitials $\left(\frac{\beta_d}{\beta_V} \geq 1\right)$, in a cold-worked material, the dislocations provide so many sinks for vacancies that the effect of a vacancy supersaturation is essentially multiplied, resulting in low void nucleation and growth rates. By the same mechanism, grain boundaries provide *unbiased* sinks for point defects and will keep the vacancy supersaturation too low for growth, provided that the grain boundary area is large enough (i.e., very small grains). Figure 8.22(a) shows a plot

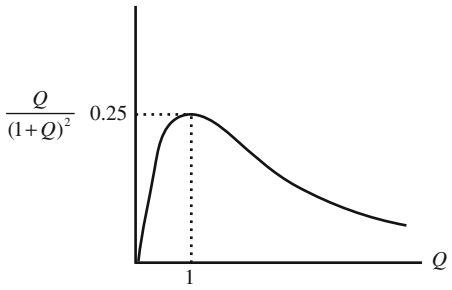

Fig. 8.21 Dependence of swelling on the dislocation/void sink strength ratio, Q, in Eq. (8.149)

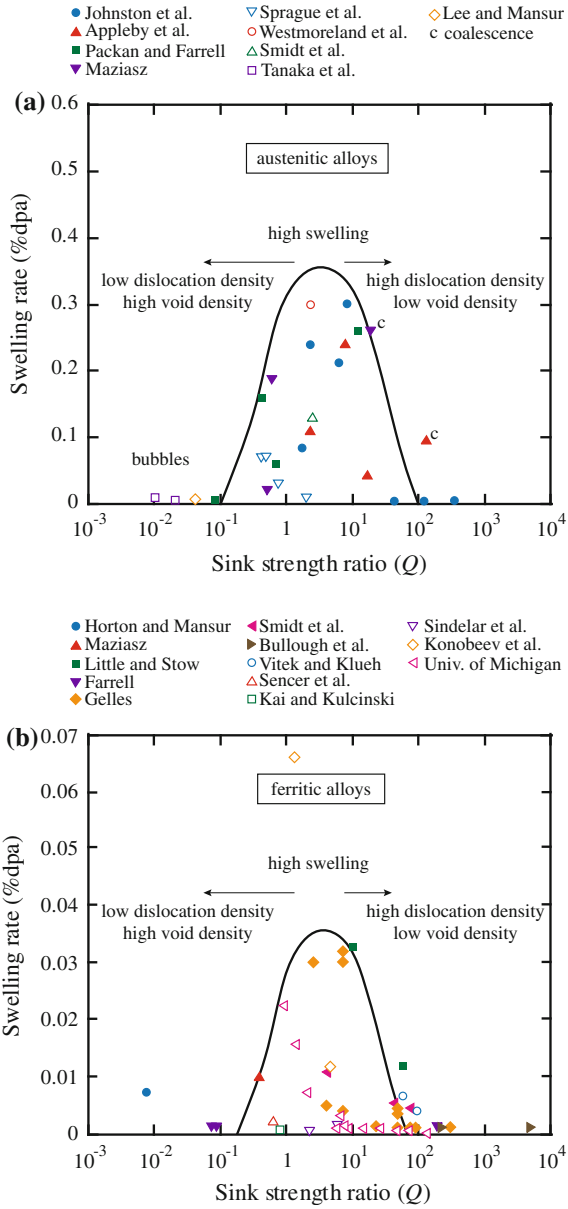

Fig. 8.22 Experimentally observed swelling rates as a function of Q for (**a**) austenitic stainless steels (after [5]) and (**b**) ferritic–martensitic steels

of swelling rate versus the sink strength ratio, Q, for several austenitic stainless steels, and Fig. 8.22(b) shows the same for ferritic–martensitic alloys. Indeed, the dependence shown in Fig. 8.21 is obeyed in practice.

The effect of cold-work on swelling in reactor exposures is shown in Fig. 8.23. Figure 8.23(a) shows the effect of cold-work on swelling in 316 stainless steel

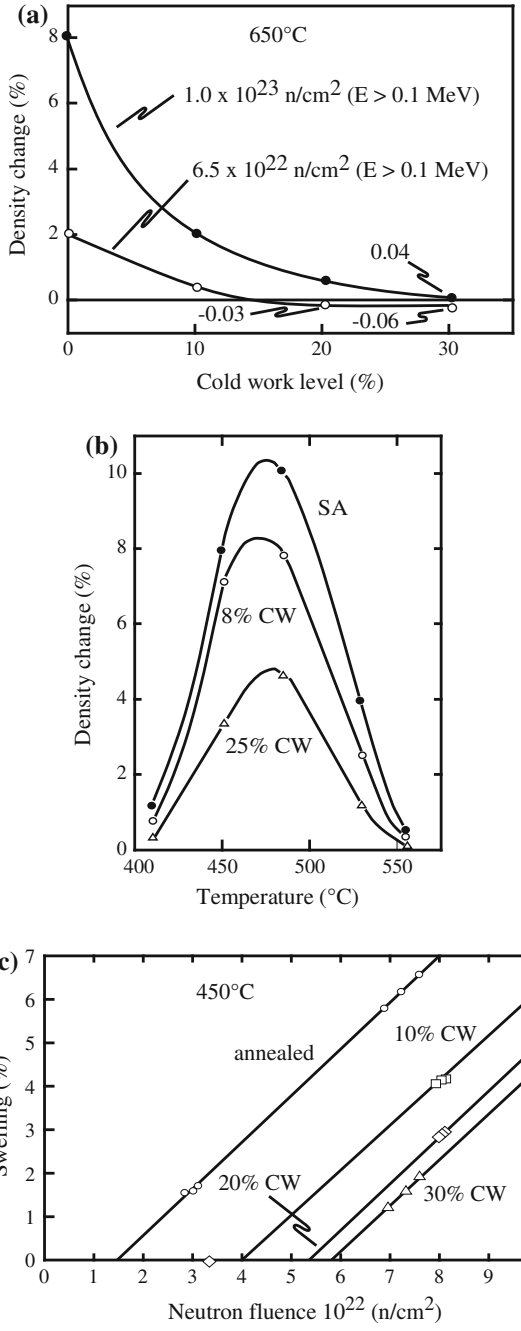

Fig. 8.23 (**a**) Effect of cold-work level on the swelling of 316 stainless steel irradiated at 650 °C in EBR-II to 33 and 50 dpa (after [22]). (**b**) Dependence of swelling on cold-work for various temperatures for 316 stainless steel irradiated in the RAPSODIE reactor to doses of 20–71 dpa (after [23]). (**c**) Effect of cold-work on swelling in 304 stainless steel at 450 °C in EBR-II (after [24])

irradiated in EBR-II at 650 °C to levels of 33 and 50 dpa. Note that for both cases, the amount of swelling decreases with increasing cold-work. Figure 8.23(b) shows that cold-work affects the temperature dependence of swelling by suppressing the magnitude of the swelling peak with increasing levels of cold-work. The data are taken from a stainless steel irradiated to doses of 20–61 dpa in the RAPSODIE reactor. Figure 8.23(c) shows the effect of cold-work on the dose dependence of swelling in 304 stainless steel and that increasing cold-work decreases the amount of swelling, but at reduced rates as the amount of cold-work increases. Note also that these data show that the primary effect of cold-work is to extend the transient swelling regime, rather than to alter the steady-state swelling rate.

8.3.4 Dose Rate Dependence

The location of the peak swelling temperature depends on the dose rate, sink strength, and the predominant mode of defect loss. When the dose rate increases, more point defects are created, but their migration velocities are unchanged. To remove defects at the higher dose rate at steady state requires point defect concentrations to be higher, resulting in greater recombination and a reduction in the net absorption of vacancies by voids and hence a reduction in the void growth rate. As a result, the *bell-shaped* swelling curve is displaced to higher temperatures with increasing dose rate. Figure 8.24 is a plot of the temperature dependence of the term $F(\eta)$ in Eq. (8.125) and illustrates the shift of the swelling peak with dose rate, K_0, similar to that for RIS shown in Fig. 6.9. Alternatively, at a given temperature, the void growth rate decreases for increasing dose rate. At temperatures where thermal emission is non-negligible, the void growth rate is a complicated function of dose rate. Nevertheless, the experimental data substantiate the effect of dose rate on swelling. Figure 8.25 shows swelling in annealed and cold-worked 316 stainless

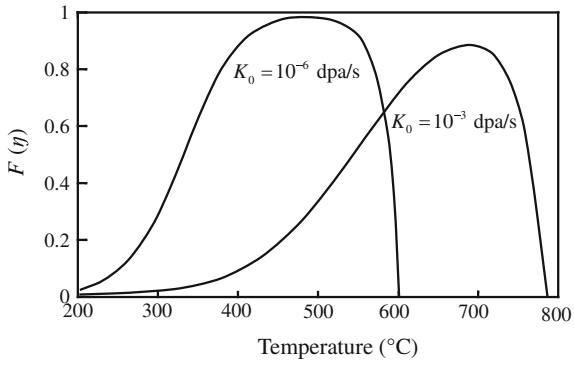

Fig. 8.24 Variation of the function $F(\eta)$ in Eq. (8.124) with temperature, illustrating the shift of the peak with dose rate, K_0. Parameters used to construct the curves are as follows: $\rho_d = 10^9$ cm^{-2}, $E_f^v = 1.6$ eV, $z_i - z_v = 0.01$, $z_v = 1$, $4\pi R\rho_V = 10^{-11}$ cm^{-2}, $D_v = \exp(-1.4\text{ eV}/kT)$ cm^2 s^{-1} (after [15])

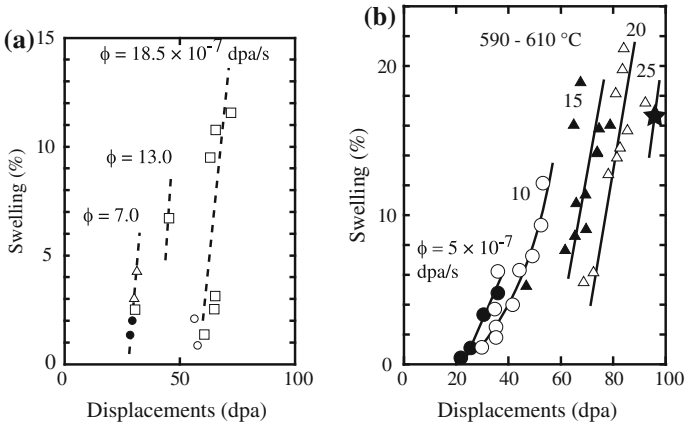

Fig. 8.25 (**a**) Effect of displacement rate on swelling of annealed 316 stainless steel in the RAPSODIE reactor fuel pin cladding at 562 °C. (**b**) Swelling in cold-worked 316 stainless steel in the PHENIX reactor fuel pin cladding at 590–610 °C (after [25, 26])

steel at temperatures between 562 and 610 °C over a range of dose rates. Note that increasing dose rate has the effect of reducing the swelling rate at a given dose, but that at steady state, all data have a similar slope, indicating that the primary effect of dose rate is on the duration of the swelling transition period.

If we move up the temperature scale, we can restore the same relative ratio of recombination rate to absorption rate at sinks. In fact, by requiring that this ratio be invariant, we can obtain a relationship between temperature and dose rate, termed the *temperature shift*.

8.3.5 Irradiation Variable Shifts

The concept of variable shifts was developed to provide a better understanding of the relationship between variables in swelling [16]. The idea is that when one irradiation variable is changed, a shift in other variables can be determined that will preserve a physical quantity describing the behavior of defects during irradiation. There are two such quantities that pertain to the limiting case where recombination dominates defect loss. The number of defects per unit volume that have *recombined* up to a time τ is:

$$N_{\mathrm{R}} = K_{\mathrm{iv}} \int_0^{\tau} C_{\mathrm{i}} C_{\mathrm{v}} \, \mathrm{d}t. \tag{8.151}$$

When the solid is at steady state and defect concentrations are controlled by recombination, Eq. (8.116) gives:

$$C_{\mathrm{v}} = \left(\frac{K_0}{K_{\mathrm{iv}}}\frac{z_{\mathrm{i}}D_{\mathrm{i}}}{z_{\mathrm{v}}D_{\mathrm{v}}}\right)^{1/2}$$
$$C_{\mathrm{i}} = \left(\frac{K_0}{K_{\mathrm{iv}}}\frac{z_{\mathrm{v}}D_{\mathrm{v}}}{z_{\mathrm{i}}D_{\mathrm{i}}}\right)^{1/2}, \tag{8.152}$$

and substituting into Eq. (8.151) yields:

$$N_{\mathrm{R}} = K_0\tau. \tag{8.153}$$

The number of defects *lost to sinks* per unit volume up to a time τ is:

$$N_{\mathrm{Sj}} = \int_0^{\tau} K_j C_j \mathrm{d}t, \tag{8.154}$$

where K is the loss rate and C is the defect concentration and the subscript j denotes the defect type. Substituting Eq. (8.152) into Eq. (8.154) gives for vacancies:

$$N_{\mathrm{Sv}} = \frac{K_{\mathrm{v}}}{(K_0K_{\mathrm{iv}})^{1/2}}\left(\frac{z_{\mathrm{i}}D_{\mathrm{i}}}{z_{\mathrm{v}}D_{\mathrm{v}}}\right)^{1/2}\Phi, \tag{8.155}$$

where Φ is the dose and the expression for interstitials is identical.

These definitions can be used to determine relationships between any two of the three variables: temperature, dose, and dose rate, taking the third to be constant. For example, in the steady-state recombination-dominated regime, we may require N_{s} to be equal for dose 1 and dose rate 1 to that for dose 2 and dose rate 2 at a *fixed temperature*:

$$\frac{K_{\mathrm{v}}}{(K_{0_1}K_{\mathrm{iv}})^{1/2}}\left(\frac{z_{\mathrm{i}}D_{\mathrm{i}}}{z_{\mathrm{v}}D_{\mathrm{v}}}\right)^{1/2}\Phi_1 = \frac{K_{\mathrm{v}}}{(K_{0_2}K_{\mathrm{iv}})^{1/2}}\left(\frac{z_{\mathrm{i}}D_{\mathrm{i}}}{z_{\mathrm{v}}D_{\mathrm{v}}}\right)^{1/2}\Phi_2,$$

and canceling terms in the equality gives:

$$\frac{\Phi_2}{\Phi_1} = \left(\frac{K_{0_1}}{K_{0_2}}\right)^{1/2}. \tag{8.156}$$

For a given change in dose rate, the shift in temperature required at constant dose to keep N_{s} invariant is determined by equating the same terms, but with *fixed dose* resulting in:

$$\left(\frac{D_{\mathrm{v}}}{K_0}\right)_1^{1/2} = \left(\frac{D_{\mathrm{v}}}{K_0}\right)_2^{1/2}, \tag{8.157}$$

or substituting in for D_v from Eq. (4.55), $D_v = D_0 \exp\left(-E_m^v/kT\right)$:

$$T_2 - T_1 = \frac{\dfrac{kT_1^2}{E_m^v}\ln\left(\dfrac{K_{0_2}}{K_{0_1}}\right)}{1 - \dfrac{kT_1}{E_m^v}\ln\left(\dfrac{K_{0_2}}{K_{0_1}}\right)}. \tag{8.158}$$

For a change in dose, the shift in temperature required to maintain N_s invariant at *fixed dose rate* is:

$$\left(D_v^{1/2}\Phi\right)_1 = \left(D_v^{1/2}\Phi\right)_2, \tag{8.159}$$

and substituting in for D_v:

$$\frac{\Phi_2}{\Phi_1} = \exp\left[\frac{E_m^v}{2k}\left(\frac{1}{T_2} - \frac{1}{T_1}\right)\right], \tag{8.160}$$

and rearranging gives:

$$T_2 - T_1 = \frac{\dfrac{-2kT_1^2}{E_m^v}\ln\dfrac{\Phi_2}{\Phi_1}}{1 + \dfrac{2kT_1}{E_m^v}\ln\dfrac{\Phi_2}{\Phi_1}}. \tag{8.161}$$

There is another important temperature shift that, instead of requiring that N_s be invariant, requires the net flux of vacancies over interstitials to a particular type of sink (voids in this case) to be invariant, where the net flux is relevant to void swelling. The temperature shift derived in this way for the recombination-dominated regime to keep swelling rate (N_R) invariant is [16]:

$$T_2 - T_1 = \frac{\dfrac{kT_1^2}{E_m^v + 2E_f^v}\ln\dfrac{K_{0_2}}{K_{0_1}}}{1 - \dfrac{kT_1}{E_m^v + 2E_f^v}\ln\dfrac{K_{0_2}}{K_{0_1}}}. \tag{8.162}$$

where E_f^v is the vacancy formation energy.

The various variable shifts described in this section are shown in the following figures. Figure 8.26 shows the relationship between dose versus dose rate dependence at a reference temperature of 200 °C for the case of N_s invariant, as in Eq. (8.156). Figure 8.27 shows the temperature shift as a function of dose rate at constant dose for three values of vacancy migration energy for N_s invariant, as in Eq. (8.158), and Fig. 8.28 shows the same relationship for the constant dose rate case, as in Eq. (8.161). Figure 8.29 shows the temperature shift as a function of dose for constant dose rate to keep the swelling rate, N_R, invariant, as in

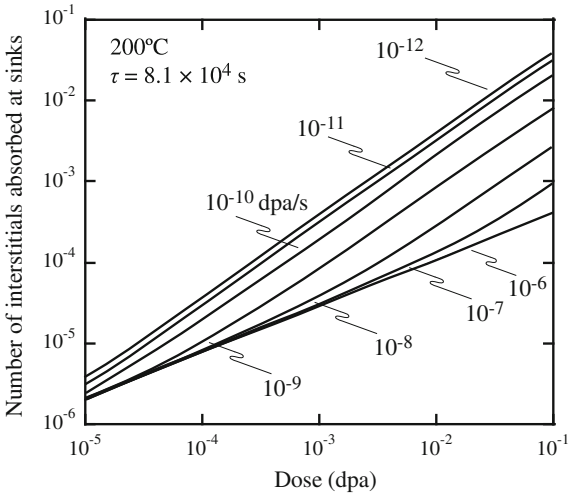

Fig. 8.26 Number of interstitials absorbed at sinks as a function of dose at 200 °C for different dose rates (after [27])

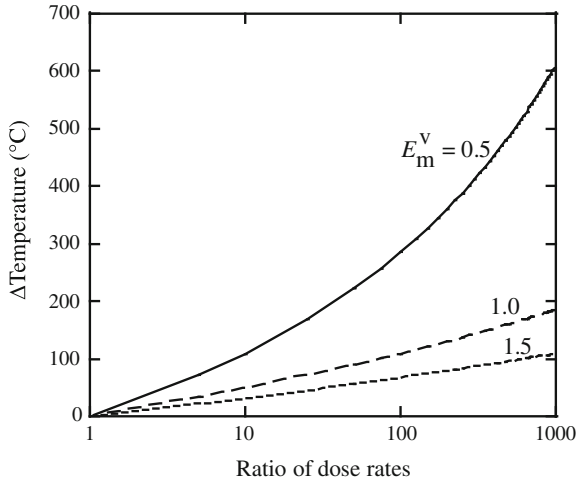

Fig. 8.27 Temperature shift from the reference 200 °C required at constant dose in order to maintain the same point defect absorption at sinks as a function of dose rate, normalized to initial dose rate. Results are shown for three different vacancy migration energies (after [27])

Eq. (8.162). Figure 8.30 shows that the temperature shift concept works well in describing the shift in the peak in the swelling versus temperature curve in nickel over more than five orders of magnitude in the dose rate as given by Eq. (8.162).

The general form of the temperature shift equation is [28, 29]:

$$T_2 - T_1 = \frac{\dfrac{kT_1^2}{E_m^v + n(E_f^v + E_*^v)}M}{1 - \dfrac{kT_1}{E_m^v + n(E_f^v + E_*^v)}M}, \tag{8.163}$$

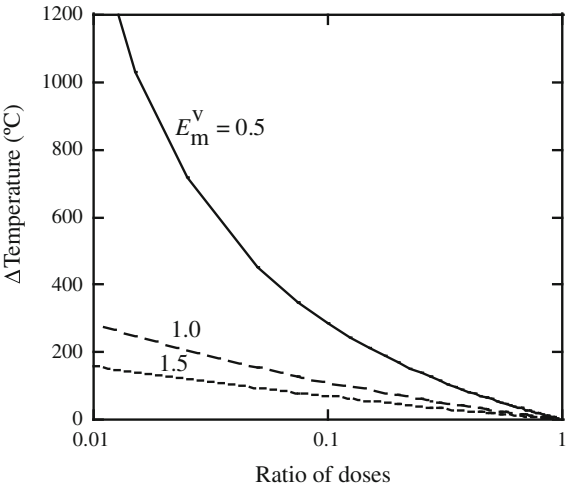

Fig. 8.28 Temperature shift from the reference 200 °C required at constant dose rate in order to maintain the same point defect absorption at sinks as a function of dose, normalized to initial dose. Results are shown for three different vacancy migration energies (after [27])

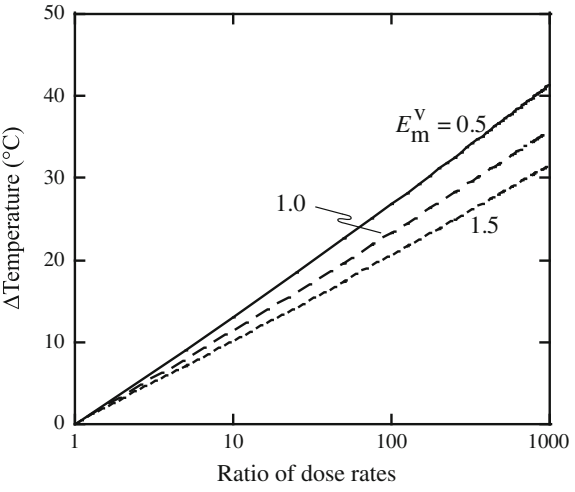

Fig. 8.29 Temperature shift from the reference 200 °C required at constant dose in order to maintain swelling invariance as a function of dose rate, normalized to initial dose rate. Results are shown for three different vacancy migration energies and a formation energy of 1.5 eV

where

$$M = \left[\ln \frac{K_{0_2} k_{i_1}^2 k_{v_1}^2}{K_{0_1} k_{i_2}^2 k_{v_2}^2} + \ln B \right], \tag{8.164}$$

and

$$B = \left[\frac{k_{i_2}^2 \exp(-E_*^v/kT_2) - k_{v_2}^2 \exp(-E_*^i/kT_2)}{k_{i_1}^2 \exp(-E_*^v/kT_1) - k_{v_1}^2 \exp(-E_*^i/kT_1)} \right]^2. \tag{8.165}$$

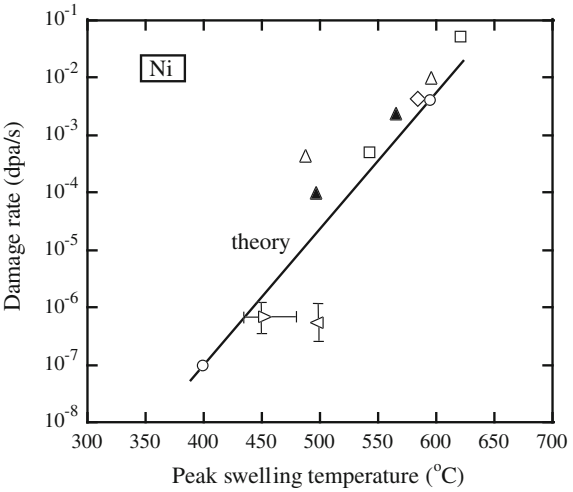

Fig. 8.30 Temperature shift of peak swelling as a function of dose rate. *Points* are experimental data, and the *line* is from theory (after [5])

The value of n is determined by the dominant process responsible for point defect removal, $n = 1$ for sink-dominated cases and $n = 2$ for recombination-dominated cases, while the value of B is determined both by the dominant process and by the mode of void growth. In the case where both interstitials and vacancies are diffusion controlled:

$$B = \frac{\rho_{d_2}}{\rho_{d_1}}, \quad \text{for} \quad n = 1, \tag{8.166}$$

$$B = \frac{r_{c_1}}{r_{c_2}} \left[\frac{\rho_{d_2}}{\rho_{d_1}}\right]^2, \quad \text{for} \quad n = 2, \tag{8.167}$$

where r_c is the radius of the recombination volume and ρ_d is the dislocation density. The term $E_*^{\mathrm{v,i}}$ represents the additional energy above the normal lattice migration energy that the point defect must overcome on diffusing to the void and is nonzero only for the case of reaction rate control. For interstitial and vacancy reaction rate control:

$$B = \frac{\rho_{d_2}}{\rho_{d_1}} \left[\frac{z_i^d \exp(-E_*^{\mathrm{v}}/kT_2) - z_{\mathrm{v}}^d \exp(-E_*^i/kT_2)}{z_i^d \exp(-E_*^{\mathrm{v}}/kT_1) - z_{\mathrm{v}}^d \exp(-E_*^i/kT_1)}\right], \quad \text{for} \quad n = 1, \tag{8.168}$$

$$B = \frac{r_{c_1}}{r_{c_2}} \left[\frac{k_{i_2}^2 \exp(-E_*^{\mathrm{v}}/kT_2) - k_{\mathrm{v}_2}^2 \exp(-E_*^i/kT_2)}{k_{i_1}^2 \exp(-E_*^{\mathrm{v}}/kT_1) - k_{\mathrm{v}_1}^2 \exp(-E_*^i/kT_1)}\right], \quad \text{for} \quad n = 2. \tag{8.169}$$

For interstitial reaction rate control and vacancy diffusion control,

$$B = \frac{\rho_{d_2}}{\rho_{d_1}} \left[\frac{bz_i^d - z_v^d R_v \exp(-E_*^i/kT_2)}{bz_i^d - z_v^d R_v \exp(-E_*^i/kT_1)} \right], \quad \text{for} \quad n = 1, \tag{8.170}$$

$$B = \frac{r_{c_1}}{r_{c_2}} \left[\frac{bk_{i_2}^2 - k_{v_2}^2 R_v \exp(-E_*^i/kT_2)}{bk_{i_1}^2 - k_{v_1}^2 R_v \exp(-E_*^i/kT_1)} \right]^2, \quad \text{for} \quad n = 2, \tag{8.171}$$

where R_v is the void radius and b is the Burgers vector. The dominant process of point defect loss as well as the mode of void growth affects the form of the temperature shift expression. When recombination dominates, the temperature shift is smaller since $2E_f^v$ occurs in the denominator. But when sinks dominate, the value is E_f^v. The reason for this is that the radiation-induced void growth rate is proportional to generation rate when sinks dominate, while it is proportional to the square root of the generation rate if recombination dominates (see Eqs. 8.146 and 8.147), However, the thermal emission rate depends on the same exponential in temperature in both cases. Thus, a given initial ratio of thermal emission rate to radiation-induced growth rate of voids may be recovered after a given increase in dose rate by a smaller increase in temperature where recombination dominates.

8.3.6 *Effect of Production Bias*

We now must consider the case of cascade formation in which both vacancy and interstitial clusters and loops are formed during the damage process. The vacancy clusters, however, are not stable and will emit vacancies that become freely migrating vacancies and are available to various sinks, including voids. Due to their high formation energies, immobilization of interstitials in clusters is permanent. So there is a bias between vacancy and interstitial production in cascade damage. Recall the point defect balance equations Eq. (5.1) that account for the incorporation of both vacancies and interstitials into clusters and the emission of vacancies from vacancy clusters. The following [30] point defect balance equations are rewritten using sink strengths instead of reaction rate constants yielding:

$$\begin{aligned} \frac{dC_v}{dt} &= K_0(1-\varepsilon_r)(1-\varepsilon_v) - k_v^2 D_v C_v - K_{iv} D_i C_i C_v + L_v \\ \frac{dC_i}{dt} &= K_0(1-\varepsilon_r)(1-\varepsilon_i) - k_i^2 D_i C_i - K_{iv} D_i C_i C_v, \end{aligned} \tag{8.172}$$

where ε_r is the fraction of defects that recombine in the cascade and ε_v and ε_i are the fraction of clustered vacancies and interstitials, respectively, and k_v^2 and k_i^2 are the total sink strengths for vacancies and interstitials, respectively, where:

$$k^2 = k_{\mathrm{V}}^2 + k_{\mathrm{N}}^2 + k_{\mathrm{vcl}}^2 + k_{\mathrm{icl}}^2 \tag{8.173}$$

where subscripts "V" and "N" refer to voids and network dislocations, respectively, and subscripts "vcl" and "icl" represent vacancy and interstitial loops or clusters, respectively, K_{iv} is the recombination coefficient, and L_{v} is the thermal emission term given by:

$$L_{\mathrm{v}} = L_{\mathrm{v}}^{V} + L_{\mathrm{v}}^{N} + L_{\mathrm{v}}^{\mathrm{icl}} + L_{\mathrm{v}}^{\mathrm{vcl}}. \tag{8.174}$$

The swelling rate is given in Eq. (8.110) as:

$$\frac{\mathrm{d}(\Delta V/V)}{\mathrm{d}t} = 4\pi R\Omega[D_{\mathrm{v}}(C_{\mathrm{v}} - C_{\mathrm{v}}^0) - D_{\mathrm{i}}C_{\mathrm{i}}],$$

and accounting for production bias caused by the formation of clusters, we can determine the steady-state swelling rate from Eqs. (8.172) and (8.174), neglecting recombination, to give [30]:

$$\frac{\mathrm{d}(\Delta V/V)}{\mathrm{d}t} = \frac{z_{\mathrm{i}}k_{\mathrm{V}}^2k_{\mathrm{d}}^2(1-\varepsilon_{\mathrm{v}})K}{k_{\mathrm{v}}^2k_{\mathrm{i}}^2} + \frac{k_{\mathrm{V}}^2(\varepsilon_{\mathrm{i}} - \varepsilon_{\mathrm{v}})K}{k_{\mathrm{i}}^2} + \frac{k_{\mathrm{V}}^2L_{\mathrm{v}}}{k_{\mathrm{v}}^2} - k_{\mathrm{V}}^2D_{\mathrm{v}}C_{\mathrm{v}}^{V}, \tag{8.175}$$

where z_{-i} is the dislocation bias, $K = (1 - \varepsilon_{\mathrm{r}})K_0$, and $C_{\mathrm{v}}^{\mathrm{V}}$ is the vacancy concentration at the void surface. The swelling rate in Eq. (8.175) can be rewritten as a sum of two contributions: a dislocation bias–driven contribution and a production bias–driven contribution, i.e.,

$$\frac{\mathrm{d}(\Delta V/V)}{\mathrm{d}t} = \left.\frac{\mathrm{d}(\Delta V/V)}{\mathrm{d}t}\right|_{\mathrm{db}} + \left.\frac{\mathrm{d}(\Delta V/V)}{\mathrm{d}t}\right|_{\mathrm{pb}}$$

or

$$\left.\frac{\mathrm{d}(\Delta V/V)}{\mathrm{d}t}\right|_{\mathrm{db}} = \frac{z_{\mathrm{i}}k_{\mathrm{V}}^2k_{\mathrm{d}}^2(1-\varepsilon_{\mathrm{v}})K}{k_{\mathrm{v}}^2k_{\mathrm{i}}^2} + \frac{k_{\mathrm{V}}^2}{k_{\mathrm{v}}^2}\left[L_{\mathrm{v}}^{\mathrm{V}} + L_{\mathrm{v}}^{\mathrm{N}} - (k_{\mathrm{V}}^2 + k_{\mathrm{N}}^2)D_{\mathrm{v}}C_{\mathrm{v}}^{\mathrm{V}}\right] \tag{8.176}$$

$$\left.\frac{\mathrm{d}(\Delta V/V)}{\mathrm{d}t}\right|_{\mathrm{pb}} = \frac{k_{\mathrm{V}}^2(\varepsilon_{\mathrm{i}} - \varepsilon_{\mathrm{v}})K}{k_{\mathrm{i}}^2} + \frac{k_{\mathrm{V}}^2}{k_{\mathrm{v}}^2}\left[L_{\mathrm{v}}^{\mathrm{vcl}} + L_{\mathrm{v}}^{\mathrm{icl}} - (k_{\mathrm{vcl}}^2 + k_{\mathrm{icl}}^2)D_{\mathrm{v}}C_{\mathrm{v}}^{\mathrm{V}}\right]. \tag{8.177}$$

In Eq. (8.176), the first term corresponds to swelling due to the biased arrival (caused by the usual dislocation bias) of mobile vacancies at the voids. The second term corresponds to effects caused by the emission of vacancies from the voids (that tends to anneal the voids) and from the dislocation network (that increases swelling). The swelling rate in Eq. (8.176) does not contain effects due to the interstitial and vacancy clusters formed during cascade damage. In Eq. (8.177), the first term represents the reduction of the interstitial flux to voids due to interstitial clustering

(which would help swelling). The second term represents the flux to the voids of vacancies evaporating under the line tension from the vacancy loops. The line tension of the interstitial loops, on the other hand, favors the absorption of vacancies that are otherwise available to the voids.

Where interstitials are assumed not to cluster, i.e., $\varepsilon_i = 0$, and the lifetimes of the vacancy loops are limited to those due to thermal and bias-driven annealing, the second term in Eq. (8.177) can then be shown to cancel the first term and the ε_v contribution in Eq. (8.176). The collapse of a cascade into vacancy loops then does not produce any appreciable effects on the swelling rate. With the immobilization of the interstitials in interstitial loops and their subsequent destruction by dislocation sweep and cascade collapse, the re-emission of vacancies from the vacancy loops essentially produces a production bias that drives the swelling according to Eq. (8.177), as discussed earlier in this section.

Under electron irradiation, there is no cascade effect, i.e., $\varepsilon_i = \varepsilon_v = 0$ and $K = K_0$. Therefore, in this case, the swelling is purely dislocation bias driven and $\left.\frac{d(\Delta V/V)}{dt}\right|_{db}$ is the only contribution. In the case of cascade damage, however, neither ε_i nor ε_v are likely to be zero. For simplicity, we may use a previously obtained result [30] that the vacancy loop contribution in Eq. (8.177) vanishes due to mutual cancelation. Then, $\left.\frac{d(\Delta V/V)}{dt}\right|_{pb}$ is given by:

$$\frac{d(\Delta V/V)_{pb}}{dt} = \frac{k_V^2}{k_i^2}\varepsilon_i K. \tag{8.178}$$

Note that ε_i need not be very large, just a few percent is enough to make a significant contribution to the total steady-state swelling rate of the order of 1 % K.

As described in the preceding paragraphs, the origin of the "production bias" lies in the special features of damage production in the form of cascades. The physical reason for this bias is the immobilization of a certain fraction of interstitials in the form of thermally stable clusters in the cascade zone. During irradiation at elevated temperatures, the vacancies would evaporate from the collapsed or uncollapsed cascade and would diffuse not only to the interstitial clusters but also to the cavities. Thus, the number of interstitials tied up in the clusters represents approximately the number of vacancies available for the cavity growth. This is basically the strength of the production bias.

The net result of the production bias is precisely the same as that of the dislocation bias, namely the production of an excess of vacancies. However, it is also quite apparent that the physical processes involved in the two mechanisms are very different. In the case of dislocation bias, the interstitial atoms are expected to migrate to dislocations where they are preferentially annihilated due to the strain–field interaction. In the cascade damage situation, this mechanism would not operate effectively since a large number of interstitials are immobilized in the form

of interstitial clusters. In the case of production bias, it is the interstitial–interstitial interaction (and not the interstitial–dislocation interaction) that determines the bias.

However, as noted in Chap. 5, Sect. 5.1.7, and discussed in Chap. 7, Sect. 7.3.3, more recent work has shown that interstitial clusters can have very high 1D mobility. This high mobility allows them to escape to annihilate at sinks such as grain boundaries, thus creating a production bias without the need for dislocation motion. Then, SIA clusters are composed of glissile (g) and sessile (s) components, or $\varepsilon_\mathrm{i} = \varepsilon_\mathrm{i}^\mathrm{g} + \varepsilon_\mathrm{i}^\mathrm{s}$. In the case of glissile SIA clusters, an additional equation is needed in the point defect balance equations of Eq. (8.172) to account for the glissile interstitial clusters [31]:

$$\begin{aligned}
\frac{\mathrm{d}C_\mathrm{v}}{\mathrm{d}t} &= K_0(1-\varepsilon_\mathrm{r})(1-\varepsilon_\mathrm{v}) - k_\mathrm{v}^2 D_\mathrm{v} C_\mathrm{v} - K_\mathrm{iv} D_i C_i C_\mathrm{v} + L_\mathrm{v} \\
\frac{\mathrm{d}C_\mathrm{i}}{\mathrm{d}t} &= K_0(1-\varepsilon_\mathrm{r})(1-\varepsilon_\mathrm{i}) - k_\mathrm{i}^2 D_\mathrm{i} C_\mathrm{i} - K_\mathrm{iv} D_\mathrm{i} C_\mathrm{i} C_\mathrm{v} \\
\frac{\mathrm{d}C_\mathrm{gicl}(x)}{\mathrm{d}t} &= K_\mathrm{gicl}(x) - k_\mathrm{g}^2 D_\mathrm{gicl} C_\mathrm{gicl}(x),
\end{aligned} \tag{8.179}$$

where $C_\mathrm{gicl}(x)$ is the concentration, $K_\mathrm{gicl}(x)$ is the production rate, k_g^2 is the sink strength, and D_gicl is the diffusion coefficient of glissile SIA clusters of size x. The sink strength of the glissile cluster can be written as:

$$k_\mathrm{g}^2 = 2\left(\frac{\pi r_\mathrm{d} \rho_\mathrm{d}}{2} + \pi r_\mathrm{V}^2 \rho_\mathrm{V} + \sigma_\mathrm{vcl}\rho_\mathrm{vcl} + \sigma_\mathrm{icl}\rho_\mathrm{icl}\right)^2, \tag{8.180}$$

where σ_vcl and σ_icl are the interaction cross sections and ρ_vcl and ρ_icl the number densities of the sessile vacancy and mobile SIA clusters, respectively. Note that σ_vcl and σ_icl are proportional to the product of the loop circumference and the corresponding capture radius, similar to r_d for dislocations.

Swelling can be calculated from the solutions of Eqs. (8.179) and (8.110). Writing Eqs. (8.179) to include the individual sink strengths from Eqs. (8.173) yields:

$$\begin{aligned}
\frac{\mathrm{d}C_\mathrm{v}}{\mathrm{d}t} &= K_0(1-\varepsilon_\mathrm{r})(1-\varepsilon_\mathrm{v}) - (k_\mathrm{V}^2 + z_\mathrm{v}^\mathrm{d}\rho_d + z_\mathrm{v}^\mathrm{icl} k_\mathrm{icl}^2 + z_\mathrm{v}^\mathrm{vcl} k_\mathrm{vcl}^2) D_\mathrm{v} C_\mathrm{v} - K_\mathrm{iv} D_\mathrm{i} C_\mathrm{i} C_\mathrm{v} + L_\mathrm{v} \\
\frac{\mathrm{d}C_\mathrm{i}}{\mathrm{d}t} &= K_0(1-\varepsilon_\mathrm{r})(1-\varepsilon_\mathrm{i}) - (k_\mathrm{V}^2 + z_\mathrm{v}^\mathrm{d}\rho_\mathrm{d} + z_\mathrm{i}^\mathrm{icl} k_\mathrm{icl}^2 + z_\mathrm{i}^\mathrm{vcl} k_\mathrm{vcl}^2) D_\mathrm{i} C_\mathrm{i} - K_\mathrm{iv} D_\mathrm{i} C_\mathrm{i} C_\mathrm{v} \\
\frac{\mathrm{d}C_\mathrm{gicl}}{\mathrm{d}t} &= K_\mathrm{gicl} - D_\mathrm{gicl} C_\mathrm{gicl} k_\mathrm{g}^2 = K_\mathrm{gicl} - 2 D_\mathrm{gicl} C_\mathrm{gicl} \left(\frac{\pi r_\mathrm{d} \rho_\mathrm{d}}{2} + \pi r_\mathrm{V}^2 \rho_\mathrm{V} + \sigma_\mathrm{vcl}\rho_\mathrm{vcl} + \sigma_\mathrm{icl}\rho_\mathrm{icl}\right)^2,
\end{aligned} \tag{8.181}$$

At steady state and neglecting recombination, Eqs. (8.181) becomes:

$$\begin{aligned} K_{\mathrm{v}} &= D_{\mathrm{v}}C_{\mathrm{v}}(k_{\mathrm{V}}^2 + z_{\mathrm{v}}^{\mathrm{d}}\rho_{\mathrm{d}}) + D_{\mathrm{v}}C_{\mathrm{v}}z_{\mathrm{v}}^{\mathrm{icl}}k_{\mathrm{icl}}^2 + D_{\mathrm{v}}C_{\mathrm{v}}z_{\mathrm{v}}^{\mathrm{vcl}}k_{\mathrm{vcl}}^2 + 2D_{\mathrm{v}}C_{\mathrm{v}}\Lambda x_{\mathrm{g}}\sigma_{\mathrm{icl}}\rho_{\mathrm{icl}} \\ K_{\mathrm{i}} &= D_{\mathrm{i}}C_{\mathrm{i}}(k_{\mathrm{V}}^2 + z_{\mathrm{v}}^{\mathrm{d}}\rho_{\mathrm{d}}) + D_{\mathrm{v}}C_{\mathrm{v}}z_{\mathrm{v}}^{\mathrm{icl}}k_{\mathrm{icl}}^2 + D_{\mathrm{i}}C_{\mathrm{i}}z_{\mathrm{v}}^{\mathrm{vcl}}k_{\mathrm{vcl}}^2 - 2D_{\mathrm{v}}C_{\mathrm{v}}\Lambda x_{\mathrm{g}}\sigma_{\mathrm{icl}}\rho_{\mathrm{icl}} \\ K_{\mathrm{gicl}} &= D_{\mathrm{gicl}}C_{\mathrm{gicl}}k_{\mathrm{g}}^2, \end{aligned} \tag{8.182}$$

where

$$\begin{aligned} K_{\mathrm{v}} &= K_0(1-\varepsilon_{\mathrm{r}})(1-\varepsilon_{\mathrm{v}}) \\ K_{\mathrm{i}} &= K_0(1-\varepsilon_{\mathrm{r}})(1-\varepsilon_{\mathrm{i}}), \end{aligned} \tag{8.183}$$

and $\Lambda = \sqrt{k_{\mathrm{g}}^2/2}$.

The vacancy supersaturation is obtained from the difference between $D_{\mathrm{v}}C_{\mathrm{v}}$ and $D_{\mathrm{i}}C_{\mathrm{i}}$ using the first two equations in Eqs. (8.182):

$$D_{\mathrm{v}}C_{\mathrm{v}} - D_{\mathrm{i}}C_{\mathrm{i}} = B_{\mathrm{d}}\frac{z_{\mathrm{v}}^{\mathrm{d}}\rho_{\mathrm{d}}}{k_{\mathrm{V}}^2 + z_{\mathrm{v}}^{\mathrm{d}}\rho_{\mathrm{d}}}D_{\mathrm{v}}C_{\mathrm{v}} + \frac{\varepsilon_{\mathrm{i}}^{g}K_0(1-\varepsilon_{\mathrm{r}})}{k_{\mathrm{V}}^2 + z_{\mathrm{v}}^{\mathrm{d}}\rho_{\mathrm{d}}}\left(1 - \frac{\sigma_{\mathrm{vcl}}\rho_{\mathrm{vcl}} + \sigma_{\mathrm{icl}}\rho_{\mathrm{icl}}}{\Lambda}\right), \tag{8.184}$$

where $\varepsilon_{\mathrm{i}}^{\mathrm{g}}$ is the fraction of interstitials in glissile clusters and B_{d} is the dislocation bias term given by $B_{\mathrm{d}} = (z_{\mathrm{i}}^{\mathrm{d}} - z_{\mathrm{v}}^{\mathrm{d}})/z_{\mathrm{v}}^{\mathrm{d}}$. The swelling rate is given by:

$$\frac{\mathrm{d}(\Delta V/V)_{\mathrm{pb}}}{\mathrm{d}t} = k_{\mathrm{V}}^2(D_{\mathrm{v}}C_{\mathrm{v}} - D_{\mathrm{i}}C_{\mathrm{i}}) - 2D_{\mathrm{icl}}^{\mathrm{g}}C_{\mathrm{icl}}^{\mathrm{g}}x_{\mathrm{g}}\Lambda\pi r_{\mathrm{V}}^2\rho_{\mathrm{V}}, \tag{8.185}$$

and substituting Eq. (8.184) into Eq. (8.185), the swelling rate becomes:

$$\begin{aligned} \frac{\mathrm{d}(\Delta V/V)_{\mathrm{pb}}}{\mathrm{d}t} = K_0(1-\varepsilon_{\mathrm{r}})\Bigg\{ & B_{\mathrm{d}}\frac{k_{\mathrm{V}}^2 z_{\mathrm{v}}^{\mathrm{d}}\rho_{\mathrm{d}}}{(k_{\mathrm{V}}^2 + z_{\mathrm{v}}^{\mathrm{d}}\rho_{\mathrm{d}})(k_{\mathrm{V}}^2 + z_{\mathrm{v}}^{\mathrm{d}}\rho_{\mathrm{d}} + z_{\mathrm{v}}^{\mathrm{icl}}k_{\mathrm{icl}}^2 + z_{\mathrm{v}}^{\mathrm{vcl}}k_{\mathrm{vcl}}^2)} \\ & + \varepsilon_{\mathrm{i}}^{g}\left[\frac{k_{\mathrm{V}}^2}{k_{\mathrm{V}}^2 + z_{\mathrm{v}}^{\mathrm{d}}\rho_{\mathrm{d}}}\left(1 - \frac{\sigma_{\mathrm{vcl}}\rho_{\mathrm{vcl}} + \sigma_{\mathrm{icl}}\rho_{\mathrm{icl}}}{\Lambda}\right) - \frac{\pi r_V^2\rho_V}{\Lambda}\right]\Bigg\}. \end{aligned} \tag{8.186}$$

The first term in brackets on the right-hand side of Eq. (8.186) represents the influence of the dislocation bias, and the second one describes the production bias. The factor $(1 - \varepsilon_{\mathrm{r}})$ accounts for the intracascade recombination of defects, which is a function of the recoil energy and reduces the rate of defect production compared to the NRT value, K_0. Swelling rate is also a function of recoil energy by virtue of the dependence on $\varepsilon_{\mathrm{i}}^{\mathrm{g}}$, which increases with PKA energy up to about 10–20 keV.

The effect of the two biases, dislocation and production, are quite different. The dislocation bias depends only on the microstructure and predicts continued void growth. The production bias can be positive or negative, depending on the

microstructure. The first term in Eq. (8.186) decreases the effect of production bias due to recombination of the SIA clusters at sessile vacancy and SIA clusters, while the second term arises from the capture of SIA clusters by voids. The latter term may become equal to zero or even negative; hence, the combination of the two bias factors does not necessarily lead to a higher swelling rate.

Considering only Frenkel pair production, the swelling rate given by Eq. (8.122) predicts that the swelling rate will be small at a low dislocation density. If this is the case, then the swelling rate in well-annealed metals at low doses should be small. Experiments have shown that the void swelling rate in fully annealed pure copper irradiated with fission neutrons up to about 0.01 dpa is ~ 1 %/dpa [32], which is similar to the maximum swelling rate found in materials at high doses. Referring to Eq. (8.186), in annealed materials, the dislocation bias term is negligible. At low doses, the void size is small, and therefore, the void cross section for the interaction with SIA glissile clusters ($\pi r_V^2 \rho_V / \Lambda$) is small. (Also, at low dose, the cluster density will be small, so the term in parentheses in the second line of Eq. (8.186) ~ 1). Thus, the swelling rate is driven by the production bias:

$$\frac{\mathrm{d}(\Delta V/V)}{\mathrm{d}t} \approx K_0(1-\varepsilon_\mathrm{r})\varepsilon_\mathrm{i}^\mathrm{g} \frac{k_V^2}{k_V^2 + z_\mathrm{v}^\mathrm{d}\rho_\mathrm{d}}. \tag{8.187}$$

When $z_\mathrm{v}^\mathrm{d}\rho_\mathrm{d} \ll k_V^2$, the swelling rate is determined by the cascade parameters:

$$\frac{\mathrm{d}(\Delta V/V)}{\mathrm{d}t} \approx K_0(1-\varepsilon_\mathrm{r})\varepsilon_\mathrm{i}^\mathrm{g}. \tag{8.188}$$

Note that the swelling rate given in Eq. (8.188) is the maximum swelling rate that can be achieved by production bias. Referring to Eq. (8.187) and assuming that there is no interaction of mobile SIA clusters with voids and sessile clusters, the swelling rate is given by:

$$\frac{\mathrm{d}(\Delta V/V)}{\mathrm{d}t} \approx 1/2 K_0(1-\varepsilon_\mathrm{r})\varepsilon_\mathrm{i}^\mathrm{g}, \tag{8.189}$$

where the sink strength ratio, $\frac{k_V^2}{k_V^2 + z_\mathrm{v}^\mathrm{d}\rho_\mathrm{d}} = ½$, the value achieved when $Q = 1$ in Eq. (8.148). Data have shown that $1 - \varepsilon_\mathrm{r} = 0.01$ and $\varepsilon_\mathrm{i}^\mathrm{g}$ in good agreement with MD simulations of cascades, yielding a maximum swelling rate of ~ 1 %/dpa.

Production bias helps to explain some additional observations. Golubov et al. [31] and Singh et al. [34] compared the microstructure of annealed copper irradiated with 2.5 MeV electrons, 3 MeV protons, and fission neutrons at ~ 520 K. For all irradiations, the damage rate was $\sim 10^{-8}$ dpa/s. The average recoil energies were estimated to be about 0.05, 1, and 60 keV, respectively, and the primary damage form was Frenkel pairs for electrons, small cascades for protons, and large cascades for neutrons. Thus, the cascade efficiency $(1 - \varepsilon_\mathrm{r})$ was highest for electrons and lowest for neutrons. If dislocation bias is responsible for swelling, then the swelling rate is

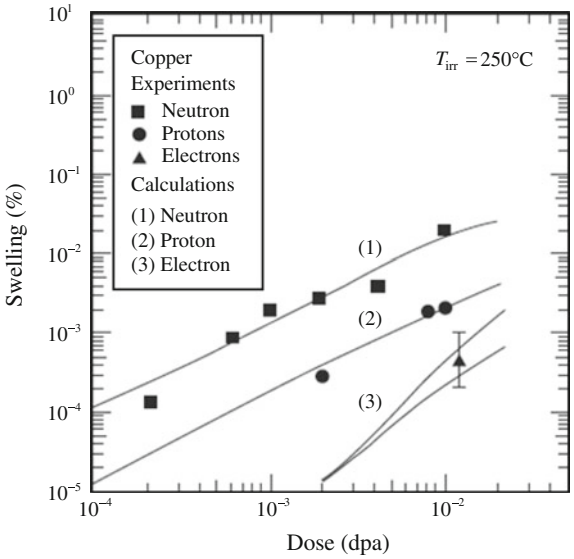

Fig. 8.31 Experimentally measured and calculated void swelling in pure copper after irradiation with 2.5 MeV electrons, 3 MeV protons, and fission neutrons. The calculations were performed in the framework of the Frenkel pair 3D model (PF3DM) for electron irradiation and using the production bias model (PBM) for irradiation with protons and fission neutrons (after [31])

proportional to the damage rate and must be highest for electron irradiation and lowest for neutron irradiation. Figure 8.31 shows just the opposite with a swelling rate for neutron irradiation of about 50 times that for electrons, with protons in between. These results can be understood from Eq. (8.186). Under electron irradiation, only the first term on the right-hand side operates as $\varepsilon_i^{\mathrm{g}} = 0$. The swelling rate is low in this case because of the low dislocation density. Under cascade damage conditions, the damage rate is smaller because of the low cascade efficiency. But in this case, $\varepsilon_{\mathrm{i}}^{\mathrm{g}} \neq 0$ and the second term on the right-hand side of Eq. (8.186) is dominant.

Cascade production of SIA clusters can also affect the nucleation of voids through damage accumulation. The sink strengths of the clusters, k_{vcl}^2 and k_{icl}^2, at steady state are given by [31]:

$$k_{\mathrm{vcl}}^2 = \frac{\varepsilon_{\mathrm{v}}^{\mathrm{s}} K_{\mathrm{v}}}{D_{\mathrm{v}} \exp(-E_{\mathrm{vcl}}/kT)(k_V^2 + z_{\mathrm{v}}^{\mathrm{d}}\rho_{\mathrm{d}}) - \varepsilon_{\mathrm{i}}^{\mathrm{g}} K_{\mathrm{v}}} (k_V^2 + z_{\mathrm{v}}^{\mathrm{d}}\rho_{\mathrm{d}}) \left(1 - \frac{1}{x_{\mathrm{vcl}}^{\mathrm{s}}}\right) \tag{8.190}$$

$$k_{\mathrm{icl}}^2 = \frac{\varepsilon_{\mathrm{i}}^{\mathrm{s}}}{\varepsilon_{\mathrm{i}}^{\mathrm{g}}} (k_{\mathrm{V}}^2 + z_{\mathrm{v}}^{\mathrm{d}}\rho_{\mathrm{d}}) \left(1 - \frac{1}{x_{\mathrm{icl}}^{\mathrm{s}}}\right), \tag{8.191}$$

where E_{vcl} is an effective binding energy of vacancies with the vacancy clusters, $x_{\mathrm{vcl,\,icl}}$ are the mean sizes of the vacancy and SIA glissile clusters, and $\varepsilon_{\mathrm{i}}^{\mathrm{s,g}}$ are the fraction of interstitials in sessile (s) and glissile (g) clusters. From Eq. (8.191), the

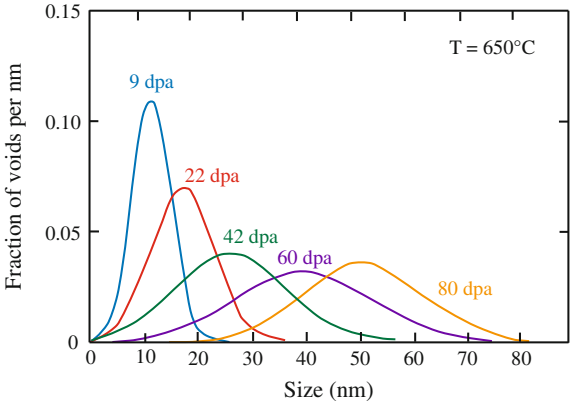

Fig. 8.32 Experimentally measured void size distribution in a Fe–Cr–Ni alloy irradiated at 650 °C (after [33])

steady-state sink strength of sessile SIA clusters is inversely proportional to the fraction of SIAs produced in cascades in the form of mobile SIA clusters, and thus, $k_{\mathrm{icl}}^2 \rightarrow \infty$ when $\varepsilon_{\mathrm{i}}^{\mathrm{g}} \rightarrow 0$, or as the fraction of interstitials in glissile clusters goes to zero, the sink strength of the (sessile) clusters approaches infinity. Such a case may be reached in large cascades as produced from neutron irradiation combined with impurities that may provide cluster immobilization. The "incubation period" of swelling observed in many alloys may be due to this process. A possible scenario may be that during the incubation period, the material is purified by RIS on SIA clusters because of their high density. At high enough doses, the high number density of SIA clusters decreases via the absorption of excess vacancies, restoring conditions for damage accumulation and consequent void growth.

As presented in the description of clusters using the Fokker–Planck formulation (Sect. 7.6), it was noted that the cluster size distribution is broadened by the parameter D and shifted by the parameter F. Thus, with increasing dose, the solution to the Fokker–Planck equation describes the broadening of the void size distribution and the increase in the mean void size of the distribution with dose. This general behavior can be compared with experimental swelling results for Fe–Cr–Ni irradiated at 650 °C. Figure 8.32 shows that the mean size of the distribution increases from about 11 nm at 9 dpa to over 50 nm by 80 dpa with a corresponding broadening of the distribution. Since swelling is mainly sensitive to the shift of the mean size of the distribution, linear swelling ($\Delta V/V \propto$ dose) is obtained when the growth rate is large compared to the diffusional broadening, in which case the swelling rate is then given by the drift force alone.

8.3.7 Stress Dependence

Equation (8.125) shows that the void growth rate consists of two components. $\dot{R}_{\mathrm{th}}$ is the thermal emission term and hence is the only part affected by the state of stress or

internal gas pressure. Consequently, the internal gas pressure and stress begin to affect the growth rate only when $\dot{R}_{\text{th}}$ becomes significant, i.e., for temperatures greater than the peak swelling temperature. When the solid is under a hydrostatic stress and when voids contain gas that exerts a pressure on the void surface, the equilibrium vacancy concentration at voids and dislocations will be different from that in the stress-free, gas-free state. Brailsford and Bullough showed that the pressure, but not the external stress, will affect the concentration of vacancies in equilibrium with the void. Hence, the force balance for the gas-containing void in mechanical equilibrium, as in Eq. (8.82), becomes:

$$\sigma = p - \frac{2\gamma}{R}, \tag{8.192}$$

where σ is the hydrostatic stress and p is the gas pressure in the void. (In the case of a non-equilibrium bubble, the appropriate stress is the radial component of the stress tensor, σ_{r}.) The vacancy concentration at the surface of the void, given by Eq. (8.85) in the gas-free case, becomes:

$$C_{\text{v}}^{\text{V}} = C_{\text{v}}^{0} \exp\left[-\frac{\Omega}{kT}\left(p - \frac{2\gamma}{R}\right)\right]. \tag{8.193}$$

Similarly, the equilibrium vacancy concentration adjacent to the network dislocations becomes:

$$C_{\text{v}}^{\text{N}} = C_{\text{v}}^{0} \exp\left[-\frac{\sigma\Omega}{kT}\right]. \tag{8.194}$$

Repeating the solution to the void growth equation using the equilibrium vacancy concentration at the void surface given by Eq. (8.193) and the equilibrium vacancy concentration at the network dislocations given by Eq. (8.194) revises the thermal emission term, R_{th}, in Eq. (8.135) (with $\rho_{\text{CP}} = \rho_{\text{L}} = 0$) as follows:

$$\dot{R}_{\text{th}} = \frac{D_{\text{v}} C_{\text{v}}^{0} \Omega^2 z_{\text{v}} \rho_{\text{d}} \left(\sigma + p - \frac{2\gamma}{R}\right)}{RkT(z_{\text{v}}\rho_{\text{d}} + 4\pi R \rho_{\text{V}})}. \tag{8.195}$$

Note that shrinkage due to thermal emission becomes instead stress-enhanced growth when the sum of the external stress and gas pressure exceeds the stress due to surface tension:

$$\sigma + p > \frac{2\gamma}{R}. \tag{8.196}$$

Note that for a stressed solid containing no gas, stress-enhanced growth will occur when $\sigma > \frac{2\gamma}{R}$. For a void containing x gas atoms, Eq. (8.196) becomes:

$$\sigma = \frac{2\gamma}{R} - \left(\frac{3xkT}{4\pi R^3}\right). \tag{8.197}$$

The void radius at which $\frac{d\sigma}{dR} = 0$ is called the critical void radius and is given by:

$$R_{cr} = \left(\frac{9xkT}{8\pi\gamma}\right)^{1/2}, \tag{8.198}$$

and substituting into Eq. (8.197) gives the stress at the critical void size, which is the critical stress for unlimited void growth:

$$\sigma_{cr} = \frac{4\gamma}{3}\left(\frac{8\pi\gamma}{9xkT}\right)^{1/2}. \tag{8.199}$$

The effect of stress on void growth in steel is given in Fig. 8.33. Note that there is little effect of stress out to high dose when the stress is low. But when stress is increased, the swelling increases rapidly at relatively lower doses. Figure 8.34 also accounts for the presence of helium in the growth of voids under stress.

However, this formulation predicts that the void growth rate is proportional to stress, which is counter to the 1 %/dpa observations. Also, as shown in Fig. 8.34, the effect of stress is only significant at very high temperatures. Experimental data have since shown that the prime role of stress is on shortening the transient swelling regime, rather than increasing the swelling rate in the steady-state regime. Figure 8.35 shows the effect of stress on swelling in modified 316 stainless steel alloys irradiated in the PHENIX reactor. Note that with increasing stress, the swelling rate (slope) approaches a constant value at lower doses. Stress can also

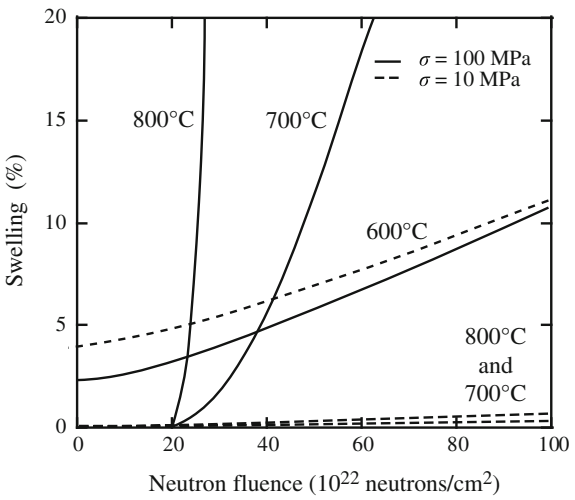

Fig. 8.33 Stress-enhanced swelling for various stress levels and temperatures as a function of fluence (after [35])

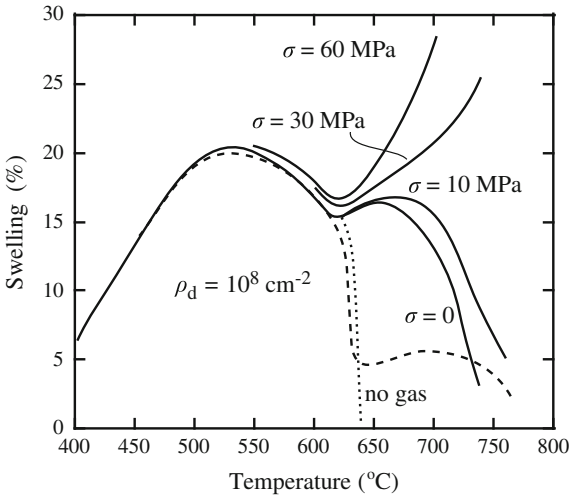

Fig. 8.34 Temperature dependence of stress-enhanced void growth in steel. The *solid curves* apply to a dislocation density of 10^8 cm^{-2} and a helium production rate of 10^{-6} appm/s (after [36])

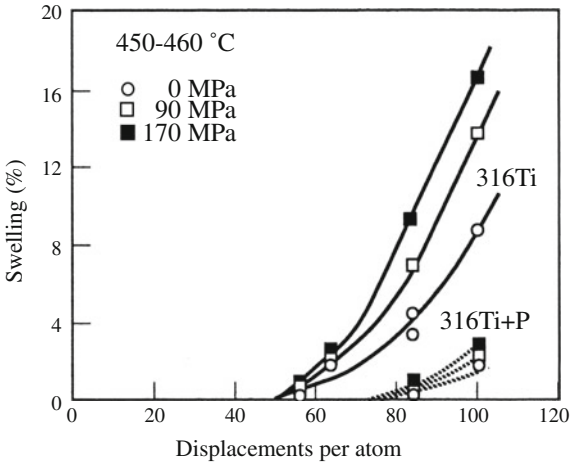

Fig. 8.35 Effect of stress on swelling of two modified 316 stainless steels irradiated in the form of pressurized tubes in the PHENIX reactor (after [37])

affect the stability of void nuclei, which would explain the observation of more rapid nucleation.

In the development of the nucleation rate of voids, the nucleation current and number density of voids of size n were described by Eqs. (8.18) and (8.19), respectively, for the case of vacancy condensation excluding interstitials:

$$J_n = Z\beta N_0 \exp\left(\frac{-\Delta G_n^0}{kT}\right), \quad \text{and} \quad \rho^0(n) = N_0 \exp\left(\frac{-\Delta G_n^0}{kT}\right).$$

with the free energy of formation of void of size n given by Eq. (8.17):

$$\Delta G_n^0 = -nkT \ln S_v + \left(36\pi\Omega^2\right)^{1/3} \gamma n^{2/3}.$$

Accounting for the application of an external hydrostatic stress, σ_h, gives:

$$\Delta G_n^0(\sigma_h) = -nkT \ln S_v + \left(36\pi\Omega^2\right)^{1/3} \gamma n^{2/3} - n\sigma_h \Omega, \tag{8.200}$$

and

$$\Delta G_n^0(\sigma_h) = \Delta G_n^0(0) + n\sigma_h \Omega. \tag{8.201}$$

Note that the effect of gas pressure, p, in the void can also be accounted for by the addition of a term, $np\Omega$.

When interstitials are present, the free energy is given by Eq. (8.33):

$$\Delta G_n' = kT \sum_{j=0}^{n-1} \ln \left[\frac{\beta_i(j+1)}{\beta_v(j)} + \exp\left(\frac{\delta G_j^0}{kT} \right) \right],$$

where δG_j^0 is the increment in free energy of a void in going from j vacancies to $j + 1$ vacancies if no interstitials are present. By assuming that stress affects only the free energy barrier (and not the critical nucleus size) and that the stress contribution of the energy per atom is not dependent on the number of atoms in the cluster, then we can approximate the free energy in Eq. (8.33) in a manner similar to that done in Eq. (8.201) [38]:

$$\Delta G_n'(\sigma_h) = \Delta G_n'(0) + n\sigma_h \Omega. \tag{8.202}$$

Then, from Eq. (8.35), the ratio of stressed to unstressed steady-state nucleation rates in a homogeneous, coprecipitation environment is:

$$\frac{J_n(\sigma_h)}{J_n(0)} = \frac{\exp\left[-\left(\Delta G_n' - n\sigma_h \Omega\right)/kT\right]}{\exp\left[-\Delta G_n'/kT\right]}. \tag{8.203}$$

Using Eqs. (8.22) and (8.23) to write the ratio of nucleation currents in terms of the ratio of void number densities in the stressed and unstressed states gives:

$$\frac{J_n(\sigma_h)}{J_n(0)} = \frac{Z'(\sigma_h)\beta_n(\sigma_h)\rho_n(\sigma_h)}{Z'(0)\beta_n(0)\rho_n(0)} = \frac{Z'(\sigma_h)\beta_n(\sigma_h)\exp\left[-\left(\Delta G_n'(\sigma_h)\right)\right]}{Z'(0)\beta_n(0)\exp\left[-\Delta G_n'(0)\right]}, \tag{8.204}$$

and provided that neither the arrival rate ratio, $\beta_n(\sigma_h)/\beta_n(0)$, nor Z' is sensitive to the stress level [39], then Eq. (8.204) becomes:

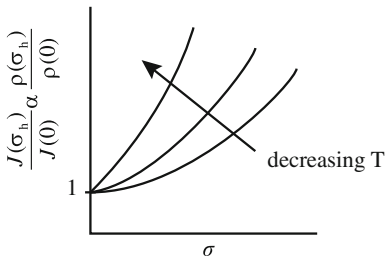

Fig. 8.36 Variation of the void nucleation rate and the void number density as a function of stress and temperature, as described by Eq. (8.205)

$$\frac{\rho_n(\sigma_h)}{\rho_n(0)} \approx \exp(n\sigma_h \Omega/kT). \tag{8.205}$$

Example 8.1 Effect of stress on void density

Assuming an external stress of 100 MPa and a void cluster size of ~15 at a temperature of 450 °C, Eq. (8.205) gives an increase in the void number density by a factor of ~6. However, for a stress of 200 MPa, the increase is 34, and for 300 MPa, the factor becomes ~200. Since both stress and temperature appear in the exponent, the factor rises rapidly with an increase in stress and with a decrease in temperature (Fig. 8.36). Referring back to Fig. 8.35, the decreasing time to reach the steady-state swelling rate as stress is increased is explainable by stress-enhanced nucleation, which will be more important at lower temperatures, contrary to the effect of stress on the steady-state swelling rate.

8.3.8 *Effect of RIS*

Recall from Chap. 6, Sect. 6.4, that RIS (radiation-induced segregation) of alloying elements occurs at sinks, which can include voids. The result is a *coated void* in which the void develops a shell of composition that is different from that in the matrix. As we have seen, for austenitic stainless steels, the void coating is enriched in nickel and depleted in chromium relative to the matrix. A primary effect of the composition change is a change in diffusion coefficient leading to a change in the void capture efficiency. The capture efficiency for the vacancy in the shell is [16, 40]:

$$z_v^V(r_V) = \frac{1 + \delta/r_V}{1 + D_v \delta / D_v^S r_V}, \tag{8.206}$$

where r_V is the void radius, δ is the thickness of the shell, and D_v^S is the vacancy diffusion coefficient in the shell. Recall that an expression for the composition dependence of D_v in the shell, D_v^S, was determined in Sect. 6.4 of Chap. 6. Using the expression for the capture efficiency in the void growth equations results in a reduction in void growth if $D_v^S < D_v$ and $D_i^S \sim D_i$.

A more important effect of the coating is the elastic interaction between a point defect and a void surrounded with a coating that has different elastic constants than the matrix. The result is a change in capture efficiency of the void for defects. The capture efficiency due to a difference in elastic constants is given as:

$$z_{i,v}^V(r_V) = \left[\frac{r_V}{r_c} + \frac{r_V}{(r_c+\delta)^2}\frac{D_{i,v}}{w_{i,v}}\right]^{-1}, \tag{8.207}$$

where r_c is the void plus coating radius and the transfer velocity, $w_{i,v}$, is

$$w_{i,v} = \frac{D_{i,v}\exp\left(-E_{i,v}^*/kT\right)}{a}, \tag{8.208}$$

where a is the lattice parameter and E^* is the repulsive interaction energy at its largest positive value. The sign of E^* is positive (repulsion) if the matrix of the shell is stiffer than that of the matrix. Since E^* is proportional to the square of the point defect relaxation volume, the sink efficiency is much smaller for the interstitial than for the vacancy due to the larger repulsion for the interstitial. So the stiffer shell results in a repulsion that is greater for the interstitial than for the vacancy, making void nucleation and growth more rapid in the case of a coated void (Fig. 8.37).

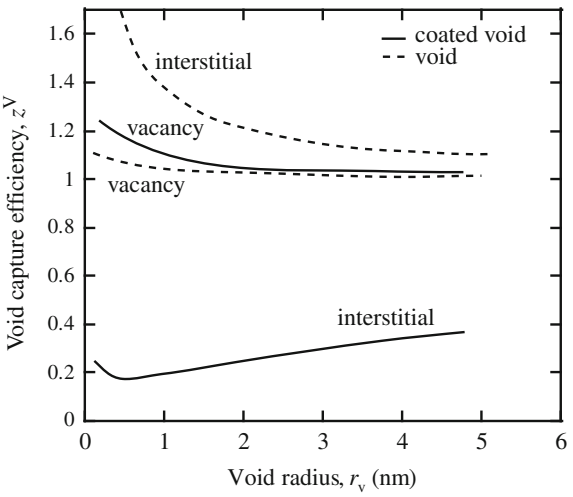

Fig. 8.37 Capture efficiencies for point defect diffusion to a void and a coated void as a function of void radius, r_V. The void prefers interstitials, especially at small void sizes. The preference is reversed for the coated void (after [16])

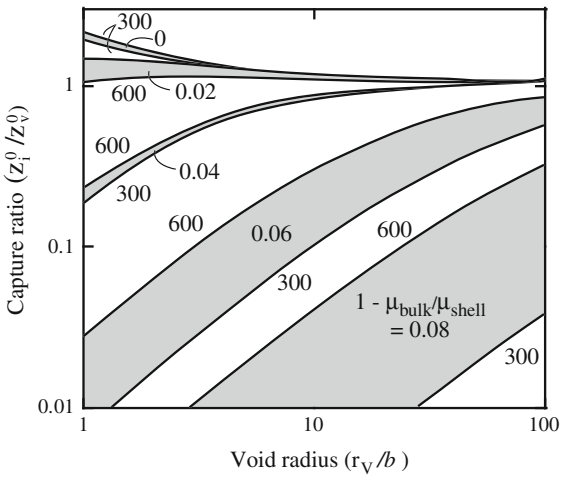

Fig. 8.38 Capture ratio z_i^0/z_v^0 for coated voids with a shell thickness of two atomic layers and zero surface stress (after [41])

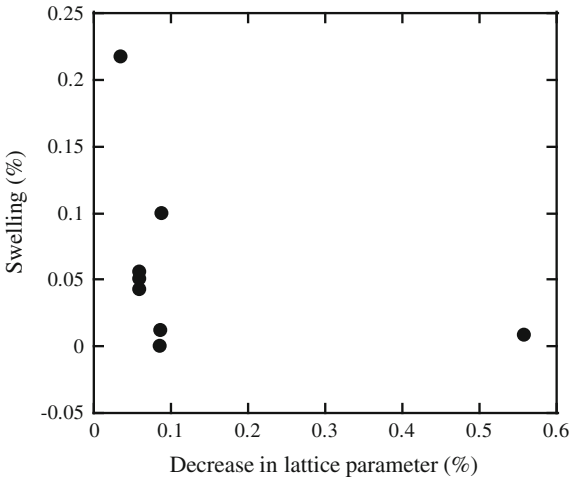

Fig. 8.39 Decrease in swelling as a function of changing lattice parameter. Swelling decreases with decreasing lattice parameter, which is caused by RIS at the void surface (after [42])

A change in the shear modulus or lattice parameter in the shell can also alter the preference of the void for vacancies and interstitials [41] by creating a barrier to defect diffusion through the shell due to a change in the strain energy. When segregation leads to a shell with a shear modulus or lattice parameter only slightly higher than in the surrounding matrix, the void becomes a highly preferential sink for vacancies and swelling is increased. Conversely, a reduction in the shear modulus and lattice parameter should result in reduced void swelling. Figure 8.38 shows the effect of the shear modulus ($1 - \mu_{bulk}/\mu_{shell}$) on the interstitial/vacancy capture ratio. For small voids, a few percent change in the shear modulus can result in orders of magnitude change in the capture ratio. Allen et al. [42] compared the

swelling and RIS behavior of a range of alloys with different nickel content. Calculation of the lattice parameter for the void shell composition shows that the swelling behavior can be explained by a decrease in lattice parameter at the void surface (Fig. 8.39). In fact, segregation leads to a smaller lattice parameter with a lower shear modulus, and the *softer* shell reduces void swelling.

8.3.9 Void Lattices

Voids have also been found to organize themselves in periodic arrays or lattices in a metal under irradiation and also in periodic walls of defect clusters. Figure 8.40(a) shows a void lattice in bcc Nb following irradiation with 8.5 MeV Ta^+ to a dose of 300 dpa at 800 °C, and Fig. 8.40(b) shows a periodic array of planar {001} walls of defects in Cu at 3 dpa. The lattices are much easier to form in bcc metals than in fcc metals, though lattices have been observed in Ni, Al, and stainless steel. Their formation is independent of the type of irradiating particle as long as cascades are produced. Void lattices are a form of self-organization that occurs as responses of complex systems to external stimuli. It is believed that self-organization results from the collective interaction between system components under external forces that drive the system far from equilibrium. In irradiated solids, the void patterns are believed to be linked to the collective action of the point defects on the lattice structure. Wall formation is restricted to a temperature range between 0.2 and 0.4 T_m, while void lattice formation occurs at somewhat higher temperatures. Characteristic is the partial or complete isomorphy of the ordered defect structure with the host lattice [44].

A full understanding of the formation of void lattices is still lacking, but the theory is able to account for many of the parametric effects in lattice formation. Kinetic rate theory and the determination of an instability threshold can explain many of the observations to date. Transport and reactions of defects during bombardment have been modeled by nonlinear diffusion–reaction equations for the cases of periodic defect walls and of void lattices. The isotropic diffusion–reaction models can describe conditions for the destabilization of the homogeneous defect cluster distributions and predict characteristic periodicity lengths but have to be modified substantially to account for the structural and orientation relationships between ordered defect arrangements and crystal structure. Possible reasons for these properties are (1) elastic interactions between defects that are probably important in wall formation and (2) low-dimensional defect transport that is probably important for void and bubble lattice formation. In general, ordered defect structures form when the following general conditions are satisfied [43]:

1. Agglomeration of vacancies into clusters during the collisional phase of cascade cooling.
2. A bias for dislocations toward preferential absorption of interstitials over vacancies.

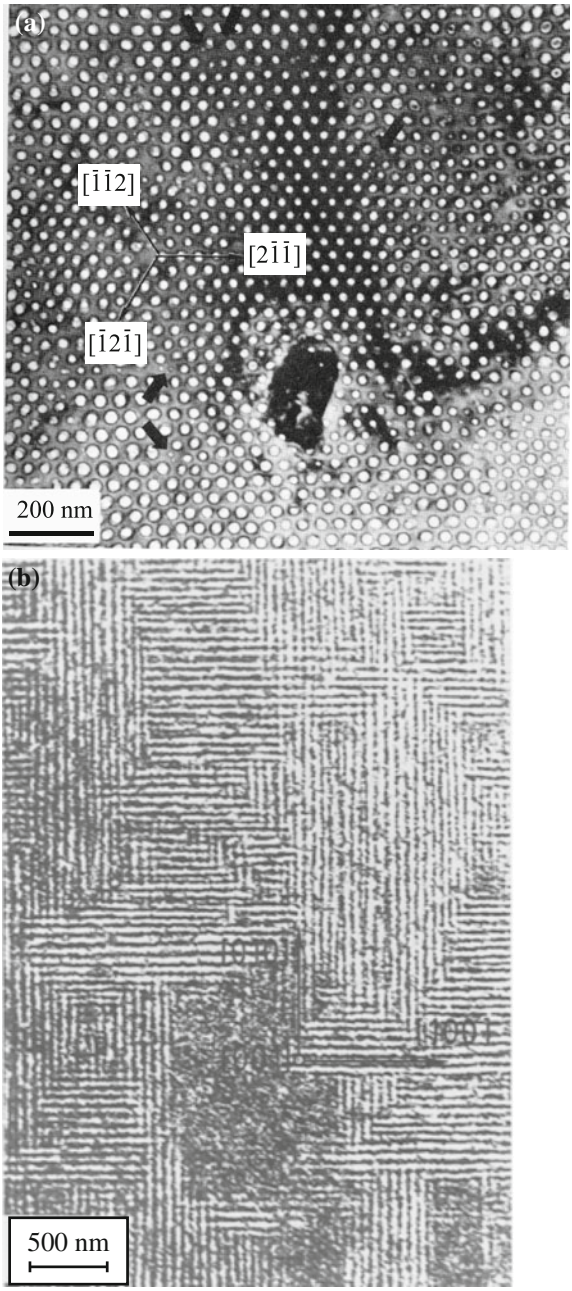

Fig. 8.40 Void lattice in (**a**) Nb irradiated with 8.5 MeV Ta^+ at 800 °C to 300 dpa (after [43]) and (**b**) periodic arrays of planar {001} walls of defects in Cu irradiated to 0.65 dpa (after [44])

3. An asymmetry in the production and diffusion of mobile point defects (production bias).
4. Some degree of anisotropy during the evolution of clustered defects. This could be triggered either by diffusional anisotropies of point defects, or by anisotropic elastic interaction between defect clusters during the latter stages of their evolution.

Two features of void ordering are as follows: (1) The symmetry and crystallographic orientation of a void lattice are always the same as those of the host lattice and (2) the void lattices are formed under neutron and heavy ion but not electron irradiation. The occurrence of void lattice formation under cascade damage conditions (neutron or ion irradiation) and its absence under single Frenkel pair production (electron irradiation) are strong evidence for a key role of the 1D motion of thermally stable SIA clusters directly produced in cascades. In cubic metals, void ordering is probably due to one-dimensional SIA loop glide. This mechanism would also provide an explanation for the enhanced swelling adjacent to grain boundaries. The role of crowdions is unclear because of their limited effective diffusion range [44]. However, it has been shown that when there is anisotropic transport of self-interstitial atoms by the crowdion mechanism (i.e., transport in which some crystal directions are preferred over others), voids occupying spatial positions that form a regular lattice grow faster, on average, than the randomly distributed voids [45]. However, for the void lattice to form, randomly distributed voids have to disappear. This can occur through stochastic void coarsening. Since void evolution in this case is sensitive to the spatial variations in the void growth rate, even a small fraction of interstitials moving as crowdions can significantly affect the spatial behavior of the void ensemble, resulting in the dissolution of randomly distributed voids with lower growth rates by stochastic fluctuations, and the nucleation and growth of voids forming a regular lattice. A general result of all models proposed to explain void lattice formation is that the existence of fundamental asymmetries in the behavior of v-type and SIA-type defects (production, diffusion, and annihilation), in spite of their principle particle–antiparticle relation, is a necessary prerequisite for the formation of ordered defect structures in metals under particle bombardment [44].

8.3.10 Effect of Microstructure and Composition

The alloy microstructure can exert significant effects on void nucleation and growth. Microstructure features such as composition, solute addition, and precipitate structure are among the most important in influencing void behavior.

Major Element Composition

In simple Fe–Cr–Ni austenitic alloys, swelling drops dramatically with increasing nickel content, reaching a minimum at about 50 at.%. Figure 8.41 shows that the

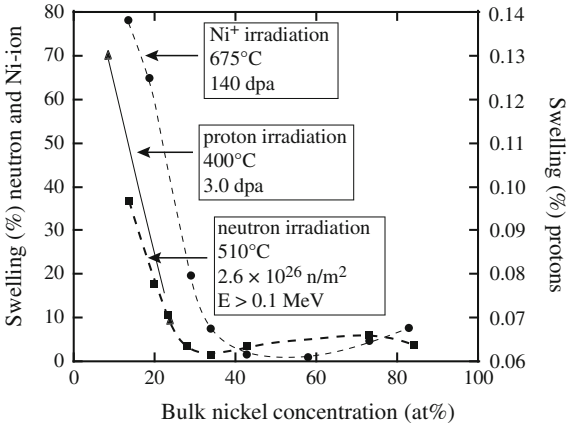

Fig. 8.41 The effect of bulk nickel concentration on swelling resulting from irradiation with different particles: neutrons, nickel ions, and protons (after [42])

swelling dependence of nickel holds for various particle irradiations. The effect of Ni content on swelling is primarily due to the change in incubation dose as shown in Fig. 8.42. In fact, the data in Fig. 8.43 show that at steady state, the swelling rate is the same over a wide range of nickel content.

Chromium content also affects swelling of austenitic alloys. Figure 8.44 shows that increasing chromium over the range 15 to 30 % results in greater swelling. Less data are available on the systematic effect of Cr than for Ni, but the available data suggest that swelling increases monotonically with Cr content. Swelling is much less of a problem in ferritic alloys, but reaches a maximum with a chromium content of about 15 at.%. Figure 8.45 summarizes the effect of Ni and Cr on swelling in Fe–Cr–Ni alloys at 675 °C.

Solute Additions

Void swelling should be inhibited by additions of minor elements that bind either vacancies or interstitials with sufficient strength to reduce the effective mobility, thus preventing defects from reaching sinks and promoting recombination. The effect of solutes on the point defect balance equations was presented in Chap. 6, Sect. 6.4. The effect of solute addition on void swelling behavior can be determined by solving Eq. (6.66) through Eq. (6.70) and the nucleation rate, as in Eq. (8.35), and the void swelling rate, as in Eq. (8.112). Results of numerical methods solution [47] show that with increasing values of binding energy, the activation energy for void nucleation increases (Fig. 8.46). The void swelling rate decreases with increasing binding energy as shown in Fig. 8.47. The net effect of solute addition on void swelling is shown in Fig. 8.48, which indicates that for increased solute concentration and binding energy, void swelling decreases. Data on the role of solutes in swelling are in general agreement with the model. Figure 8.49 shows that Si and P strongly influence the swelling of austenitic stainless steels. In fact, Si is a fast diffuser and is known to alter the ratio of diffusivities of the solvent atoms. As shown in Fig. 8.50, the effect of P on swelling is indeed in extending the incubation period

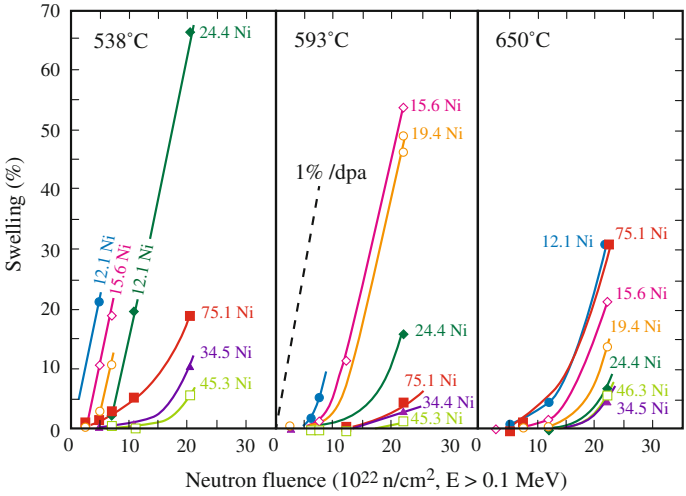

Fig. 8.42 The influence of temperature and nickel content on swelling of ternary Fe–15Cr–*x*Ni alloys in EBR-II (after [46])

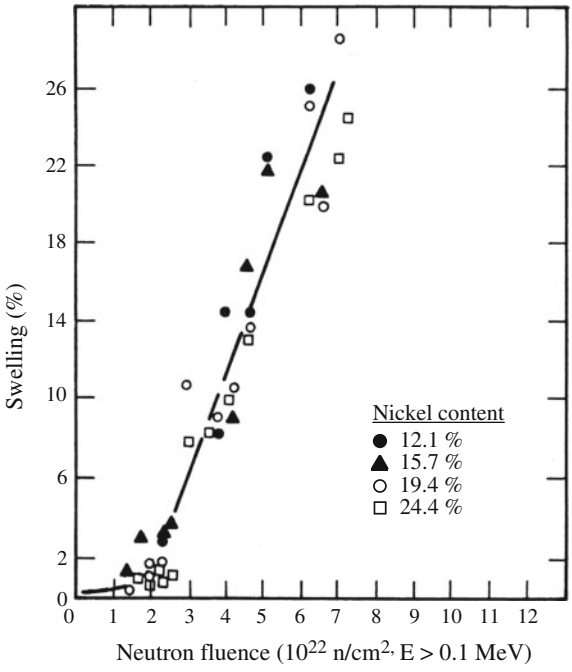

Fig. 8.43 Swelling of Fe–15Cr–xNi ternary alloys in EBR-II at temperatures between 400 and 510 °C for nickel levels between 12.1 and 24.4 wt% (after [46])

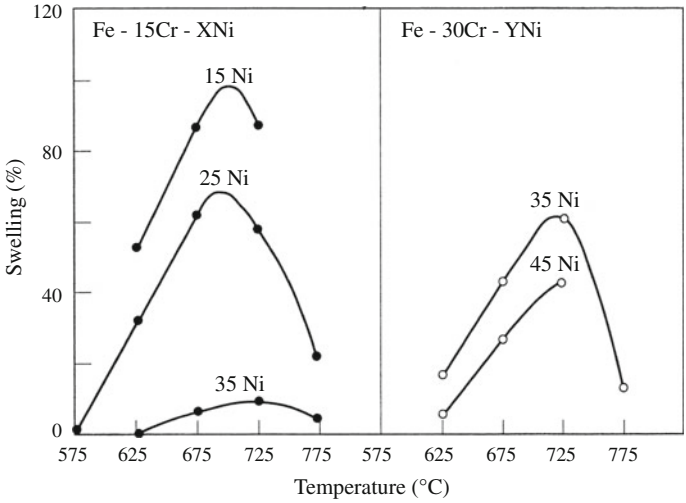

Fig. 8.44 Effect of chromium content on swelling in Fe–Cr–Ni alloys following 5 MeV Ni^+ ion irradiations to a dose of 140 dpa (after [19])

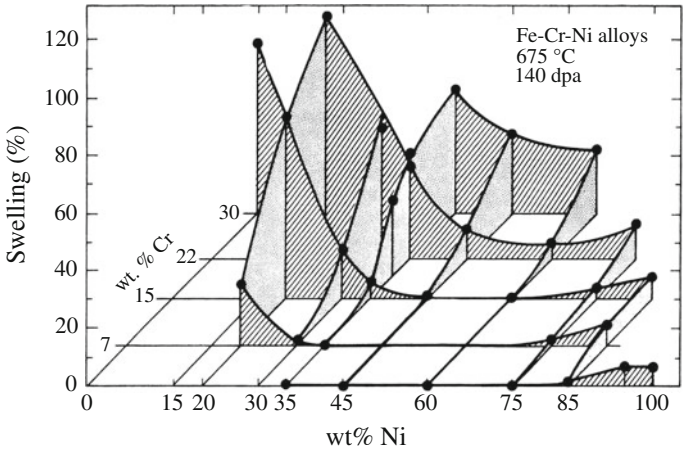

Fig. 8.45 Two-dimensional plot of the nickel and chromium dependence of swelling in Fe–Cr–Ni alloys irradiated with 5 MeV Ni^+ ions at 675 °C to a dose of 140 dpa. Swelling was measured by the step-height technique (after [19])

to larger doses. Oversize solutes such as Hf have a similar effect in suppressing the nucleation of voids in stainless steels irradiated at ~300 °C. While other factors are important, Fig. 8.51 shows that the addition of ~1 wt% Hf to 316 stainless steel results in the suppression of void formation during Ni^{++} ion irradiation at 500 °C through a dose of 50 dpa, compared to an incubation dose of only 2 dpa for the reference 316 stainless steel alloy.

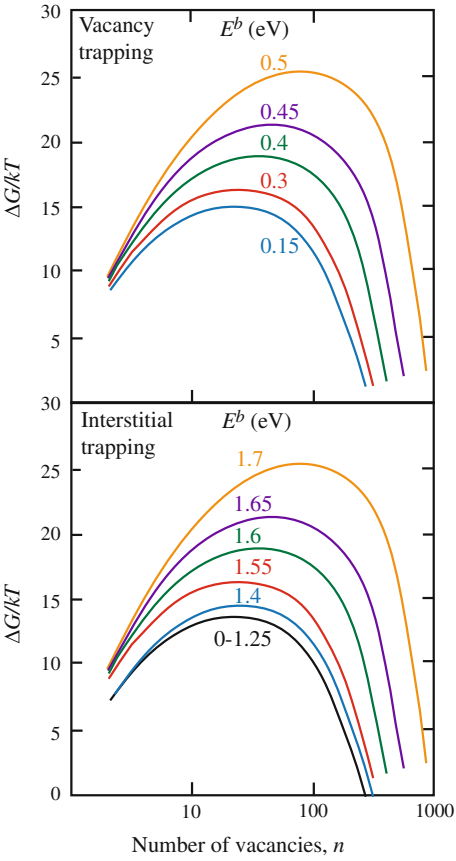

Fig. 8.46 The effect of impurity trapping on the free energy of void nucleation. Upper curves are for vacancy trapping and lower curves for interstitial trapping. The nucleation rates calculated from the curves are given as a function of binding energy in eV (after [47])

Precipitates

Precipitates can act as recombination sites for vacancy–interstitial annihilation to reduce void swelling. Precipitates can also inhibit dislocation climb necessary for dislocations to act as a preferential sink for interstitials and hence retard void growth.

In fact, precipitates can affect cavity growth in three ways [51]. The first is a direct effect in which voids that are attached to precipitates can undergo large growth rates because the precipitate acts as a collector of point defects. Precipitates can indirectly affect void growth by changing the overall sink strength of the solid or by changing the characteristics of the matrix.

As discussed in Sect. 5.8, the coherent precipitate is considered to be a site where constrained recombination of defects occurs due to the distribution of saturable traps that acquire a steady-state occupation probability as a result of a balance between defect capture, defect thermal release, and extrinsic recombination with the anti-defect. However, incoherent precipitates accept any excess point defect flux that

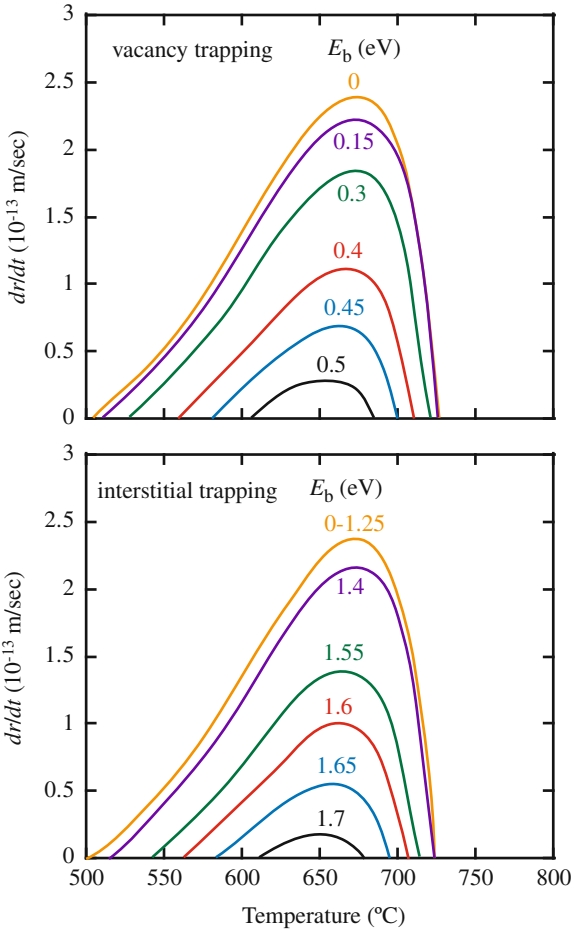

Fig. 8.47 The effect of impurity trapping on void growth rates. *Upper curves* are for vacancy trapping, and *lower curves* are for interstitial trapping (after [47])

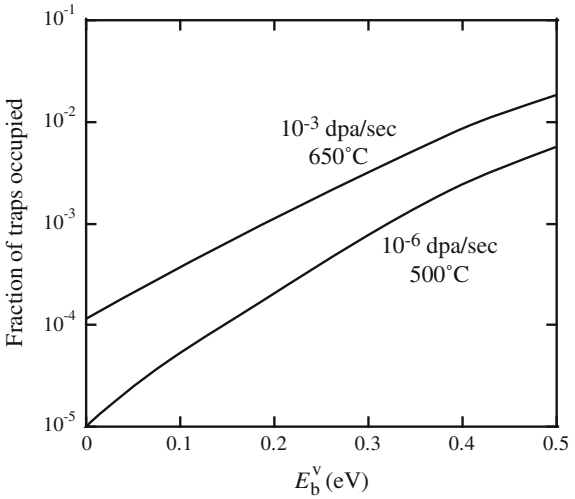

Fig. 8.48 The fraction of traps occupied for vacancy trapping at typical charged particle and fast reactor dose rates and temperatures versus binding energy. Under these conditions, the fraction of traps occupied is small even at high vacancy binding energies (after [47])

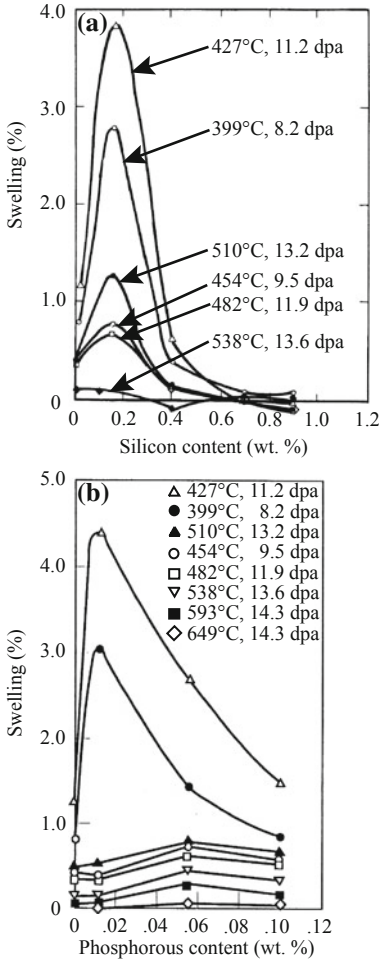

Fig. 8.49 Influence of (**a**) silicon and (**b**) phosphorus on the swelling in EBR-II of annealed Fe–25Ni–15Cr at various combinations of temperature and fluence (after [48])

happens to impinge on it. These precipitates can accumulate defects and may act as sites for rapid transport of defects, similar to grain boundaries. In fact, they can serve as sites for the collection of defects which are then channeled to voids.

While the potential exists for precipitates to strongly influence void growth through their action as sinks or recombination sites, measurements of the effect of precipitation on void growth have failed to show that they play a significant role.

Grain Boundaries

In polycrystalline materials, voids are not homogeneously distributed throughout a grain. A common observation is that a region adjacent to the grain boundaries is absent of voids. This region extends to a roughly fixed distance into the grain from the grain boundary and is referred to as the void-denuded zone, shown in Fig. 8.52

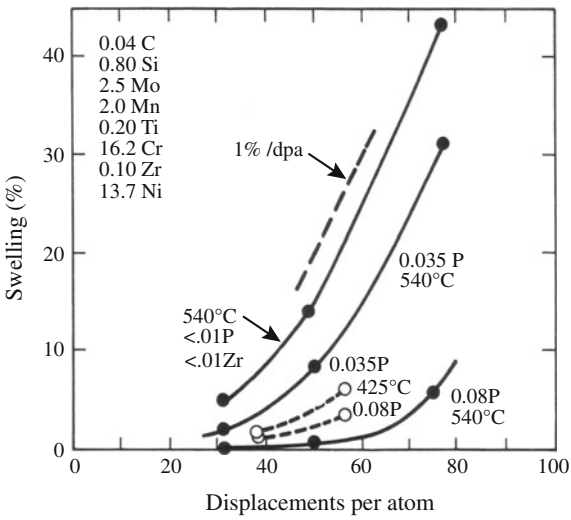

Fig. 8.50 Influence of phosphorus level on swelling in EBR-II for a titanium-modified 316 steel at 425 and 540 °C (after [49])

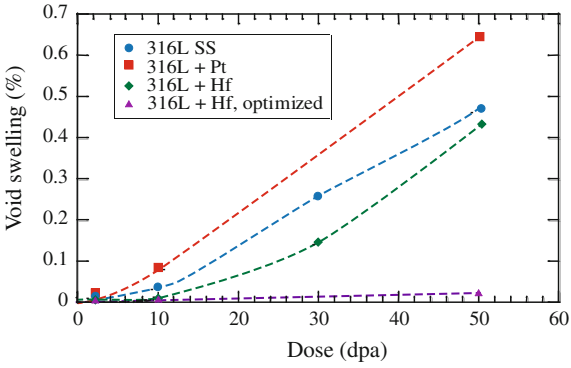

Fig. 8.51 Suppression of swelling to at least 50 dpa in 316 SS doped with ~1 wt% Hf after irradiation with 5 MeV Ni^{++}ions at 500 °C (after [50])

for ion-irradiated Ni and for lath boundaries in ferritic–martensitic alloy HT9. Considering only Frenkel pair production, e.g., electron irradiation, these denuded zones occur because of the diffusion of vacancies to the grain boundary sink that reduces the vacancy supersaturation near the grain boundary below the level needed to sustain void nucleation. Note in Fig. 8.53 that denuded zone occurrence is dependent on the sink strength of the grain boundary. In the same sample, a random high-angle grain boundary (RHGB) exhibits a clear denuded zone (Fig. 8.53(a)), but a coincident site lattice boundary (CSLB) shows no such zone (Figure 8.53(b)). The difference is likely due to the low energy of the CSLB, resulting in a low sink strength. Figure 8.53(c) is an extreme example of a heterogeneous void distribution in ferritic–martensitic alloy HT9 that is, perhaps, due to the many void-denuded zones next to grain boundaries.

Figure 8.54 shows the normalized vacancy supersaturation (S/S_0) profiles as a function of distance from the grain boundary, represented as a fraction of the grain

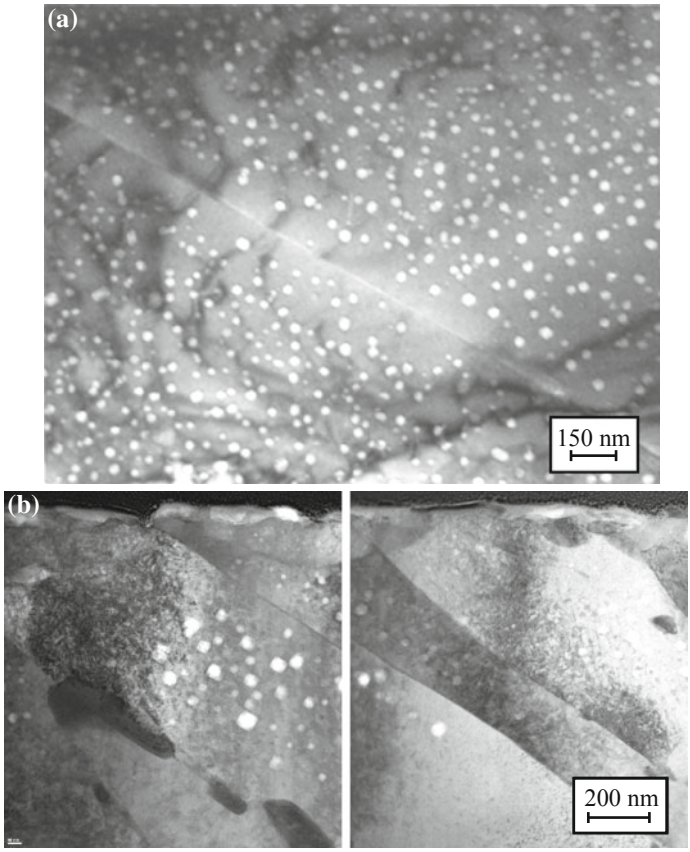

Fig. 8.52 Transmission electron micrographs of the void denuded zone (**a**) in ion-irradiated nickel (after [52]) and (**b**) near lath boundaries in alloy HT9 irradiated with 5 MeV Fe^{++} ions at 460 °C to 375 dpa after preimplantation with 1 appm He (*courtesy* A. Monterrosa)

diameter, d_g. Two features are of significance. First, regardless of grain size, the vacancy concentration drops to nearly zero at the grain boundary, greatly reducing the vacancy supersaturation in its vicinity. Second, with increasing grain size, the depth-dependent portion of the vacancy supersaturation profile extends deeper into the grain interior and its peak value becomes smaller as the grain size gets smaller. Figure 8.55 shows the calculated grain size–dependent supersaturation and experimentally measured swelling as a function of grain size. With decreasing grain size, more and more vacancies produced in the grain interior manage to diffuse to and annihilate at the grain boundaries. Thus, the volume of solid in which the vacancy supersaturation can support void nucleation decreases with decreasing grain size. The implication is that void swelling can be suppressed by reducing the grain size below some critical size.

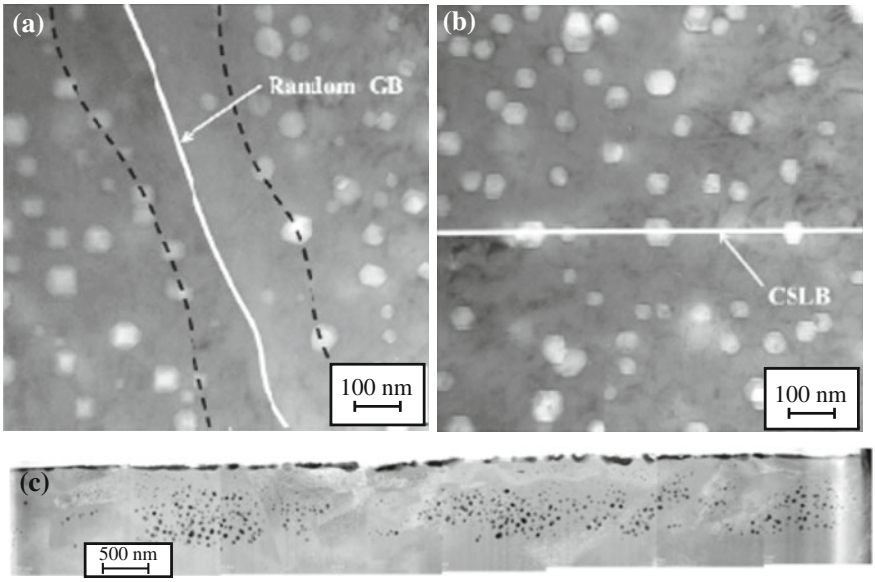

Fig. 8.53 Denuded zone (**a**) at a random grain boundary, (**b**) at a CSLB in Fe–15Cr–15Ni following neutron irradiation at 476 °C to 18 dpa (after [53]), and (**c**) in HT9 irradiated at 460 °C to 375 dpa (*courtesy* K. Sun)

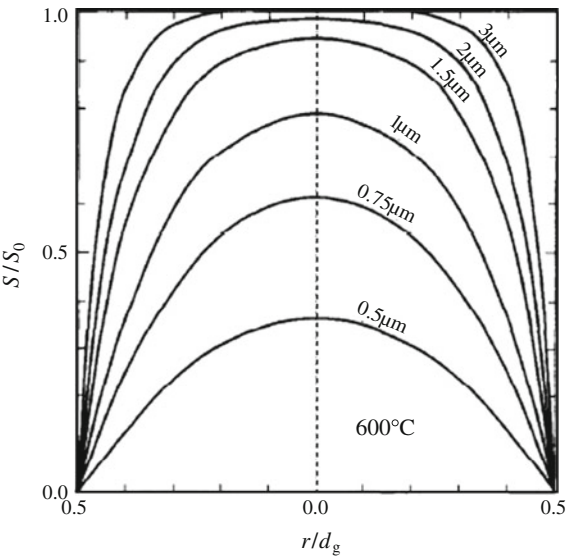

Fig. 8.54 Normalized vacancy supersaturation (S/S_0) profiles calculated for different grain sizes (d_g) in an austenitic stainless steel under 1 MeV electron irradiation at 873 K; $r/d_g = 0$ refers to the grain center, and $r/d_g = 0.5$ refers to the position of the grain boundaries (after [54])

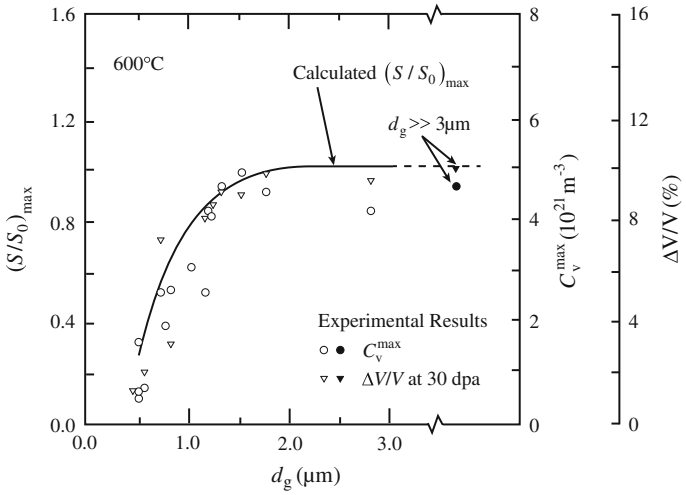

Fig. 8.55 Variation of the maximum vacancy supersaturation $(S/S_0)_{max}$ (i.e., at $r/d_g = 0$) with grain size (d_g) in an austenitic stainless steel irradiated with 1 MeV electron at 873 K. For comparison, the measured values of void density (C_v^{max}) and swelling are also plotted for different grain sizes (after [54])

The data shown in Fig. 8.55 come from 1 MeV electron irradiation that produces isolated Frenkel pairs distributed homogeneously in the solid. In this case, damage accumulation can be understood in terms of random, three-dimensional diffusion and biased attraction of monointerstitials to dislocations using conventional rate theory. Conversely, under cascade damage conditions, the nucleation and growth of cavities are significantly enhanced in the zone immediately adjacent to the void-denuded zone along the grain boundaries, referred to as the peak zone, as in Fig. 8.56. This peak zone is believed to be a consequence of the production bias. One-dimensional glide of small interstitial clusters will remove SIAs from the grain interior to grain boundaries over distances up to several microns. The result is the generation of a high vacancy supersaturation in the peak zone adjacent to the denuded zone in cases where cascades are formed. Thus, the observation of the peak zone formation under cascade damage conditions and its absence during single-displacement conditions likely arise because of differences in recoil energy. The consequence is that under cascade damage conditions, void swelling would first increase with increasing grain size, reaching a maximum at a grain size when the peak zone maxima overlap. Swelling would then decrease with grain size, becoming independent of the grain size at sizes greater than the peak zone width.

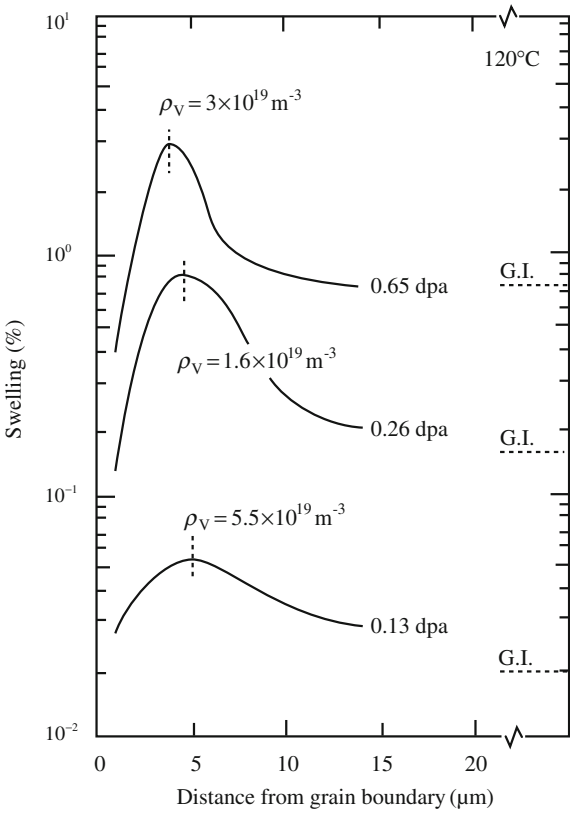

Fig. 8.56 Variation of void swelling with the distance from the grain boundary in aluminum irradiated with fission neutrons at 393 K. The cavity density (ρ_V) in the peak swelling zone is also indicated. The levels of the void swelling in the grain interior (G.I.) are also marked (after [54])

8.3.11 Effect of Reactor Operating History

Much of our understanding of void behavior in metals comes from irradiation in reactors. The experimental data are used to validate models and to provide material parameters to benchmark the models. Given that most models assume that reactor parameters (temperature, dose rate, stress) are constant over time, it is often true that in both commercial and test reactors these parameters can vary considerably during operation and due to the shutdown–start-up cycle. It is not unusual for irradiation experiments to experience numerous power (and hence temperatures) reductions over the course of a six-month to one-year irradiation. Garner [55] cites one instance in which a 600 °C, three-year irradiation, experienced 237 temperature setbacks in the first year, during which the temperature fell to as low as 50 °C. While the dose accumulated at these lower-than-target temperatures is low (0.12 dpa in the 3.5 dpa accumulated in year 1), they can have a profound effect on the microstructure.

Figure 8.57(a) shows the difference of dislocation loop size and number density in Ni–2.0Si samples irradiated in JMTR at 400 °C for the case of "conventional"

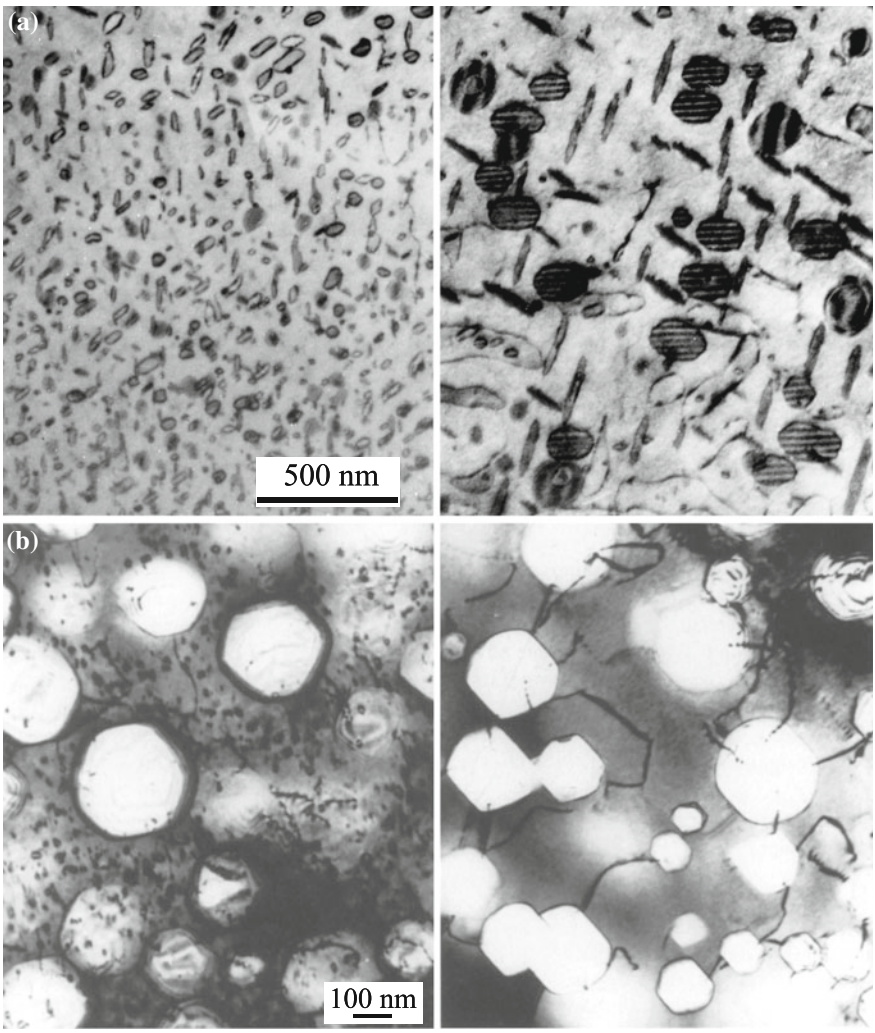

Fig. 8.57 (**a**) Effect of temperature control on dislocation loop formation and growth in Ni–2 %Si irradiated at 400 °C in the Japan Materials Test Reactor (JMTR) to a dose of $\sim 10^{24}$ n/m^2. LHS is conventional control (0.92×10^{24} n/m^2, $E > 1.0$ MeV), and RHS is improved control (0.96×10^{24} n/m^2). (**b**) Effect of shutdown rate on the formation of small dislocation loops in Fe–15Cr–16Ni irradiated at in FFTF at 600 °C. The image *on the left* underwent a slow temperature decrease during power shutdowns compared to a very rapid reduction in temperature at shutdown for the sample *on the right* (after [55])

temperature control versus one where the temperature control was considerably improved. The smaller mean loop size and larger density are likely the result of additional loop nucleation during the periods where temperature was low, but the neutron flux was nonzero. This low-temperature microstructure persisted at the

nominal irradiation temperature and resulted in an alteration of the loop size distribution as compared to the case in which temperature was controlled. Low-temperature loop nucleation in a high-temperature microstructure can also affect the evolution of the void microstructure.

Figure 8.57(b) shows the microstructure of a Fe–15Cr–16Ni alloy irradiated at 600 °C in the Materials Open Test Assembly (MOTA) in the Fast Flux Test Facility (FFTF) to comparable doses. The sample on the left was in an assembly, and reactor shutdown occurred over a six-hour period during which the temperature was reduced by 50–100 °C and then to gradually over the six-hour period during which the flux was also decreased. Irradiation during cooling is responsible for the formation of the fine dislocation loop structure. Following rapid shutdown during which the neutron flux and temperature are decreased over a several minute period, no fine loop structure is observed. The fast drop in temperature does not provide an opportunity to accumulate enough dose in this intermediate-temperature regime to cause loop nucleation.

The significance of these observations is twofold. First, that a low-temperature dislocation microstructure introduced into a high-temperature microstructure can alter the further development of that microstructure, affecting both loop and void evolution. Second, only very small doses (<0.1 dpa) are required to nucleate the fine loop structure that remains stable during the continuation of the irradiation at high temperature. These data also provide additional information on the loop nucleation rate, indicating that it is perhaps higher than current models can explain.

8.4 Bubbles

Up to this point, we have been treating voids as essentially empty cavities that grow and shrink by the absorption of vacancies. We have accounted for the effect of gas atoms on the nucleation of voids and also on the equilibrium vacancy concentration at the void surface. But we have not discussed the magnitude of the pressure in the void due to the gas and the effect this may have on the growth of the void. We also have made no distinction between a void and a bubble. One question that we would like to answer is how much gas must a void have in order to be considered a bubble? In a practical sense, the distinction is largely one of degree and character. A cavity is considered to be a bubble if the effect of the gas (on the surface energy and due to the pressure) causes the cavity to become spherical. This is essentially how voids and bubbles are distinguished in transmission electron microscopy. Due to the periodicity of the lattice, cavities will be faceted with the facets lying on the close-packed planes. But if the surface energy is changed by the gas, or if the gas pressure is high enough, then the cavity will become spherical in shape. Of course, very large voids will approach a spherical shape as the contribution of the facets diminishes with increasing void radius.

Because insoluble gases are often formed by transmutation when certain elements are irradiated, inert gas bubbles form, which alter the mechanical and

physical properties of an alloy. Bubble formation depends on the mobility of the gas (in the form of either individual atoms or complexes), the minimum number of gas atoms which are able to form a stable nucleus and the rate at which lattice vacancies can be supplied to enhance the stability of a nucleated core.

Bubbles nucleate under irradiation and then grow or redissolve. The criterion is that nucleation ceases when a gas atom diffusing at random is most likely to encounter a pre-existing nucleus rather than take part in creating a new one. The resulting bubble density varies inversely as the square root of the gas atom diffusion coefficient and thus increases with decreasing temperature.

The following assumptions about bubble nucleation under irradiation are made. Homogeneous nucleation is predicated on the premise that bubbles grow by the interaction of gas atoms from a background atomic population on a random basis. Thus, no account is taken of local effects such as cascade processes or precipitation on lattice defects or impurity agglomerates. Concerning stable nuclei, we assume that a pair of gas atoms is stable against thermal dissociation and that its activation energy is such that its motion may be ignored with respect to that of single gas atoms.

In this section, we will first consider the mechanics of bubbles followed by the development of bubble growth models that will closely parallel void growth.

8.4.1 Bubble Mechanics

For a bubble of radius R, embedded in a solid medium, the change in the free energy of the solid due to the bubble is:

$$\mathrm{d}G = V\,\mathrm{d}p + \gamma \mathrm{d}A. \tag{8.209}$$

Since

$$V\,\mathrm{d}p = \mathrm{d}(pV) - p\,\mathrm{d}V, \tag{8.210}$$

and for an ideal gas, pV = constant and $V = 4/3\pi R^3$, then:

$$\frac{\mathrm{d}G}{\mathrm{d}r} = -4\pi R^2\left(p - \frac{2\gamma}{R}\right). \tag{8.211}$$

Setting $\mathrm{d}G/\,\mathrm{d}r = 0$ yields:

$$p = 2\gamma/R. \tag{8.212}$$

Thus, the equilibrium condition for a bubble is expressed by the force balance $p = 2\gamma/R$, in which the force due to the outward pressure of the gas, p, is balanced by

the inward-acting force due to the surface tension, $2\gamma/R$. In the presence of a stress, the force balance becomes:

$$p = \frac{2\gamma}{R} - \sigma. \tag{8.213}$$

where positive stress is tension.

All bubble models require a specific relation between the number of gas atoms in a bubble and its radius. The van der Waals equation of state is used to describe the thermodynamic state of inert gas in bubbles. Let n_x be the number of gas atoms in a spherical bubble of radius R and the gas density is ρ_g. Then,

$$n_x = (4/3\pi R^3)\rho_g. \tag{8.214}$$

From the ideal gas law ($pV = nkT$), we have:

$$p\frac{V}{n} = kT \quad \text{or} \quad \frac{p}{\rho_g} = kT \quad \text{or} \quad p = \frac{3nkT}{4\pi R^3}. \tag{8.215}$$

Using Eq. (8.212) for mechanical equilibrium to eliminate ρ_g and p in Eqs. (8.214) and (8.215) gives:

$$\begin{aligned} n_x &= 4/3\pi R^3 \frac{2\gamma}{RkT} \\ &= \frac{8\pi R^2\gamma}{3kT}. \end{aligned} \tag{8.216}$$

For small R, $1/\rho_g$ is not proportional to R and we must account for the volume occupied by the gas atoms themselves. We do this by modifying Eq. (8.215) to include a term B which is a function of temperature and pressure. This gives us van der Waals equation of state:

$$p\left(\frac{1}{\rho_g} - B\right) = kT \quad \text{or} \quad \frac{1}{\rho_g} = B + \left(\frac{kT}{2\gamma}\right)R, \tag{8.217}$$

and Eq. (8.216) becomes:

$$n_x = \frac{8\pi R^2\gamma}{3(kT + 2B\gamma/R)} = \frac{4/3\pi R^3}{B + (kT/2\gamma)R}. \tag{8.218}$$

For large R, the perfect gas approximation applies, and for very small R, the dense gas limit applies. Physically, there is a minimum volume occupied by each atom, B, and as R decreases, the volume per atom approaches this limit. The result is:

$$\frac{1}{\rho_g} = B\frac{\text{nm}^3}{\text{atom}} : \text{dense gas limit}, \tag{8.219}$$

and

$$\frac{1}{\rho_g} \cong \left(\frac{kT}{2\gamma}\right)R : \text{ideal gas limit}. \tag{8.220}$$

Note that for stainless steel at 500 °C, where $\gamma \sim 1.75$ J/m^2, $2\gamma/kT \sim 328$ nm^{-2}, then $\frac{1}{\rho_g} \cong 3 \times 10^{-4} R\frac{\text{nm}^3}{\text{atom}}$.

The limiting cases corresponding to Eqs. (8.219) and (8.220) are:

$$n_x = \left(\frac{4\pi R^3}{3B}\right) \text{for small } R \tag{8.221}$$

$$= \left(\frac{4\pi R^2}{3}\right)\left(\frac{2\gamma}{kT}\right) \text{for large } R. \tag{8.222}$$

If Eq. (8.212) is not satisfied, then the bubble is described as a non-equilibrium bubble. That is, the bubble is not in equilibrium with the solid. Mechanical equilibrium is usually maintained by a flow of vacancies to the bubble to provide the additional volume needed to accommodate the influx of gas atoms. Whether Eq. (8.212) is satisfied depends on the relative absorption rate of vacancies and gas atoms by the bubble. A bubble of radius R can be considered as the absence of $(4/3\pi R^3)/\Omega$ matrix atoms where Ω is the atomic volume. The empty sphere of radius R can be thought of as consisting of n_v vacancies given by:

$$n_v = \frac{4/3\pi R^3}{\Omega}. \tag{8.223}$$

The number of gas atoms in a sphere of radius R in mechanical equilibrium is given by Eq. (8.218). The number of vacancies per gas atom in an equilibrium bubble is then:

$$\frac{n_v}{n_x} = \left(\frac{kT}{2\gamma}\right)\frac{R}{\Omega} + \frac{B}{\Omega}. \tag{8.224}$$

Note that n_x increases as R^2, but n_v increases as R^3, so increasing numbers of vacancies are needed per gas atom in order to maintain equilibrium.

Stress is accounted for by taking Eq. (8.213) and substituting for p from Eq. (8.215) to give:

$$\sigma = \frac{2\gamma}{R} - \frac{3n_x kT}{4\pi R^3}, \tag{8.225}$$

where σ is the hydrostatic tensile stress. The critical bubble radius for unstable bubble growth is determined by setting $d\sigma/dr = 0$ and solving for R, yielding:

$$R_c = \left(\frac{9n_x kT}{8\pi\gamma}\right)^{1/2}. \tag{8.226}$$

Substituting for R_c in Eq. (8.226) into Eq. (8.225) gives:

$$\sigma_c = \left(\frac{128n\gamma^3}{81n_x kT}\right)^{1/2}, \quad \text{or} \quad n_x = \frac{128n\gamma^3}{81\sigma_c^2 kT}. \tag{8.227}$$

The critical bubble radius, R_c, is related to the equilibrium bubble radius, R_0, by expressing Eqs. (8.216) and (8.226) in terms of the number of gas atoms in the bubble, n_x, and eliminating n_x, giving:

$$R_c = \sqrt{3}R_0, \tag{8.228}$$

and the critical stress in terms of R_0 is:

$$\sigma_c = \frac{4\sqrt{3}\gamma}{9R_0}. \tag{8.229}$$

Substituting for Eq. (8.222) into Eq. (8.225) to eliminate n_x gives a relation between the applied stress, the initial bubble size, and the critical bubble size:

$$\sigma_c = \frac{2\gamma}{R_c}\left(1 - \frac{R_0^2}{R_c^2}\right). \tag{8.230}$$

Equations (8.229) and (8.230) provide the bubble stability criterion in terms of the applied stress and the bubble size. For bubbles of size R_0, Eq. (8.229) gives the critical stress for stability. For a solid with bubbles of size $R_0 < R_c$, application of a tensile stress σ_c will cause the bubble to grow to size R_c specified by Eq. (8.230). If $R_0 > R_c$ or if σ_c is greater than the right-hand side of Eq. (8.229), then the bubble will grow without bound. Or, for a given applied stress, Eq. (8.229) gives the critical bubble radius for stability. Equation (8.226) can be compared to the stability equation for a gas-free void in a solid subject to a stress, σ. For $p = 0$ in Eq. (8.213), we have that $\sigma = 2\gamma/R$. The numerical coefficient in Eq. (8.229) is about 0.77, which is less by about a factor of 3 than the coefficient for the void. The difference is due to the effect of the gas pressure in the bubble that assists the stress.

8.4.2 Growth Law

Analogous to void growth, the time rate of change of the volume of a bubble is equal to the difference in the rates at which vacancies and interstitials are absorbed and to the volume carried by each of these point defects:

$$\frac{\mathrm{d}}{\mathrm{d}t}\left(\frac{4}{3}\pi R^3\right) = \Omega\left[4\pi R D_\mathrm{v}(C_\mathrm{v} - C_\mathrm{v}^\mathrm{v}) - 4\pi R D_\mathrm{i}(C_\mathrm{i} - C_\mathrm{i}^\mathrm{v})\right], \tag{8.231}$$

and so the growth law is:

$$\frac{\mathrm{d}R}{\mathrm{d}t} \equiv \dot{R} = \frac{\Omega}{R}\left[D_\mathrm{v}(C_\mathrm{v} - C_\mathrm{v}^\mathrm{V}) - D_\mathrm{i}(C_\mathrm{i} - C_\mathrm{i}^\mathrm{V})\right], \tag{8.232}$$

where C_v^V and C_i^V are the concentrations of vacancies and interstitials at the bubble surface and C_v and C_i are the point defect concentrations in the bulk solid. The thermodynamic vacancy concentration at the bubble surface given by Eq. (8.85) is modified to include the effect of gas pressure in the bubble:

$$C_\mathrm{v}^\mathrm{V} = C_\mathrm{v}^0 \exp\left[\frac{-\Omega}{kT}\left(p - \frac{2\gamma}{R}\right)\right], \tag{8.233}$$

and for interstitials

$$C_\mathrm{i}^\mathrm{V} = C_\mathrm{i}^0 \exp\left[\frac{\Omega}{kT}\left(p - \frac{2\gamma}{R}\right)\right], \tag{8.234}$$

where C_v^0 and C_i^0 are the thermodynamic equilibrium concentrations of vacancies and interstitials, respectively, for a stress-free solid and the exponential terms reflect the presence of a mechanical stress acting on the solid equal in magnitude to $p - 2\gamma/R$. Because C_i^0 is so small, the interstitial term, as in Eq. (8.234), can be neglected.

Setting $\mathrm{d}R/\mathrm{d}t = 0$ in Eq. (8.232) and substituting Eq. (8.233) for C_v^V into the resulting expression, taking logarithms and rearranging gives [56, 57]:

$$R_\mathrm{c} = \frac{2\gamma}{p + \dfrac{kT}{\Omega}\ln S_\mathrm{v}}, \tag{8.235}$$

where S_v is the effective vacancy supersaturation given by:

$$S_\mathrm{v} = \frac{D_\mathrm{v}C_\mathrm{v} - D_\mathrm{i}C_\mathrm{i}}{D_\mathrm{v}C_\mathrm{v}^0}. \tag{8.236}$$

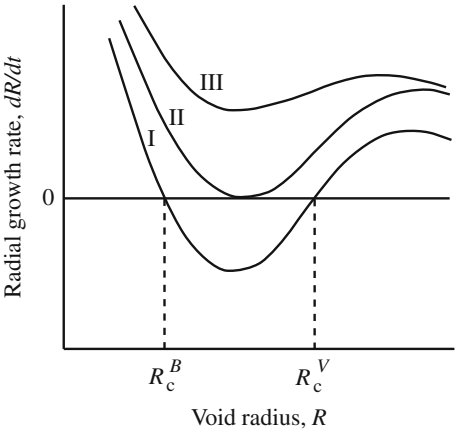

Fig. 8.58 Schematic plot of cavity growth rate as a function of cavity radius for increasing amount of helium gas in the void or S_v (after [56])

Now, substituting Eq. (8.215) for p into Eq. (8.235) and rearranging gives:

$$g(R_c) = R_c^3 - \frac{2\gamma\Omega}{kT \ln S_v} R_c^2 + \frac{3n_x\Omega}{4\pi \ln S_v} = 0, \tag{8.237}$$

where the expression denoted by the function $g(R_c)$ is zero when R_c is a root. The growth rate is plotted as a function of void radius in Fig. 8.58 for three conditions. The lower curve is the case where Eq. (8.237) has three real roots, the middle curve shows the case in which at least two of the roots are equal, and the upper curve has one real root [57]. In case I, the roots are denoted R_c^B and R_c^V. A void containing enough gas atoms that it is between R_c^B and R_c^V will shrink back to R_c^B. A void with the same number of gas atoms but with radius below R_c^B will grow to R_c^B and stop. Finally, a void with the same number of gas atoms and with radius above R_c^V will grow without limit by bias-driven growth. As the number of gas atoms increases, Eq. (8.237) is represented by curves that progress from I to II to III. In the case of curve III, the number of gas atoms is large enough that there will be no intersections with the $dR/dt = 0$ axis and these cavities will only grow by bias-driven growth. At some critical number of gas atoms, there is just one intersection of the function dR/dt with the $dR/dt = 0$ axis. This case is represented by curve II. In this case, the corresponding number of gas atoms is denoted as n_x^* and the corresponding minimum critical radius where R_c^B and R_c^V coincide is denoted as R_c^*. The quantity, n_x^*, is the maximum number of gas atoms that may be contained in a cavity for there to still exist a critical radius, with a minimum value of R_c^*.

The minimum critical radius, R_c^*. can be found by taking the derivative of Eq. (8.237) with respect to R_c, giving:

$$\frac{dg(R_c)}{dR_c} = 3R_c^2 - \frac{4\gamma\Omega}{kT \ln S_v} R_c. \tag{8.238}$$

Setting Eqs. (8.237) and (8.238) to zero simultaneously yields the minimum critical radius:

$$R_c^* = \frac{4\gamma\Omega}{3kT\ln S_v}, \tag{8.239}$$

and from Eq. (8.226):

$$n_x^* = \frac{128\pi\gamma^3\Omega^2}{81(kT)^3(\ln S_v)^2}. \tag{8.240}$$

Stoller et al. [57] noted that Eq. (8.240) can be written for non-spherical cavities using a shape factor, F_V, such that:

$$n_x^* = \frac{32F_V\gamma^3\Omega^2}{27(kT)^3(\ln S_v)^2}, \tag{8.241}$$

where $F_V = 4\pi/3$ for a spherical void. He also notes that more physically reasonable solutions are obtained using a hard sphere equation of state rather than the ideal gas law, which tends to overpredict swelling incubation times.

It should also be noted that Eqs. (8.240) and (8.228) are the same when σ is replaced with $\Omega/\ln S$, indicating that the stability criterion is the same regardless of whether the solid is acted on by an actual stress or an effective stress defined by the irradiation-induced vacancy supersaturation. A bubble is stable for negative vacancy supersaturation and can be stable or metastable for positive vacancy supersaturation, depending on the magnitude of the supersaturation, the gas content, and the bubble size according to Fig. 8.58. For a constant stress or irradiation-induced vacancy supersaturation, when the stability limit is reached by gas absorption, a bubble starts to grow by vacancy absorption and is transformed into a cavity. Equations (8.239) and (8.226) describe the bubble-to-void conversion criterion.

Equation (8.232) can be used to calculate the swelling rate due to bubble swelling by assuming all gas to be in the bubbles, resolution to be insignificant, and the gas to be ideal such that:

$$p = \frac{n_x kT}{4/3\pi R^3\rho_B}, \tag{8.242}$$

where ρ_B is the total bubble density and $n_x = \dot{x}t$ is the gas concentration in the solid being produced by transmutation at a rate of $\dot{x}$ The swelling rate due to bubble growth is:

$$\mathrm{d}(\Delta V/V)/\mathrm{d}t = (4\pi R^2\rho_B/\Omega)\mathrm{d}R/\mathrm{d}t. \tag{8.243}$$

8.4.3 Bubble Growth by Dislocation Loop Punching

While vacancy diffusion is the prime mechanism contributing to bubble growth on a fine scale, an additional mechanism for bubble growth in the case of high gas pressure is dislocation loop punching. If the pressure in the bubble is large enough, the stress in the solid nearby may reach a level where dislocation sources can be activated, resulting in the growth of the bubble by *punching out* a dislocation loop (Fig. 8.59). Recall that the stress required to operate a Frank–Read source is $\sim \mu b/l$, where l is the spacing between pinning points. Dislocation sources that are easiest to activate will be those with $l \sim r_0$, where r_0 is the radius of the bubble. So the excess pressure required for the bubble to generate dislocations is then $\sim \mu b/r_0$. The magnitude of the excess pressure required to generate prismatic dislocations can be determined by comparing the free energy change of the bubble upon creation of a dislocation loop of size equal to the bubble, to the energy of the loop itself [59]. The work to increase the bubble size is:

$$\Delta F = -pdV = -\left(p - \frac{2\gamma}{r_0}\right)\pi r_0^2 b, \tag{8.244}$$

where p is the pressure in the bubble, V is the bubble volume, γ is the surface energy, and b is the Burgers vector magnitude. Neglecting the stacking fault energy contribution, the energy of the prismatic dislocation loop of radius r_0 given by Eq. (7.64) is approximated as:

$$E_{\mathrm{L}} = \frac{\mu b^2 r_0}{2(1-\nu)} \ln \frac{4r_0}{r_{\mathrm{c}}}, \tag{8.245}$$

where r_{c} is the dislocation core radius. For dislocation loop formation to be energetically possible,

$$\left(p - \frac{2\gamma}{r}\right)\pi r_0^2 b > \frac{\mu b^2 r_0}{2(1-\nu)} \ln \frac{4r_0}{r_{\mathrm{c}}}, \tag{8.246}$$

or approximating E_{L} as $\pi \mu b^2 r_0$:

$$p > (2\gamma + \mu b)/r_0. \tag{8.247}$$

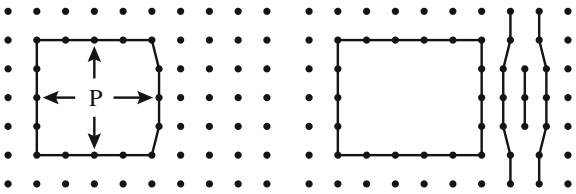

Fig. 8.59 Schematic illustration of the growth of a bubble by dislocation loop punching (after [58])

For typical values of γ and μ, the gas pressure in the bubble must be about an order of magnitude greater than $2\gamma/r_0$ before dislocations can be generated and allow the bubble to expand.

8.4.4 Bubble Lattices

Similar to void lattices described earlier, high levels of He can result in the organization of gas bubble lattices. In fact, gas bubble lattice formation has been observed in bcc, fcc, and hcp metals following He injection at temperatures $<0.3T_m$ [60]. Helium bubbles in Cu are aligned with dense-packed rows parallel to matrix {111} directions. Johnson et al. [60] measured the lattice constant of the He bubble superlattice in Cu to be a_{He} = 7.6 nm, corresponding to a bubble density of 10^{25} bubbles/m^3. Figure 8.60 shows a bright-field transmission electron micrograph of a helium gas bubble lattice in molybdenum following 40 keV He^+ irradiation to a dose of 5×10^{21} He^+/m^2 at 500 °C. While the same forces driving the formation of void lattices are expected to apply to bubble lattices, additional interactions may arise due to the close spacing of overpressurized bubbles, such as bubble growth by dislocation loop punching.

8.4.5 Helium Production

An important ingredient in bubble formation and growth is the production of helium. In a reactor, He production is governed by the boron and nickel contents of the alloy through the reactions:

$$^{10}\mathrm{B}(n,\alpha)^{7}\mathrm{Li}\,, \tag{8.248}$$

Fig. 8.60 He gas bubble superlattice formed in molybdenum following 40 keV He^+ irradiation to a dose of 5×10^{21} He^+/m^2 at 500 °C (after [43])

and the two-step reaction:

$$^{58}\mathrm{Ni}(n,\gamma)^{59}\mathrm{Ni}(n,\alpha)^{56}\mathrm{Fe}\,. \tag{8.249}$$

The thermal neutron (n, α) cross section for ^{10}B is very large, about 3837b, while the thermal neutron cross sections for the reactions in Eq. (8.249) are 4.6b and 12.3b, respectively. For thermal reactors then, a large amount of helium is produced early in life from transmutation of boron, but this source burns out by about 1 dpa ($\sim 10^{21}$ n/cm^2).

The presence of nickel in stainless steels provides a smaller but sustained source of helium at higher dose. ^{59}Ni is not a naturally occurring isotope and is produced from ^{58}Ni. Thus, this helium contribution involves a delay relative to that of single-step threshold (n, α) reactions [61]. Since both steps of the sequence involve cross sections that increase with decreasing energy and the second step exhibits a resonance at 203 eV, the generation rate per dpa in fast reactors increases near the core boundaries and out-of-core areas.

Nickel has five naturally occurring stable isotopes with ^{58}Ni comprising 67.8 % natural abundance, ^{60}Ni comprising 26.2, and ~6.1 % total of ^{61}Ni, ^{62}Ni, and ^{64}Ni. There is no natural ^{59}Ni or ^{63}Ni at the beginning of radiation. During irradiation in a highly thermalized neutron spectrum, all nickel isotopes are strongly transmuted, primarily to the next higher isotopic number of nickel. ^{59}Ni has a half-life of 76,000 years and is progressively transmuted to ^{60}Ni, while ^{58}Ni is continuously reduced in concentration. Therefore, the ^{59}Ni concentration rises to a peak at a thermal neutron fluence of 4×10^{22} n cm^{-2} where the 59/58 ratio peaks at ~0.04 and then declines, as shown in Fig. 8.61.

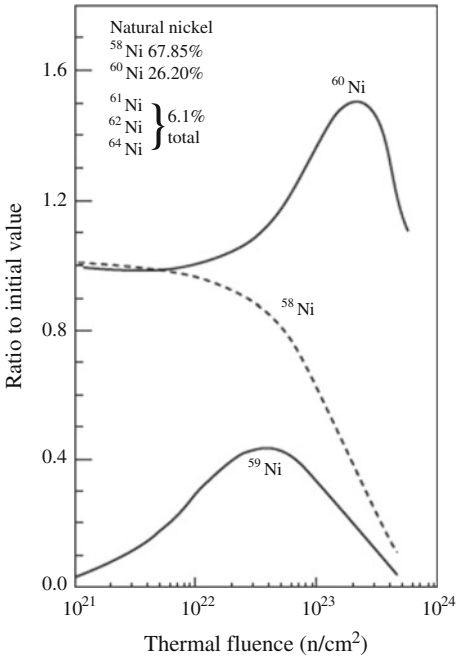

Fig. 8.61 Transmutation-induced evolution of three nickel isotopes during irradiation in thermalized neutron spectrum (after [62])

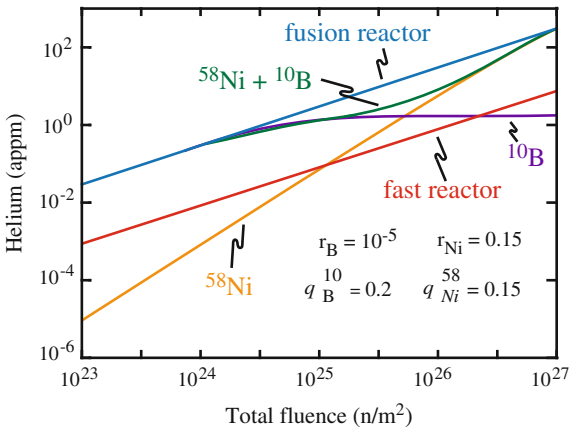

Fig. 8.62 Helium buildup versus fluence for stainless steel in HFIR (thermal reactor), a fusion reactor spectrum, and a fast reactor spectrum. In the figure, r is the atom fraction of boron or nickel in the alloy and q is the initial fraction of the isotope listed in the figure (after [27])

In this regard, thermal reactors produce greater amounts of helium at low-dose and in a lower-dose-rate environment, making low-dose helium-induced swelling a potentially greater problem in a thermal reactor than in a fast reactor. Figure 8.62 shows the production rate of helium from an alloy containing ^{58}Ni and ^{10}B in the HFIR (thermal) reactor. Note that the production rate of helium is dominated at low fluence by the contribution from ^{10}B and at higher fluence by ^{58}Ni. Helium buildup for the same alloy in a fast reactor and a fusion reactor is shown for comparison. Note that the helium buildup in a fusion reactor matches that in HFIR, and both are higher than that in a fast reactor.

The reaction in Eq. (8.249) has another important consequence. The recoil of the ^{59}Ni upon emission of the gamma ray produces only about five displacements per event and usually is not a significant addition to the displacement dose. However, the isotope ^{59}Ni undergoes three strong reactions with thermal and resonance ($\sim$0.2 keV) neutrons, two of which are highly exothermic and can significantly add to the dpa level. These reactions, in order of highest-to-lowest thermal cross section, are (n, γ) to produce ^{60}Ni, followed by (n, α) and (n, p) to produce helium and hydrogen, respectively.

Even at relatively low thermal-to-fast neutron ratios, the reaction sequence can produce significant amounts of helium. For example, He/dpa ratios in the order of $\sim$3–8 appm dpa^{-1} can be experienced along the length of a 316 stainless baffle bolt in the baffle–former assembly of a pressurized water reactor [61], while comparable rates in fast reactors are in the order of 0.1–0.2 appm dpa^{-1}. In thermalized spectra, the latter two reactions can quickly overwhelm the gas production produced by nickel at high neutron energies. The ^{59}Ni(n, α) reaction releases 5.1 MeV in the form of a 4.8 MeV alpha particle, which loses most of its energy by electronic losses that results in the deposition of significant thermal energy but the production

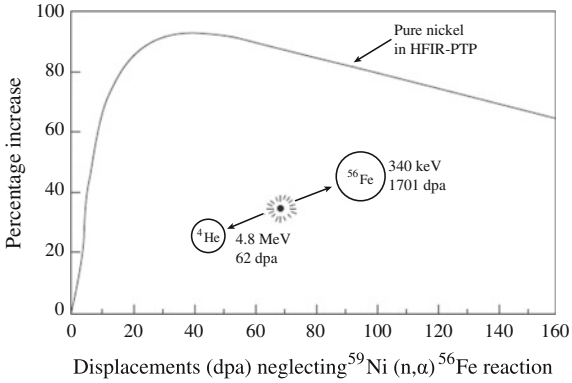

Fig. 8.63 Increase in dpa arising from the effect of ^{59}Ni to produce helium when pure nickel is irradiated in the HFIR test reactor in the peripheral target position where the thermal-to-fast ratio is 2.0 (after [62])

of only ~62 atomic displacements per each event, and a recoiling ^{56} Fe carrying 340 keV, which is very large compared to most primary knock-on energies, and produces ~1700 displacements per event.

An example of the time-dependent increase in dpa rate in highly thermalized light water spectra is shown for pure nickel in Fig. 8.63 for a thermal-to-fast ratio of 2.0. Note that the calculated increase in this figure addresses only the ^{59}Ni(n, α) reaction. Additional increases occur as a result of the ^{59}Ni(n, p) and ^{59}Ni(n, γ) reactions, resulting in roughly doubling the dpa due to the three ^{59}Ni reactions before a calculated dose of ~40 dpa is attained.

An even stronger example of the linkage of the ^{59}Ni transmutation effect and the displacement process has been observed [62]. In-core thermal-to-fast ratios in heavy water-moderated reactors such as CANDUs are on the order of ~10, but far from the core, the ratio can be near ~1000. Compression-loaded springs constructed of high nickel alloy X-750 were examined after 18.5 years of operation far from the core and were found to be completely relaxed. Calculating the ^{59}Ni contribution, it was deduced that full relaxation occurred in ~3–4 years rather than the 650–700 years one would predict based on dpa calculated without taking into account the ^{59}Ni contribution. Therefore, in this case, ^{59}Ni contributed ~95 % of the dpa damage. Additionally, 1100 appm of helium was calculated to have been produced at the midsection of the spring in ~3 years, with ~20,000 appm helium having been produced when the spring was examined after 18.5 years of exposure. Figure 8.64 shows calculations of H, He, and displacement damage in alloy X-750 garter springs used in CANDU reactors as a function of fluence. Note that at end of life (~4.5×10^{23} n/cm^2), the damage level is ~65 dpa of which ~62 dpa comes from the recoil of ^{59}Ni, the He level is 22,000 appm (338 appm He/dpa), and the H level is ~4500 appm (69 appm H/dpa). Such levels of He and potentially H will cause significant bubble formation and swelling in the alloy.

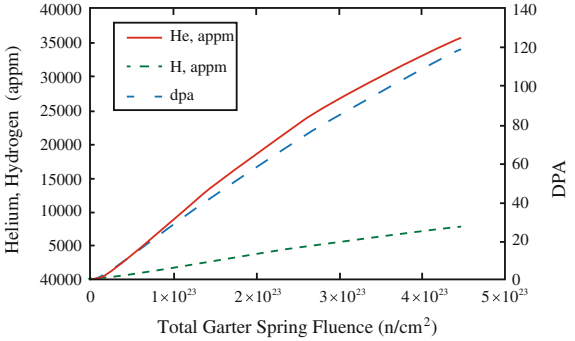

Fig. 8.64 He, H, and dpa production as a function of fluence for X-750 garter springs in a CANDU reactor (*courtesy* CANDU Owners Group)

Another consequence of the ^{59}Ni sequence is the inducement of temperature increases due to gamma heating. At the peak ^{59}Ni level reached at 4×10^{22} n cm^{-2} (Fig. 8.61), the nuclear heating rates from the energetic (n, α) and (n, p) reactions are 0.377 and 0.023 Wg^{-1} of nickel, significantly larger than the neutron heating level of $\sim$0.03 Wg^{-1} of natural nickel. Thus, an increase in nuclear heating of $\sim$0.4 Wg^{-1} of nickel must be added to the gamma heating rate at the peak ^{59}Ni level. Depending on the nickel level of the steel and the level of gamma heating, which is the primary cause of temperature increases in the interior of thick plates, this additional heating contribution may or may not be significant.

Gamma heating is also a strong function of the thermal-to-fast (T/F) neutron ratio and the neutron flux, being $\sim$54 Wg^{-1} in the center of the HFIR test reactor where the T/F ratio is $\sim$2.0. In pressurized water reactors in austenitic core internals, however, the T/F ratios are lower by a factor of 2–10, depending on location, and the gamma heating rates in the baffle–former assembly are $\sim$1–3 Wg^{-1}. In this case, an additional 0.4 Wg^{-1} of nuclear heating can be a significant but time-dependent addition to total heating, especially for high-nickel alloys.

Nomenclature

a	Lattice constant
$A^{X}_{v,i}$	Absorption rate of vacancies, interstitials by sink X
B	Volume occupied by a gas atom in a bubble
B_d	Dislocation bias term defined below Eq. (8.184) as $B_d = (z^d_i - z^d_v)/z^d_v$
C_{giL}	Concentration of glissile SIA loops
C_j	Concentration of species j
C^0_j	Thermal equilibrium concentration of species j
C^L_v	Vacancy concentration in equilibrium with a dislocation loop
C^V_v	Vacancy concentration at the void surface
D_j	Diffusion coefficient of species j
D^c	Diffusive spread due to cascades
D^e	Diffusive spread due to vacancy emission
D^s	Diffusive spread due to single defect jumps
E	Energy

E_{b}^{j} Binding energy of specie j
E_{f}^{J} Formation energy of specie j
E_{m}^{j} Migration energy of specie j
E_{vL} Effective binding energy of vacancies with vacancy clusters
$E_{*}^{\mathrm{v,i}}$ See definition after Eq. (8.167)
F_{V} Shape factor (= $4\pi/3$ for spherical void)
$g(R_{\mathrm{c}})$ Void growth rate factor, defined in Eq. (8.216)
G Free energy
G_0 Free energy of perfect lattice
ΔG Change in free energy
ΔG_n^0 Activation barrier for void nucleation without interstitials
$\Delta G_n^{'}$ Activation barrier for void nucleation with interstitials
H Enthalpy, also Henry's law constant, as in Eq. (8.57)
J Nucleation current
k Boltzmann's constant
k_{g}^2 Sink strength for 1D diffusing SIA clusters
k_X^2 Sink strength of sink X
k_j^2 Total sink strength species j
$k_{\mathrm{cl}}^{\mathrm{eff}}$ Effective production rate of defects in clusters and free form
K_j Loss rate of species j
K_{iv} Vacancy–interstitial recombination rate
k_j^{eff} Effective production rate of free defects of type j
K_0 Defect production rate
k_x^{c} Rate of gas atom resolution
l Distance of cluster to a grain boundary
L_j Thermal emission rate of species j
m_{i} Number of interstitial in an interstitial loop
M Helium concentration
M_x Helium cluster of x gas atoms
n Number of vacancies in a void
n_{cr} Number of vacancies in a void of critical size
$n_{\mathrm{k}}, n_{\mathrm{k}}'$ Critical void nucleus cluster size
n_{vi} Number of vacancies and interstitials
$N_{\mathrm{d}j}$ Average number of defects of type j generated in a single cascade
N_0 Number of lattice sites per unit volume
N_{R} Number of defects per unit volume that have recombined
N_{S} Number of defects per unit volume lost to sinks
p Gas pressure
P_m Probability of nucleating a void embryo of size m
Q Sink strength ratio
R Radius
r_{c} Recombination volume radius, or dislocation core radius (Eq. 8.245)
r_0 Prismatic dislocation loop radius

R	Void or bubble radius
R_g	Grain radius
R_c	Critical bubble radius
R_cr	Critical void radius
R_iv	Vacancy–interstitial recombination rate
R_max	Saturation void size
R_0	Equilibrium bubble radius
$\dot{R}$	Rate of change of radius, growth rate
r_k, $r_k^{'}$	Critical void nucleus radius
S	Entropy
S_j	Supersaturation of species j
T	Temperature
V	Volume
$\Delta V/V$	Fractional volume
w_n	Number of ways of removing $\rho^0(n)$ voids of size n from a solid
x	Number of gas atoms in a void
$x_\mathrm{vcl,icl}$	Mean sizes of vacancy and SIA glissile clusters
z_v	Vacancy bias factor
z_i	Interstitial bias factor
z_iv	Combinatorial factor for vacancy–interstitial recombination
Z	Zeldovich factor
Z'	Zeldovich factor in the presence of interstitials or in a stressed solid
α_j	Emission rate of species j
β	$2\gamma\Omega/kT$ defined in Eq. (8.71)
β_j	Absorption rate of species j
δ	Thickness of void shell
$\varepsilon_\mathrm{i}^\mathrm{g}$	Fraction of interstitials in glissile clusters
ε_j	Fraction of defect j that is lost to clusters
ε_r	Fraction of Frenkel pairs that recombine during cascade cooling
Φ	Fluence or dose
γ	Surface energy
γ_{SFE}	Stacking fault energy
Λ	Defined in Eq. (8.182) as $\sqrt{k_\mathrm{g}^2/2}$
η	Defined in Eq. (8.117)
μ	Shear modulus
μ_x	Chemical potential of species x
ν	Poisson's ratio
θ	Angle between surface and tangent to void, as in Eq. (8.81)
Θ	Defined in Eq. (8.98)
ρ	Void size distribution
ρ_x	Density of entity x
σ_icl	Interaction cross section for SIA loops
σ_vcl	Interaction cross section for vacancy loops

σ_h Hydrostatic stress
Σ_s Macroscopic neutron scattering cross section
τ Time Constant
Ω Atomic volume
ξ Defined in Eq. (8.15)
ζ Defined in Eq. (8.130)

Subscripts

B Bubbles
cr Critical size
CP Coherent precipitates
d Dislocations
db Dislocation bias
g Glissile clusters or gas
gb Grain boundary
g Glissile SIA loops
hom Homogeneous
i Interstitials
icl SIA loops
j Defect specie representation
IP Incoherent precipitates
L Dislocation loops
N Network dislocations
pb Production bias
s Sinks
v Vacancy
V Void
vcl Vacancy loops
0 Equilibrium

Superscripts

c Cascades
E Vacancy emission
g Glissile
L Loops
m Number of vacancies in a void embryo of size m
s Single defects, sessile
V Voids
0 Equilibrium
* Minimum critical value
′ In the presence of interstitials

Problems

8.1 In a solid where the effect of interstitials is neglected (i.e., where $\beta_i/\beta_v = 0$),

(a) Determine the critical void embryo size (in terms of the number of vacancies *and* void radius).
(b) Show schematically how the number of vacancies in the critical size void embryo varies with:

(i) Temperature
(ii) Degree of vacancy supersaturation
(iii) Void surface energy
(iv) The presence of interstitials.

(c) How do your answers to parts (a) *and* (b) change when an inert gas is present?

8.2 Determine the critical void embryo size for 316 stainless steel ($a = 0.3$ nm, $\gamma = 1.75$ J/m^2) irradiated at 500 °C so as to produce a vacancy supersaturation of 10^3.

8.3 Derive Eq. (8.40).

8.4 Calculate and plot the relative void growth rate $\dot{R}/\dot{R}_o$ for stainless steel ($T_m = 1823$ K) as a function of T/T_m, given that

$$
\begin{aligned}
Q_f^v &= 1.4\,\text{eV} \\
Q_m^v &= 1.09\,\text{eV} \\
\rho_d &= 10^{10}\,\text{cm}^{-2} \\
\Sigma s &= 0.3\,\text{cm}^{-1} \\
\phi &= 10^{14}\,\text{n/cm}^2\text{s} \\
\nu &= \#\ \text{displacements/neutron} = 100 \\
z_{iv} &= 30 \\
z_i &= 1.02 \\
z_v &= 1.00 \\
a^3 &= \Omega = 0.011\,\text{nm}^3 \\
kT/2\gamma &= 0.01\,\text{nm}^2 \\
\nu &= 10^{13}\,\text{s}^{-1}
\end{aligned}
$$

Neglect voids as sinks ($\rho_V \simeq 0$) and precipitates ($\rho_{CP} \simeq 0$) and loops as sinks ($\rho_L \simeq 0$). Assume the vacancy diffusion coefficient is given by

$$D_v = va^2 \exp(-Q_m^v/kT)$$

and the equilibrium vacancy concentration is given by

$$C_v^0 = \Omega^{-1} \exp(-Q_f^v/kT)\,.$$

Assume the void diameter is 50 nm.

8.5 The equation for growth of a cavity is given by:

$$\frac{dR}{dt} = \frac{\Omega}{R}[D_v(C_v - C_v^V) - D_i C_i]\,.$$

Explain what happens to the cavity growth rate if the radiation dose rate doubles. Assume low sink strength and low temperature. Explain what happens if the radiation stops, but the sample is held at the same temperature at which it was irradiated.

8.6 A solid is subjected to a neutron flux, resulting in void formation and growth. At time t_1, a condition is reached where the dislocation density is 10^9 cm^{-2}, the voids are all 100 nm in diameter at a density of 10^{14} cm^{-3}, and the void growth rate is zero. In the absence of thermal emission, however, $\dot{R} = 10^{-2}$ nm/s. The metal is instantaneously strained such that the dislocation density increases by a factor of 10 and the void growth rate in the absence of thermal emission increases to 8×10^{-2} nm/s. Determine the direction and magnitude of the hydrostatic stress needed to suppress void growth. Assume that the solid contains no dislocation loops or precipitates and that the voids are gas free.

8.7 Pure nickel has been found to be highly susceptible to void formation when irradiated in a fast neutron spectrum. Along with voids, perfect dislocation loops are found in nickel. In comparison, Fe–18Cr–8Ni stainless steel is less susceptible to void formation and faulted Frank loops are found, but voids are also present.

As the nickel content in the stainless steel is increased, two other observations are made. The susceptibility to void formation decreases, and voids that are present are surrounded by a nickel-rich shell.

Given the following information, explain each of these observations.

$$\gamma/\gamma_{SFE}|_{Ni} < \gamma/\gamma_{SFE}|_{Fe}, \quad R_{Ni} < R_{Fe}$$

Element	Cr	Fe	Ni
$\sigma_{eff}(n, \alpha)$	0.20	0.23	4.20

8.8 (a) Explain the reason for the characteristic bell-shaped plot of swelling versus irradiation temperature.
(b) How and why is the shape changed by:

(i) Cold-work prior to irradiation
(ii) The addition of impurities
(iii) Grain size

(c) Explain why swelling and creep can affect each other.

8.9 You are designing the stainless steel fuel cladding for the advanced breeder reactor. Your objective is to delay void nucleation *and* minimize void growth. Concerning cladding fabrication, you can control:

(a) Grain size
(b) Degree of cold-work
(c) Precipitate density
(d) Impurity content of the steel.

From a design standpoint, you can control the normal operating temperature of the cladding over a window of 100 °C.
Using void nucleation and growth theory, how can you utilize these *five* parameters to reach this goal? Be quantitative where possible.

8.10 Annealing is a means of removing radiation damage from an alloy. For stainless steel with both dislocation loop and void populations, explain what will occur when the steel is annealed at 600 °C for several hours. In describing the changes during annealing, indicate relative rates and end points.

8.11 In the absence of gas atoms, we wish to eliminate voids in Cu by thermal treatment at 400 °C. Calculate the length of time needed to accomplish this for initial void radii of 5 and 30 nm. The surface free energy of copper is 1.73 J/m^2.

8.12 Given that the number of gas atoms in a bubble can be described as

$$m = (4/3\pi R^3)\rho_g$$

and that the gas atom density, ρ_g, can be described by

$$1/\rho_g = B + (kT/2\gamma)R$$

where B is the dense gas limit:

(a) Show that the volume increase that accompanies coalescence of equal-sized gas bubbles is

$$(\Delta V/V)_{\text{final}}/((\Delta V/V)_{\text{initial}} = /\sqrt{2}.$$

(b) Assuming that the overall gas balance in UO_2 can be given as

$$YF't = mN$$

where

Y noble gas yield of a fission event
F' fission rate density
m gas atoms per bubble
N bubble density,

and all the gas remains in bubbles, develop an expression for the volumetric swelling rate and indicate the dependence on burnup.

(c) How would you account for

(i) Gas remaining in the matrix?
(ii) Resolution?

References

1. Cauthorne C, Fulton E (1967) Nature 216:575
2. Jenkins ML, Kirk MA (2001) Characterization of radiation damage by transmission electron microscopy. Institute of Physics Publishing, Philadelphia
3. Adda U (1972) In: Corbett JW, Ianiello LC (eds) Proceedings of radiation-induced voids in metals, CONF-710601, USAEC Technical Information Center, Oak Ridge, TN, 1972, p 31
4. Olander DR (1976) Fundamental aspects of nuclear reactor fuel elements, TID-26711-P1. Technical Information Center, USERDA, Washington, DC
5. Mansur LK (1994) J Nucl Mater 216:97–123
6. Russell KC (1971) Acta Met 19:753
7. Powell RW, Russell KC (1972) Rad Eff 12:127
8. Katz JL, Wiedersich H (1972) In: Corbett JW, Ianiello LC (eds) Proceedings of radiation-induced voids in metals, CONF-710601, USAEC Technical Information Center, Oak Ridge, TN, 1972, p 825
9. Russell KC (1979) Acta Met 26:1615
10. Packan NH, Farrell K, Stregler JO (1978) J Nucl Mater 78:143
11. Wiedersich H, Katy JL (1979) Adv Colloid Interface Sci 10:33
12. Russell KC (1972) Acta Met 20:899
13. Katz JL, Wiedersich H (1973) J Nucl Mater 46:41
14. Semenov AA, Woo CH (2002) Phys Rev B 66:024118
15. Brailsford AD, Bullough R (1972) J Nucl Mater 44:121–135
16. Mansur LK (1978) Nucl Technol 40:5–34
17. Brimhall JL, Kissinger HE, Kulcinski GL (1972) In: Corbett JW, Ianiello LC (eds) Proceedings of radiation-induced voids in metals, CONF-710601, USAEC Technical Information Center, Oak Ridge, TN, 1972, p 338

18. Garner FA, Porollo SI, Vorobjev AN, Konobeev YuV, Dvoriashin AM (1999) In: Ford FP, Bruemmer SM, Was GS (eds) Proceedings of the 9th international symposium on environmental degradation of materials in nuclear power systems: water reactors, the minerals, metals and materials society, Warrendale, PA, p 1051
19. Garner FA (1984) Irradiation performance of cladding and structural steels in liquid metal reactors, chap 6. In: Frost BRT (ed) Materials science and technology, vol 10A, nuclear materials, part I. VCH, New York
20. Krasnoselov VA, Prokhorov VI, Koleskikov AN, Ostrovskii ZA (1983) Atomnaya Energiya 54(2):111–114
21. Garner FA, Bates JF, Mitchell MA (1992) J Nucl Mater 189:201–209
22. Brager HR, Garner FA (1979) Effects of radiation on structural materials the 9th international symposium, STP 683. America Society for Testing and Materials, Philadelphia, PA, 1979, pp 207–232
23. Dupouy JM, Lehmann J, Boutard JL (1978) In: Proceedings of the conference on reactor materials science, vol. 5, Alushta, USSR. Moscow, USSR Government, pp 280–296
24. Busboom HJ, McClelland GC, Bell WL, Appleby WK (1975) Swelling of types 304 and 316 stainless steel irradiated to 8 × 1022 n/cm^2, general electric company report GEAP-14062. General Electric Co., Sunnyvale
25. Seran LJ, Dupouy JM (1982) In: Effects of radiation on materials the 11th international symposium, STP 782. American Society for Testing and Materials, Philadelphia, PA, 1982, pp 5–16
26. Seran LJ, Dupouy JM (1983) In: Proceedings of the conference on dimensional stability and mechanical behavior of irradiated metals and alloys, vol 1, Brighton. British Nuclear Energy Society, London, 1983, pp 22–28
27. Mansur LK (1993) J Nucl Mater 206:306–323
28. Mansur LK (1978) J Nucl Mater 78:156–160
29. Mansur LK (1978) Nucl Technol 40:5–34
30. Woo CH, Singh BN (1990) Phys Stat Sol (b) 159:609
31. Golubov SI, Barashev AV, Stoller RE (2012) In: Konings RJM (ed) Comprehensive Nuclear Materials, 1.13. Elsevier, Amsterdam
32. Singh BN, Foreman AJE (1992) Philos Mag A 1992(66):975
33. Abromeit C (1994) J Nucl Mater 216:78–96
34. Singh BN, Eldrup M, Horsewell A, Earhart P, Dworschak F (2000) Philos Mag 80:2629
35. Brailsford AD, Bullough R (1973) J Nucl Mater 48:87
36. Brailsford AD, Bullough R (1972) British Rep AERE-TB-542
37. Dubuisson P, Maillard A, Delalande C, Gilbon D, Seran JL (1992) Effects of Radiation on materials the 15th international symposium, STP 1125. American Society for Testing and Materials, Philadelphia, PA, 1992, pp 995–1014
38. Brager HR, Garner FA, Guthrie GL (1977) J Nucl Mater 66:301–321
39. Wolfer WG, Foster JP, Garner FA (1972) Nucl Technol 16:55
40. Brailsford AD (1975) J Nucl Mater 56:7
41. Wolfer WG, Mansur LK (1980) J Nucl Mater 91:265
42. Allen TR, Cole JI, Gan J, Was GS, Dropek R, Kenik EA (2005) J Nucl Mater 341:90–100
43. Ghoniem NM, Walgraef DJ, Zinkle S (2002) Comput Aided Mater Des 8:1–38
44. Jager W, Trinkaus H (1993) J Nucl Mater 205:394–410
45. Woo CH, Frank W (1985) J Nucl Mater 137:7
46. Garner FA (1984) J Nucl Mater 122–123:459–471
47. Mansur LK, Yoo MH (1978) J Nucl Mater 74:228–241
48. Garner FA, Kumar AS (1987) Radiation-Induced Changes in Microstructure the 13th International Symposium, STP 955 (Part 1). American Society for Testing and Materials, Philadelphia, PA, 1987, pp 289–314
49. Garner FA, Brager HR (1985) J Nucl Mater 133–134:511–514
50. Gan J, Simonen EP, Bruemmer SM, Fournier L, Sencer BH, Was GS (2004) J Nucl Mater 325:94–106

51. Brailsford AD, Mansur LK (1981) J Nucl Mater 103–104:1403–1408
52. Shiakh MA (1992) J Nucl Mater 187:303–306
53. Sekio Y, Yamashita S, Sakaguchi N, Takahashi H (2014) J Nucl Mater 458:355–360
54. Singh BN, Zinkle SJ (1994) J Nucl Mater 217:161–171
55. Garner FA, Sekimura N, Grossbeck ML, Ermi AM, Newkirk JW, Watanabe H, Kiritani M (1993) J Nucl Mater 205:206–218
56. Mansur LK, Coghlan WA (1983) J Nucl Mater 119:1–25
57. Stoller RE, Odette GR (1985) J Nucl Mater 131:118–125
58. Evans JH (1978) J Nucl Mater 76–77:228–234
59. Trinkaus H (1983) Rad Eff 78:189–211
60. Johnson PB, Mazey DJ, Evans JH (1983) Rad Eff 78:147–156
61. Garner FA (2012) Radiation damage in austenitic steels. In: Konings RJM (ed) Comprehensive Nuclear Materials, 4.02:33. Elsevier, Amsterdam
62. Garner FA, Griffiths M, Greenwood LR, Gilbert ER (2010) In: Proceedings of the 14th international conference on environmental degradation of materials in nuclear power systems—water reactors. American Nuclear Society, 1344–1354